THESIS FOR THE DEGREE OF LICENTIATE OF ENGINEERING

# $WO_3$ for reflective displays in color

MARIKA GUGOLE

Department of Chemistry and Chemical Engineering

CHALMERS UNIVERSITY OF TECHNOLOGY

Gothenburg, Sweden 2021

**$WO_3$ for reflective displays in color**

MARIKA GUGOLE

Cover image: CIE coordinates for 5 samples based on the design depicted in the schematic on the top right. The gold, $WO_3$, platinum thin films make up the Fabry-Pérot cavity which is used to select the reflected wavelengths (color). The lithium ions, intercalating and de-intercalating change the optical properties of the $WO_3$ and hence the reflected color. The white points correspond to the de-intercalated state, which is also shown in the pictures of the fabricated samples, while the dark points to the intercalated state.



Licentiatuppsatser vid Institutionen för kemi och kemiteknik

Chalmers tekniska högskola.

Nr 2021:04

Department of Chemistry and Chemical Engineering

Chalmers University of Technology

SE-412 96 Gothenburg, Sweden

Phone: +46 (0)31 772 56 16

www.chalmers.se

Printed by Chalmers Reproservice

Gothenburg, Sweden, Mars 2021

# Abstract

Reflective displays, also known as electronic paper, are very attractive due to their low power consumption and great visibility under bright ambient light conditions. However, reflective displays in color are still limited on the market for two main reasons. First, their low absolute reflectivity requires the integration of a strong backlight which has the consequence of a higher power consumption and the loss of the paper-like appearance. Second, their color quality (chromaticity) is poor. Both reasons are the result of how the red, green and blue (RGB) subpixels are generated: color filters are applied on top of white surfaces. The 3 subpixels design itself, limits the reflectivity to 33% for each color, moreover the addition of color filters makes it drop to less than 30%.

Plasmonic structural colors based on metal-insulator-metal Fabry-Pérot cavities, on the other hand, have been proven to show great reflectivity (>90%) and chromaticity and, combined with electrochromic materials, could be used as pixels in reflective displays. In this thesis 2 types of these metasurfaces are fabricated, combined with the inorganic electrochromic material tungsten trioxide ($WO_3$) to generate dynamic structures.

The first type includes an aluminum mirror, an alumina spacer layer, and a top gold film with a nanoholes array. The thickness of the alumina spacer layer is tuned to select the reflected wavelengths via thin film interference to fabricate RGB surfaces. The nanoholes on the top layer, moreover, contribute to the chromaticity via plasmonic resonance. On top of the Fabry-Pérot cavities, we deposit a layer of $WO_3$. This electrochromic material, once placed in an electrochemical cell with an electrolyte containing lithium ions, undergo an optical change (it turns deep blue) when a voltage is applied, hence when the ions are intercalated or de-intercalated in the film. As a result, the RGB pixels can be turned on and off, completely or partially, to display all the other colors.

The second type is also based on a Fabry-Pérot cavity, with a platinum mirror and a top gold layer. The difference relies in the spacer layer, which is constituted by the electrochromic $WO_3$. Here are presented 2 designs based on this, one with nanoholes in the top gold film and one with nanoholes in the bottom platinum mirror. In both designs the holes only serve as passages through the metal to the $WO_3$ film and do not show any plasmonic resonance in the visible part of the spectra. The result is dynamic structures that can reflect several different colors due to the change in the optical constants of the spacer layer. With this design it could then be possible to move away from a 3 subpixels configuration towards a 2 or 1 subpixels configuration with higher reflectivity.

**Keywords:** reflective displays, plasmonic metasurfaces, structural colors, electrochromism.

# List of publications

**I.** **High-contrast switching of plasmonic structural colors: inorganic versus organic electrochromism.**
Marika Gugole*, Oliver Olsson*, Kunli Xiong, Jolie C. Blake, José Montero Amenedo, Ilknur Bayrak Pehlivan, Gunnar A. Niklasson, and Andreas Dahlin
*ACS Photonics* **2020** *7* (7), 1762-1772
*Contributed equally as first authors

**II.** **Electrochromic Inorganic Nanostructures with High Chromaticity and Superior Brightness**
Marika Gugole, Oliver Olsson, Stefano Rossi, Magnus P. Jonsson, and Andreas Dahlin
*Manuscript*

# Contribution to the listed publications

I. Fabrication of the metasurfaces, deposition of the inorganic electrochromic material and its characterization. Contribution to the writing.

II. Fabrication and test of the Fabry-Pérot cavities, simulations of Fresnel model and combination of the structures. Contribution to the writing.

# Contents

# Introduction

Displays can be divided in two categories: emissive and reflective. Emissive displays are the most commonly found displays and they produce images using light sources. The light source allows good quality images, but also consumes a lot of power [1]. Reflective displays, on the other hand, do not contain any light source, but create images by reflecting the ambient light, exactly like paper, which is why they are also referred to as electronic paper or e-paper. This results in a different image quality depending on the ambient conditions: very high reflection in sunlight, for example, but poor reflection in dark conditions. Moreover, the power consumption is low since there is no competition between the display own light source and the ambient light, but quite the opposite.

Another thing worth mentioning is the effects of emissive displays on the human body. If we think about how many hours per day we spend looking at a screen it is not surprising that such a long exposure to a light source could negatively affect us and it has probably happened to all of us that we get a headache due to the long time spent working with a computer. It is also known that looking at your phone, computer or TV before going to bed will affect your sleep quality [2].

So why are not reflective displays the most common type of screens? Mainly due to their limitation in producing highly reflective colors with good chromaticity.

This work focuses on the fabrication and characterization of highly reflective plasmonic structural colors which are combined with organic and inorganic electrochromic materials. These materials are used to switch the colors on and off, like a regular pixel, and show a very high contrast and fast switch together with a low power consumption. Moreover, they are implemented in the structure to create a dynamic monopixel.

# Background

## Reflective displays in colors

Different technologies have been presented through the years to achieve a high-quality reflective display in color [3].

The most popular one and the one is the electrophoretic ink technology, which is used in the well-known Amazon Kindle e-book reader. In electrophoretic displays (EPDs) black and white particles of opposite charge are interchanged upon a voltage switch and act like black and white pixels creating images. The step towards EPD in colors has been made, for example, introducing color filters on top of the black and white pixels (E-ink Kaleido/Triton) or pigment electronic ink (E-Ink spectra). However, independently of the technology implemented, the introduction of red, green and blue (RGB) pixels has the consequence of limiting the maximum reflected light for each pixel to 100%/3=33% and thus requiring a bright ambient light. If then a filter is added, for example on an EPD display, the reflection decreases even more [4], as it is depicted in Figure 1. The light shines on the RGB subpixels, which means only about 33% of it is reflected by each color. A common color filter has a transmission of about 90%, which means that the total reflected light, in perfect conditions, is less than 30%. In reality, this would be a lot less, considering the low background reflection of EPD displays even in black and white mode.

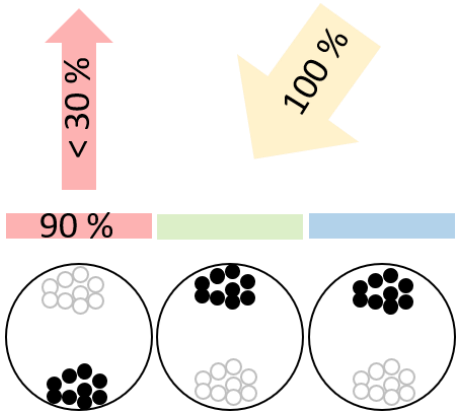


*Figure 1: Schematic of an EPD display with color filters.*

To improve this condition, two different options are considered in this work: highly reflective RGB subpixels and a dynamic monopixel. Both options have their foundation on structural coloration and plasmons.

## Plasmonic structural colors

Plasmonic structures can be used to produce vibrant and stable colors. The principle on which these types of colors are based on is structural coloration.

Structural coloration refers to the fabrication of colors without using pigments but taking advantage of light interferences to control the reflected light. This mechanism is widely found in nature, for example in the blue feathers of birds [5, 6].

The easiest structural coloration mechanism is based on thin film interference [6], shown in Figure 2, and it is also the physical principle on which the structural colors in this thesis are based.

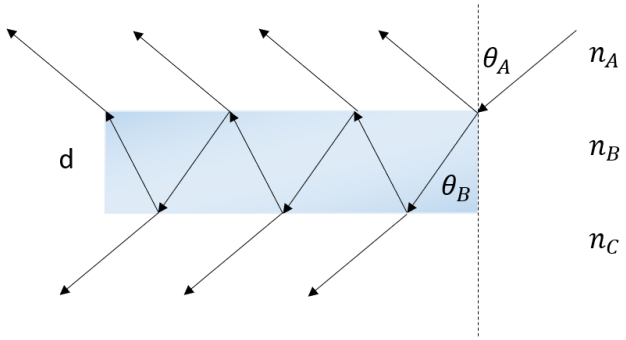


*Figure 2: Schematic of thin film interference phenomenon.*

The light hits at an angle $\vartheta_A$ a thin film of thickness d and refractive index $n_B$ and refracts at an angle $\vartheta_B$ (Snell's law). When the refracted beam hits the lower boundary of the thin film, it refracts again, but it also reflects and refract again at the upper boundary, exiting the film and interfering with the other reflected beams. Depending on the thickness d of the thin film, only the wavelengths which are a multiple integer of the optical path length will constructively interfere, while half wavelengths will destructively interfere and cancel each other. This is described by the following equation:

$$2n_B d\cos\vartheta = m\lambda \quad (1)$$

where m is an integer.

The structural colors fabricated in this thesis, are an application of thin film interference, a Fabry-Pérot cavity, which consist in a metal-insulator-metal configuration, as shown in Figure 3.

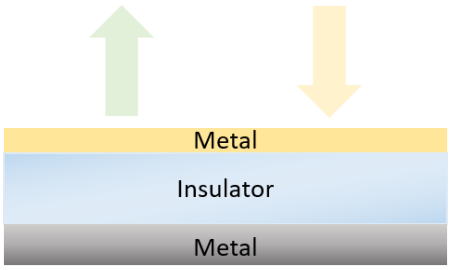


*Figure 3: Metal-Insulator-Metal structure to create a Fabry-Pérot cavity. The incident light is reflected several times in the cavity and only a selected wavelength (range) is reflected from the structure.*

In this configuration a specific wavelength can be selected by tuning the materials and thicknesses of the layers [4, 6-17] (and simulations can be done using the transfer matrix method).

In this thesis, plasmonic structural colors, refers to colors fabricated by a metal-insulator-metal structure, as shown above, to select the desired wavelength. Adding nanoholes in the top metal layer excite surface plasmons in the visible spectrum and the scattering and absorption from them allows to refine the selection of the desired wavelength range [18].

It is possible to fabricate pixels in vibrant primary colors with different combinations of metals and insulators. It is also possible to introduce a mechanism able to shut the color on and off, like a regular pixel, using an electrochromic layer on top of the structure which can turn transparent or colored when a voltage is applied. However, the electrochromic material can also be implemented in the Fabry-Pérot cavity, as middle layer, to create a dynamic monopixel.

## How the eye perceives colors and the 1931 CIE color spaces

There are two important topics to discuss in order to understand the data presented further in this thesis: how the human eye perceive colors and how it is possible to represent them in a somehow universal language.

One of the many properties of an object is to absorb or reflect part of the light that shines on it. The reflected light, when in the visible part of the spectrum, is perceived by our eyes as colors. Our eyes are characterized by three types of cone photoreceptors, long ones that are sensitive to red light, medium to green and short to blue. However, different colors with physically the same spectral radiance (the power received by an optical system looking at a surface from a specified viewing angle) appear more or less bright to the human eye depending on where they lay in the wavelength's spectrum. For this purpose, a luminosity function is introduced. As it is shown in Figure 4 the human eye will see as brighter a green color than a blue color, which means for example that if we see a blue and a green objects that appear to be equally bright, physically speaking the blue one will have a higher radiance. This luminosity function will be used further in the thesis to characterize colors considering not only their reflectance value, but also the perception of the human eye.

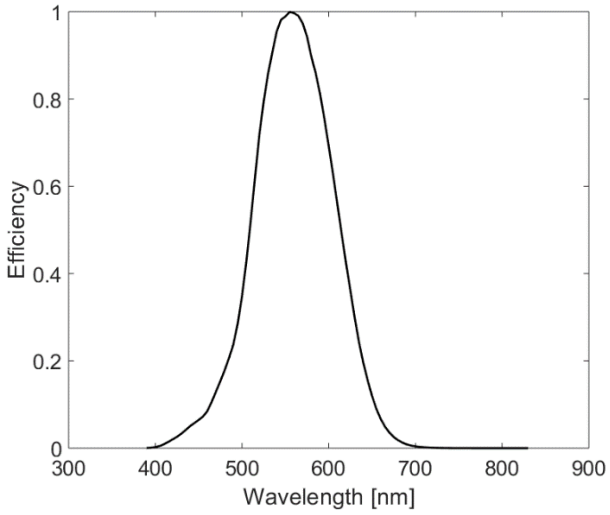


*Figure 4: Luminosity function.*

Moving towards the representation of the colors, In 1931 the International Commission on Illumination (CIE, from the French Commission Internationale de l'Éclairage) introduced the RGB color matching functions, which can be used to calculate how much of each primary color, red, green and blue, is needed to recreate a desired color when viewed by a standard observer at 2 degrees angle. In addition, a scale factor is introduced to take into consideration the brightness of each color. The result of this is three coordinates RGB, called tristimulus values. These functions, however, still have some tricky points. First, there are negative values, which means that to recreate some colors it is necessary to add a negative amount of a color, which was considered counter intuitive. Secondly, they are 3 coordinates, which are hard to visualize in a graph.

To simplify the representation, the XYZ space was introduced, where the matching functions where simply shifted so that the values where all positive. Moreover, the Y function now match the luminosity function that was mentioned above, which means that we can consider the X and Y values as a sort of coordinates for the color and Y as an expression of its brightness.

A step further to the XYZ color space is then the xyY color space, which will be used in this thesis, where x and y are called the chromaticity coordinates and Y is the brightness [19].

The x and y coordinates are calculated from XYZ as:

$$x = \frac{X}{X + Y + Z} \tag{2}$$

$$y = \frac{Y}{X + Y + Z} \tag{3}$$

The x,y coordinates are plotted in the CIE diagram which shows the color corresponding to each x,y combination. In Figure 5 an example of the CIE diagram of the standard red, green and blue color (sRGB) used by monitors, web and printers (citation needed).

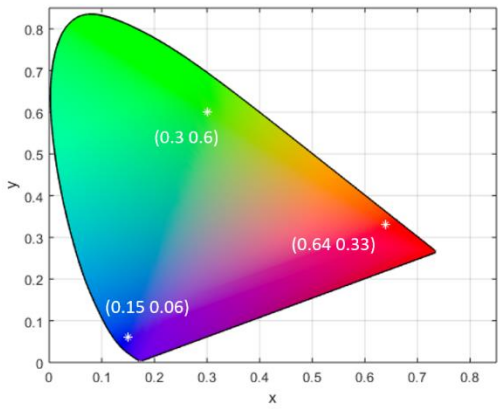


*Figure 5: CIE diagram showing the standard red, green, and blue*

## Electrochromic materials and electrochromic devices

Electrochromism is the property of some materials which can change their optical properties when a voltage is applied that causes intercalation/deintercalation of ions in the film. Some of these materials can switch between a quite transparent to a quite dark colored state. By placing them on top of a structural colored material, it is possible to switch the color on and off.

In this thesis the focus will be on the inorganic electrochromic material $WO_3$, which can switch between a bleached transparent state and a colored deep blue state. In the first, we compare its characteristics with the ones of an organic electrochromic option (ProDOT-$Me_2$). In the second paper, we fabricate dynamic structural colors using $WO_3$ as the spacer layer in a Fabry-Pérot cavity.

$WO_3$ is a very well-known and studied electrochromic inorganic material, whose electrochromic behavior have been explained with different theories through the past 50 years [20-23]. When considering this material for its electrochromic properties, amorphous and oxygen deficient $WO_3$ shows

better electrochromic properties than its stoichiometric crystalline state [24] and it is such films we fabricate in this thesis as well.

The mechanism behind electrochromism in $WO_3$ is still not completely understood [25]. The most recent literature suggests that optical absorption is associated to polaron hopping between adjacent W states with different valence states ($W^{5+} \rightarrow W^{6+}$) upon photon absorption and or between oxygen vacancies [26-28].

## Contrast, speed, lifetime, power consumption and bistability

To characterize electrochromic materials, different properties can be studied. In this work, we focus on five most important ones, which address five characteristic that are desired in a reflective screen: contrast, speed, lifetime, power consumption and bistability.

The contrast is defined as the difference in reflectivity between the (two) states of the electrochromic material, bleached and colored.

$$C(\lambda) = \Delta R(\lambda) = R(\text{colored})(\lambda) - R(\text{bleached})(\lambda) \tag{4}$$

As it is shown in eq. (4), the contrast depends on the wavelength. Thus, some specific wavelengths can be picked as reference for any comparison. In this thesis 3 wavelengths are considered: 630 nm, 530 nm and 470 nm for red, green and blue although it has to be taken into account that a color does not correspond to a single wavelength, but to a range of wavelengths. In some cases, like when we have the electrochromic materials on a colored surface, it is more meaningful to consider the highest contrast at whichever wavelength that would be. In the case of a comparison between elctrochromic materials only, without the colored surface, it is also possible to calculate a mean reflectivity difference, weighted using the luminosity function mentioned above, to express a mean difference over the wavelengths where our eyes are sensitive:

$$\overline{\Delta R} = \frac{\int_{380\ \text{nm}}^{780\ \text{nm}} L(\lambda)\Delta R(\lambda)d\lambda}{\int_{380\ \text{nm}}^{780\ \text{nm}} L(\lambda)d\lambda} \tag{5}$$

The switching speed is the time needed for the electrochromic material to completely switch between the two states and it can depend on the voltage applied to the material. Connected to this, is the power consumption, that is the power needed in a full switch. The last parameter, the bistability of the material is the time that one coloration state of the material can be maintained without a voltage applied.

# Techniques

## Thin film deposition: physical vapor deposition (PVD)

Physical vapor deposition is the production of a condensable vapor by physical means and subsequent deposition of a thin film of this vapor [29]. The means by which this vapor is created can be different. In this thesis, RF reactive magnetron sputtering and electron beam evaporation are used.

### RF reactive magnetron sputtering

Sputtering is the physical vapor deposition method in which the vapor of a target source is created via ion bombardment and deposited onto a substrate [30]. In reactive sputtering, moreover, the target substance interacts with a reactive gas, such as oxygen, and forms a compound before being deposited onto the substrate [29]. In Figure 6 a schematic of a RF magnetron sputtering chamber.

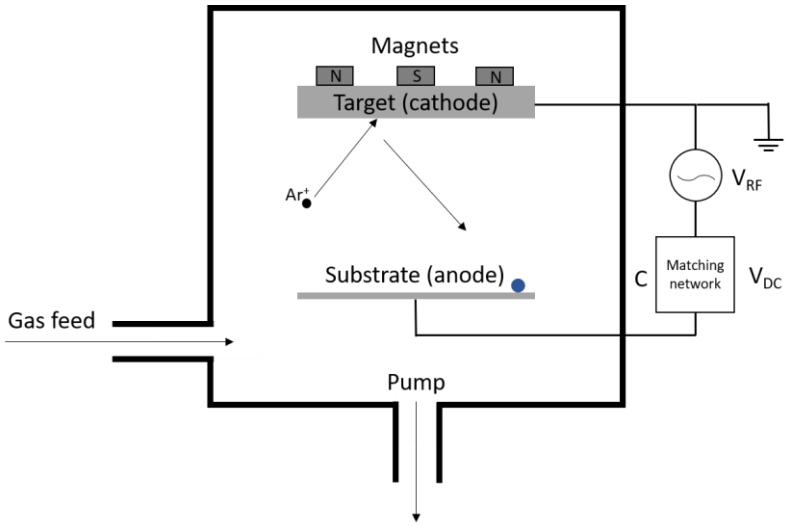


*Figure 6: Schematic of an RF magnetron sputtering chamber.*

The pumping line evacuates the chamber (in the case of the Nordiko 2000 sputter used in this work, the base pressure is about $5 \cdot 10^{-6}$ mbar) and argon is let in the chamber. Argon and oxygen flow and chamber pressure can be chosen to set sputtering conditions. The power supply is a high RF voltage source (0.5-1kV amplitude, 13.56 MHz usually [29]), a blocking capacitor and a matching network improve the power transfer to the plasma and develops the DC self-bias, which is a monitor of how much of the RF power is actually transferred to the plasma after losses [31]. The magnets around the target create a magnetic field that concentrates and intensifies the plasma in the vicinity of the target, thus enhancing the ion bombardment by confining the electrons and resulting in a higher deposition rate. This design is called magnetron [29].

### Electron beam evaporation

In electron beam evaporation, or e-gun evaporation, the target material is evaporated by a beam of energetic electrons [29]. Figure 7 shows the evaporation chamber with a 270° bent electron beam. The fundamental parts are the thermionic emitter, which emits the energetic electrons, a magnetic field, which bents the beam, a crucible source and a substrate plate.

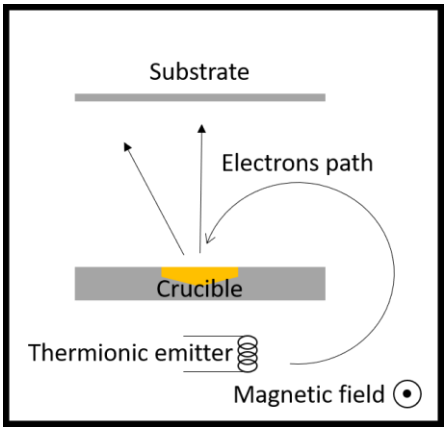


*Figure 7: Schematic of an evaporation chamber with a 270° bent electron beam.*

As in the sputtering, the chamber is also pumped and the process is done under vacuum. In electron beam evaporation the pressure is around $10^{-5}$ Torr.

In the evaporation chamber, a QCM sensor is also present, to monitor the thickness during the deposition (this is not present in the sputtering chamber and thickness has to be measured afterwards).

## Ellipsometry

Ellipsometry is an indirect method to determine the thickness and optical properties of thin films. It is based on the measurement of how the light polarization changes after being reflected from the sample [32].

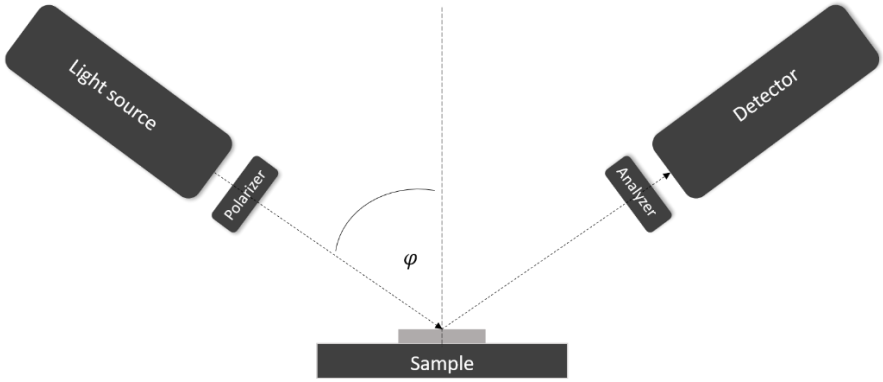


*Figure 8: Schematic of an ellipsometer.*

Figure 8 shows a schematic of an ellipsometer. The light from the light source passes through a polarizer and it is linearly polarized. Then it is reflected by the sample and it passes through another polarizer, called analyzer, and is collected by a detector. Light source and detector are both at the same angle relative to the sample normal (φ).

As previously said, ellipsometry is an indirect method, which means that the quantities that are measured directly are then analyzed by means of a model (which usually depends on the material which is analyzed) and other quantities are indirectly calculated (for example thickness). The quantities that are directly calculated are the phase difference and the amplitude ratio [33].

# Fabrication and test

## $WO_3$ sputtering

The radio frequency (RF) reactive sputtering of the electrochromic layer $WO_3$, is made using NORDIKO 2000 sputter. Argon flow is set to 32 sccm and Oxygen at 8 sccm, with a pressure of 20 mTorr and a RF power of 150 W.

## Colloidal lithography using nanoparticles

The structures that will be described more in detail in the next sections have a nanoholes array in one or more metal layers. To obtain that array, we use a technique called colloidal lithography, where polystyrene (PS) nanoparticles are deposited before the metal layer and stripped after its deposition, to leave nanoholes behind. In Figure 9 a detail representation of the process is shown.

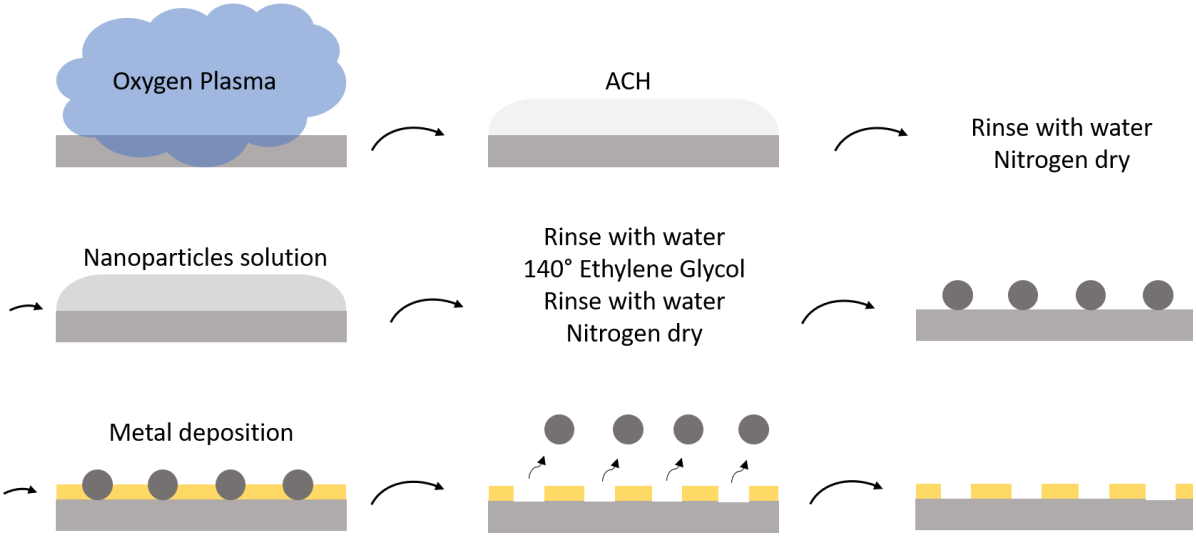


*Figure 9: Steps of the colloidal lithography technique.*

The first step is exposing the substrate to a 30 s oxygen plasma at 50W, to make the surface hydroscopic. This step is done only for the structures without $WO_3$ as a substrate, since oxygen plasma treatment of $WO_3$ film results in a non-uniform particles distribution. Then a 0.25 M solution of aluminum chlorohydrate (ACH) is deposited on the substrate and let rest for 1 min. This step makes the surface charged and it is necessary to attract the PS particles deposited successively. After the ACH adsorption, excess is rinsed away with water and the substrate is dried with nitrogen. Then a PS particles solution is deposited and let rest for 2 or 4 minutes depending on the substrate (the specific concentration and rest time is different for different structures and it will be mentioned in the successive sections). Then the particles are rinsed with water and 140°C ethylene glycol is poured on the substrate. This step partly melts the PS particles, so that they remain on the substrate after the last rinse with water and dry with nitrogen. All the steps are carried out keeping the surface in a horizontal position. When the particles have been adsorpted on the substrate, the metal layer is evaporated on top, with a maximum thickness of about the radius of the particles. Then the particles are stripped away with tape or gently rubbed away with a sponge swab.

In the next sections a more detailed description of the process is presented for 3 different structures.

## Three structures

The 3 different structures refer to different combination of layers, but also, in case of the dynamic colors, to different concepts (designs). What we will call "conventional" structure, implies having a mirror deposited on the glass support, followed by the spacer layer and the gold layer. The "reverse" structure instead has the gold layer deposited on the glass support, followed by the spacer layer and the mirror. The conventional structure may or may not present holes in the gold layer and it does not have holes in the mirror layer. The reverse structure does not have holes in the gold layer, but has holes in the mirror layer, to allow the electrolyte to flow into the $WO_3$ spacer layer. These different designs imply, then, having the electrolyte and reference and counter electrode in different places with respect to the sample (see Figure 10).

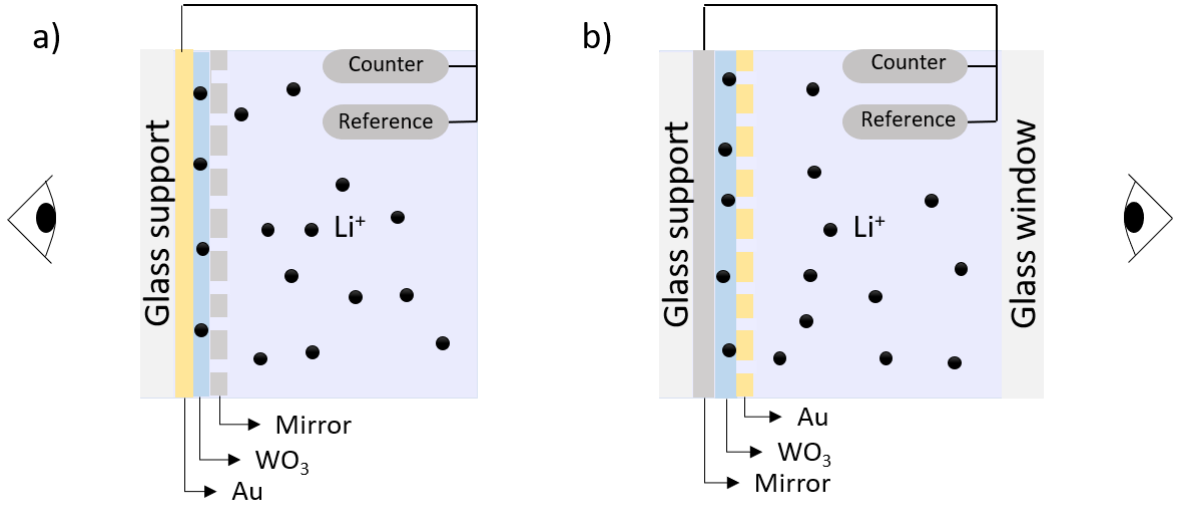


*Figure 10: schematic of a) the reverse structure and b) the conventional structure principle of operation in a flowcell. Figure also present in Paper II.*

All the structures are based on color generation by a combination of cavity resonances (Fabry-Pérot cavity) and plasmonic enhancement.

## Static colors with $Al_2O_3$ as spacer layer

A 100 nm Al mirror is first deposited by evaporation (Lesker PVD 225) onto a glass substrate with 5 nm Cr as adhesive layer. Then 61 nm, 95 nm or 110 nm of $Al_2O_3$ are deposited to obtain red, green or blue surfaces respectively. To create a nanoholes array on the las Au layer, colloidal lithography is performed on the $Al_2O_3$. First, the substrate is exposed to the oxygen plasma, then ACH is poured on the surface and let rest for 1 min, then the surface is rinsed with water and dried with nitrogen. Next, the 0.1% 147 nm polystyrene particles (microParticles GmbH) solution is poured on the surface and let rest for 2 min before being rinsed with water. After the rinsing, ethylene glycol (at approximately 140°C) is poured on the surface, followed by rinsing with water and drying with nitrogen. After the deposition of the particles, 1 nm Ti and 20 nm Au were deposited by evaporation (Lesker PVD 225) and then the particles were removed by tape stripping. In Figure 11 a schematic of the structure.

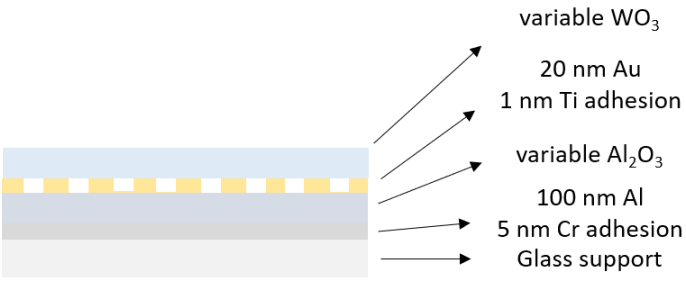


*Figure 11: schematic of the structure used to make static RGB pixels (conventional). The thickness of the $Al_2O_3$ layer is 61, 110 and 95 nm for RGB respectively while the thickness of the $WO_3$ layer is 130 nm for R and B and 180 nm for G.*

A final layer of $WO_3$ is then sputtered on top of the RGB pixels in order to switch them on and off.

## Dynamic colors with $WO_3$ as spacer layer

### Conventional structure

A 50 nm Pt mirror is first deposited by evaporation (Lesker PVD 225) onto a glass substrate with 5 nm Ti as adhesive layer. Then $WO_3$ is deposited by RF sputtering (Nordiko 2000). To create a nanoholes array on the las Au layer, as above, colloidal lithography is performed on the $WO_3$. The process was carried on via a sequence of steps, first 0.25 M ACH was poured on the surface and let rest for 1 min, then the surface was rinsed with water and dried with nitrogen. Next, the 2mM NaCl 0.1% 147 nm polystyrene particles (microParticles GmbH) solution was poured on the surface and let rest for 2 minutes.

### Reverse structure

The structure described above can also be done reversed. 1 nm Ti and 20 nm Au is deposited by evaporation (Lesker PVD 225), the particles are stripped with tape and $WO_3$ is deposited by RF sputtering (Nordiko 2000) as spacer layer. On top of the $WO_3$ film, colloidal lithography with 1 M ACH and 2mM NaCl 0.1% polystyrene particles (microParticles GmbH) solution is performed as above. Lastly 70 nm Pt is deposited by evaporation (Lesker PVD 225) and the particles are removed with a soft sponge while the sample is immersed in isopropanol.

## Electrochemical measurements setup

The electrochemical deposition of the polymer and the switching of both the organic and inorganic electrochromic material is carried out in a customized electrochemical cell. Figure 12 shows a schematic of it, where its different parts are pointed out and a side view shows the different position that the samples can take during the measurement. The cell is a customized 3-electrodes electrochemical cell, where the counter electrode is made of platinum and the reference electrode is Ag/Ag+. The cell allows the sample to be placed in different configurations. The sample can be placed in front of the electrodes, as used for the reversed structure or behind the electrodes, as for the conventional structure

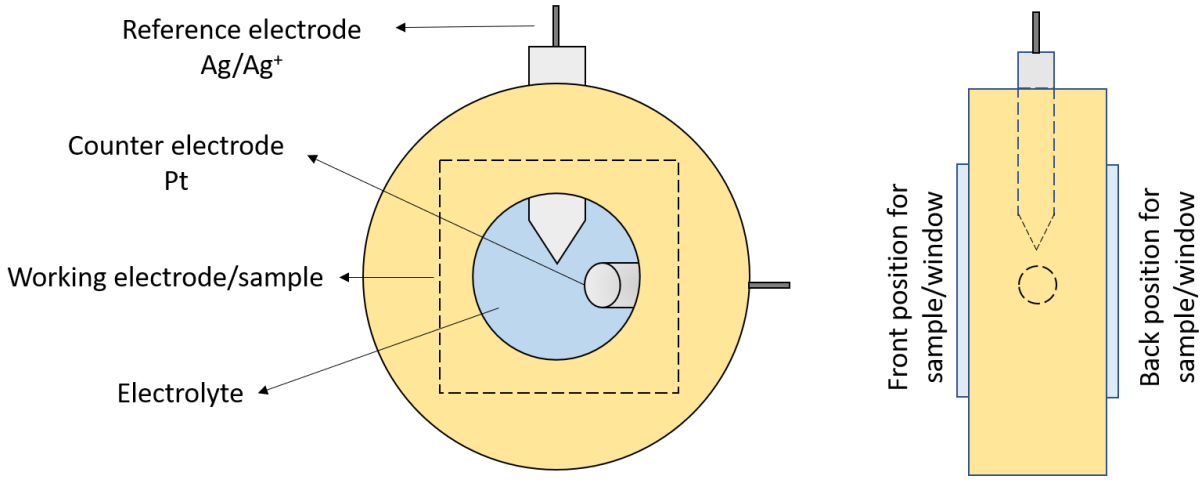


*Figure 12: On the left, front schematic of the cell. On the right, side schematic of the cell.*

## Electrochemical switching of $WO_3$

In the case of the on/off switching colors, a layer of $WO_3$ is deposited on top of the structure to allow the pixel to be switched on and off. For the dynamic colors, this step has yet to be done.

### Top electrochromic material configuration

The samples were placed in a 3 electrodes electrochemical cell (Pt as counter electrode and Ag/Ag+ as reference electrode). The switch was done using a Gamry Interface 1010E potentiostat. The electrolyte used was 1M LiClO4 (Lithium perchlorate, anhydrous, 99%, Alfa Aesar™, Fisher Scientific) in PC (propylene carbonate,reagent grade, 99%, Sigma Aldrich). The cell was placed in an optical setup were reflection or transmission could be measured. The voltages applied for the switch were -1.5 V for the dark state and 1.5 V for the bright state for the RGB structures and -1.5 V for the dark state and 1.7 V for the bright state for the 200 nm $WO_3$ on 20 nm Au sample.

### Spacer layer configuration

In the spacer layer configuration, a similar setup as described above was used, with the difference that in the case of the reverse structure the counter and reference electrode were placed behind the sample. The voltages used were ± 1.5V.

## Optical measurements

The switch of the electrochromic material was measured in a home-built reflection setup, with a tungsten lamp (Azpect Photonics), a 4x air objective with NA 0.1 and a fiber-coupled photodiode array (B&WTek) spectrometer. As reference for reflection measurements a broadband dielectric mirror (BB05-E02, Thorlabs) was used.

## Color characterization

The metasurfaces colors, without the top electrochromic film, were measured with a CM-700d spectrophotometer (Konika Minolta) which also gives the CIE coordinates.

# Results

Paper I reports the successful fabrication of plasmonic metasurfaces stable in organic solvents with high chromaticity and reflectivity. Two electrochromic materials are evaluated on the metasurfaces, one organic (ProDOT-$Me_2$) and one inorganic ($WO_3$). A method to predict the highest contrast for the organic option is also presented and proven. The comparison follows in terms of contrast, switching time, energy consumption and bistability.

Paper II reports the fabrication of dynamic structural colors, based on a Fabry-Pérot cavity with $WO_3$ as spacer layer. The dynamicity of the structures comes from the change in refractive index of the electrochromic $WO_3$ layer upon ion intercalation. The structures, when combined, show a wide color gamut while maintaining a high reflectivity.

## Paper I

### Plasmonic metasurfaces stable in propylene carbonate

In the first paper we present a new structure for the plasmonic metasurfaces, based on the previous design used in the group [14, 16], a metal-insulator-metal structure. The difference resides in the materials used: aluminum mirror, alumina spacer and gold as a top layer with or without nanoholes. The aluminum mirror, contrary to the silver one used previously, would not dissolve in 1M $LiClO_4$ in propylene carbonate, one of the electrolytes in which $WO_3$ can be switched and the one which gives better coloration efficiency [34]. The choice of this electrolyte has two more motivations: non-aqueous electrolytes have the advantage that gas formation and hydrolysis can be avoided and also that the monomers used in the comparison which will be presented later can be dissolved without surfactants, which are needed for the aqueous ones [16].

RGB pixels were easily fabricated by metal evaporation and colloidal lithography, as mentioned above (static colors with conventional structure). The spacer layer thickness was optimized via full Fresnel modeling which resulted in 61 nm, 110 nm and 95 nm of $Al_2O_3$. The red sample does not present a nanoholes array on the gold top layer, due to the scattering in the red region of the spectrum, confirmed by dark field spectra. Thus, the nanoholes do not contribute in the enhancement of the color. For green and blue samples, however, the red scattering contributed to narrowing the reflection spectrum in the desired region. The metasurfaces show CIE coordinates and reflectivity spectra comparable with other works [15] and our previous ones [14] with the advantage of being stable in non-aqueous electrolytes.

### Contrast optimization

The focus of this paper is the optimization and comparison of one organic and one inorganic established electrochromic material.

For the organic option, we derived and proved an equation which allows the determination of the highest optical contrast possible for a specific wavelength based only on one measurement on an unknown thickness. Reporting from the paper:

$$\frac{\Delta R_{max}}{R_0}(\lambda) = \left[\frac{\alpha_{colored}}{\alpha_{bleached}}\right]^{1/\left(1-\frac{\alpha_{colored}}{\alpha_{bleached}}\right)} - \left[\frac{\alpha_{colored}}{\alpha_{bleached}}\right]^{\alpha_{colored}/\frac{\alpha_{bleached}}{\left(1-\frac{\alpha_{colored}}{\alpha_{bleached}}\right)}} \quad (6)$$

Where $R_0$ $(\lambda)$ is the reflectivity of the underlying surface, $\alpha_{colored}(\lambda)$ and $\alpha_{bleached}(\lambda)$ are the absorbing capacities (inverse length), of the layers in colored and bleached state respectively.

Moreover

$$\frac{\alpha_{colored}}{\alpha_{bleached}} = \frac{E_{colored}}{E_{bleached}} \quad (7)$$

where $E_{colored}(\lambda)$ and $E_{bleached}(\lambda)$ are the extinction values of the layers which can be measured easily via transmission measurements.

Equation (7) shows that the ratio of the extinction values is not dependent of thickness and that has been proven for ProDOT-$Me_2$ (see fig. 2A in paper I).

However, the equation does not hold for $WO_3$, since the model does not consider thin film interference (which becomes strong with the real part of the refractive index being around 2.2, see figure 2D in paper I). Full Fresnel simulations (transfer matrix) are necessary to determine the optimal thickness which gives the optimal contrast at the desired wavelength. For the simulations, literature values of the permittivity in colored and bleached state of $WO_3$ have been used [27]. These values can depend on the composition and fabrication process of the film, which means simulations were only a first guideline before actual fabrication of different thicknesses of the film in order to select the optimal one.

## Organic – Inorganic: comparison

As it can be seen in Fig 2B in paper I, ProDOT-$Me_2$ has the highest extinction ratio among the tested polymers (PPy, PEDOT, ProDOT-$Me_2$), and it has been then selected for the comparison with the inorganic option $WO_3$.

The first term of comparison is contrast. Figure 4A and 4B in paper I show the spectra in bleached and colored states for the organic and inorganic options, whose thicknesses give the biggest reflectivity changes. The optimal thickness was chosen differently for the two options. For the polymer, the contrast was checked during the polymerization process (using potential sweeps) and stopped when the highest value was reached. For the inorganic option, the simulations were the first step, then different thicknesses around the simulated one were fabricated and the best one chosen. The results show that, regardless of the parameter of comparison (absolute $\Delta R$ at whichever wavelength that happened on the 3 RGB metasurfaces) or a mean $\overline{\Delta R}$ calculated over the whole spectrum with the luminosity function as a weight (equation 5) the inorganic option gives the highest contrast ($\Delta R_{max} > 50\%$). However, despite the inorganic option performing better than the organic option, the latter one is easier to fabricate and its results easier to predict.

Another important parameter for electrochromic materials is the switching speed. Figure 5A and 5B in paper I show the intensity of the reflected light of the 3 RGB wavelengths for the organic and inorganic option vs time. It is evident that the organic option outperforms the inorganic one, switching in a time of the order of ms compared to a few seconds for the inorganic option, for a layer of 200 nm on a gold surface in both cases. From the switching speed it is also possible to calculate the energy per area required for the switch, by integrating the current in time (not shown in a figure). This resulted in values of 1-2 mJ/cm$^2$ for ProDOT-$Me_2$ and up to 40 mJ/cm$^2$ for $WO_3$. This difference, despite being not huge, would become important in a device which is required to switch frequently.

Connected to the switching speed is the bistability, which is the ability of the electrochromic film to retain the coloration after the voltage pulse. Figure 6A and 6B in paper I show the intensity of the reflected light for the RGB wavelengths versus time for the organic and inorganic option respectively. The inorganic option performs better than the organic one since the color is retained for a longer time and moreover the drift is not wavelength dependent.

## Paper II

In Paper II we present the fabrication and characterization of two designs for achieving high reflectivity dynamic structural coloration: one conventional and one reverse structure (Figure 1a in Paper II). Both structures take advantage of the change in refractive index of $WO_3$ [11, 12] which is placed between two metal films in a Fabry-Pérot cavity configuration. In the conventional structure a nanoholes array is fabricated in the top gold film while in the reverse design the array is fabricated in the Pt mirror.

Opposite to the previous work [4], where the nanoholes array on the top gold film would enhance the chromaticity of the structures (paper I), the nanoholes array in the Au film show weak red scattering, while in the Pt film no scattering at all, as it is shown in the dark field images in Figure S1, in SI of paper II). Thus, there is no contribution from it to the chromaticity of both these structures and the holes only serve for the $Li^+$ ions to reach the $WO_3$ layer. This was proven, as well, by fabricating a control sample without holes (Figure S2, SI of paper II), which showed similar reflectivity spectra as well as by changing the size of the holes (from 147 nm to 99 nm), as it can be seen in Figure S2, SI of paper II. However, simulations suggested that the plasmonic activity could take place in the near infrared for the conventional design (Figure S4, SI of paper II).

The two structures have no differences in terms of optical response and the same color range could be achieved (Figure 1b in paper II), with absolute reflectivity and spectra similar in both designs. This is shown in Figure 2a in paper II, where the reverse structures are measured directly through the glass support while the conventional structures are measured through a liquid having the same refractive index as the electrolyte used to switch the structure in the upcoming results. This was done to consider part of the reflectivity loss that would occur in a device implementing the conventional structure [34].

In Figure 2b in paper II are reported simulated (full Fresnel modeling, transfer matrix, using literature data for the permittivity of each layer [27, 35, 36]) and experimental CIE coordinates for several different thicknesses of the middle $WO_3$ layer. The simulations show a wide achievable gamut, moreover the experimental values lay eve outside the simulated gamut, suggesting that our deposited $WO_3$ films have a broader permittivity change than the literature one.

By applying a potential (± 1.5 V vs $Ag^+$) to the nanostructure, hence intercalating and de-intercalating $Li^+$ ions in the $WO_3$ film, their colors could be tuned, as shown in Figure 3a in paper II for different $WO_3$ thicknesses in reverse and conventional design. Once more, if we compare the spectra for conventional and reverse design fabricated with the same $WO_3$ thickness (samples III and IV, 110-120 nm), we notice similar reflection spectra, meaning that the optical performances, in terms of color gamut, are not affected by the order of the layers. Remarkably, the reflectivity of the cavities with $WO_3$ being in the absorbing state remain high (>50%). Figure 3b in paper II reports the xy coordinates for each intermediate state of the switch in a CIE diagram. Moreover, the Y value of the initial and final state (bright and dark state of $WO_3$) are reported. The reason why the Y value is chosen is that it accounts for brightness change according to the wavelength sensitive human vision. As a comparison, Y values for commercial papers are reported: perfect mirror (Y=100), A4 printed paper ($Y_{white}$= 84, $Y_{black}$=5) and a newspaper ($Y_{white}$= 63, $Y_{black}$=9).

It should be noticed that the reported spectra for reverse structure are what one would measure in a complete device (measuring through the glass support), while for the conventional design the reported spectra only account for a glass window and electrolyte. As mentioned above, in a complete device the absolute reflectivity would be lowered by additional layers. In fact, the reason why we introduced the reverse design is to maintain the as-fabricated high reflectivity in a future device, since all the components of the electrochemical cell needed to switch the reverse structures can be placed behind the platinum mirror. This means that the counter and reference electrode can be freely chosen and do not need to be transparent, which is required in the conventional design. In the latter one, the structure would be placed behind the electrolyte and the counter and reference electrodes would be place in front of it as well. This means that the absolute reflectivity would be lowered by, as an example, an ITO glass on which a counter electrochromic material is deposited, like NiO used in smart windows [34]. In Figure 4a in paper II, we show the reflectivity loss from the conventional structure in air to the conventional structure in electrolyte with an ITO window (solid line and dashed-dot line). Without considering the (necessary) ion storage layer deposited on the ITO window, the reflectivity loss is already from~80 to~50 (at the peak).

To show how a device based on these structures would perform, we combined two samples with different $WO_3$ thicknesses (80 nm and 100 nm, reverse structure) and simulated the color range and Y values that could achieve. In the simulations we combine the reflectivity spectra of the two subpixels (35% for the 80 nm sample and 55% for the 100 nm sample) together with the spectra of a half reflector (50% reflection over the whole visible spectrum) that accounts for the remaining 10%. This would mimic a situation where two subpixels are placed on a substrate, accounting for the loss due do the need of separating the subpixels from each other. The combinations are calculated selecting 3 points for each subpixel's switch, when $WO_3$ is bright, when it is dark and one intermediate point. The xy values of the combinations and then plotted in a CIE diagram (Figure 4c in paper II) together with the rgb xy values of a commercial colored ebook reader (PocketBook Color™). Figure 4d are shows the Y values of the combinations together with the Y values of the PocketBook reader. The mean value of the Y for all the combinations is~29, which is not reached even by the "white" color in the book reader, which means that our structures have a brightness higher than the latest commercially available device.

Finally, we report the values for two other important parameters: switching time and bistability. A full switch requires~1 min, which is slightly lower than we reported for a $WO_3$ film which was directly in contact with the electrolyte in paper I. However, in this case the start and end point are not the only states of interest since every intermediate point correspond to a desirable color. For this reason, it is important that once a state is selected, the color can be retained for a long time. This is measured as bistability, which can be seen in Figure S7, SI of paper II. Both the dark state of $WO_3$ and an intermediate state show great bistability (no change over at least ~1 min) once the voltage is switched off.

# Conclusions

The focus of this work was to fabricate and characterize three different plasmonic metasurfaces based on Fabry-Pérot cavities, for application in reflective displays. All the surfaces are based on the inorganic electrochromic material $WO_3$.

The first structure, presented in Paper I, was fabricated with a combination of Al mirror, $Al_2O_3$ spacer layer and top Au layer with a nanohole array. The thickness of the spacer layer was optimized to obtain the three primary RGB colors (61 nm, 110 nm, 95 nm). This combination resulted in high reflectivity and high chromaticity primary colors as well as structures stable in non-aqueous electrolytes. On top of the RGB metasurfaces, $WO_3$ was deposited to switch the colors on and off. The thickness of $WO_3$ was selected so that for all the colors, after ion insertion and hence electrochemical switch of $WO_3$, the maximum contrast was achieved. These structures with $WO_3$ on top were then compared with the same structures with an organic electrochromic material on top, PProDOT-$Me_2$. The organic option was also proven to follow an equation that allows to predict the highest contrast for a selected wavelength and that was used to optimize the thickness of the material for the RGB metasurfaces.

The last two structures, presented in Paper II, are also based on Fabry-Pérot cavity, but with $WO_3$ as spacer layer. In this case $WO_3$ was not used to switch the colors on and off, but to tune the cavity and the resulting color by taking advantage of the change in refractive index of $WO_3$. One of these structures, what we called conventional, follows the design of the previously presented but with $Al_2O_3$ replaced by $WO_3$. The second structure, referred to as reversed, was fabricated so that both the layer order and the position of the structure itself in the electrochemical setup was inverted. In this case there was not a nanoholes array in the gold film but in the bottom Pt mirror. In both cases the nanoholes served only for the ions to flow in and out of the $WO_3$ since they did not show any plasmonic effect in the visible part of the spectra. Both designs presented high reflection as fabricated and great bistability, a wide color range and most importantly they retained a high brightness even while the $WO_3$ layer was switched to its dark state. Moreover, the advantage of the second design over the first one lays in the fact that the whole electrochemical setup was placed behind the structure itself. This would eliminate the limitations on the choice of electrolyte and electrodes in a future device design.

# Acknowledgements

I would like to thank the Swedish Foundation for Strategic Research (SSF) for the financial support and the MyFab Chalmers where part of this work has been performed.

Then I would like to thank my supervisor Andreas Dahlin for the guidance and support. A special thanks to my colleagues in the “e-paper group” Jolie, Oliver and Kunli for all the discussions and great work as well as Gustav, Rebekah, Justas, Bita, Tim, Sophia, Asaad, Zeynep and Maria for creating such an inspiring and fun environment.

A special thanks to Oliver, partner in life and at work, for supporting me through all the stress and difficulties and for explaining things to me an infinite amount of times until I understand. Thanks also to our little feathered monsters, William and Loretta the screaming parrots, for never stop being loud and keeping the stress up as well as making our zoom calls more fun.

Lastly, but most importantly, thanks to my parents for all the sacrifices they have made and still make for me and my education.

# References


1. Fernández, M.; Casanova, E.; Alonso, I., Review of Display Technologies Focusing on Power Consumption. *Sustainability* **2015,** *7* (8), 10854-10875.

2. Chang, A.-M.; Aeschbach, D.; Duffy, J. F.; Czeisler, C. A., Evening use of light-emitting eReaders negatively affects sleep, circadian timing, and next-morning alertness. *Proceedings of the National Academy of Sciences* **2015,** *112* (4), 1232-1237.

3. Heikenfeld, J.; Drzaic, P.; Yeo, J.-S.; Koch, T., Review Paper: A critical review of the present and future prospects for electronic paper. *Journal of the Society for Information Display* **2011,** *19* (2), 129.

4. Gugole, M.; Olsson, O.; Xiong, K.; Blake, J. C.; Montero Amenedo, J.; Bayrak Pehlivan, I.; Niklasson, G. A.; Dahlin, A., High-Contrast Switching of Plasmonic Structural Colors: Inorganic versus Organic Electrochromism. *ACS Photonics* **2020**.

5. Sun, J.; Bhushan, B.; Tong, J., Structural coloration in nature. *RSC Advances* **2013,** *3* (35), 14862.

6. Kinoshita, S.; Yoshioka, S., Structural Colors in Nature: The Role of Regularity and Irregularity in the Structure. *ChemPhysChem* **2005,** *6* (8), 1442-1459.

7. Daqiqeh Rezaei, S.; Dong, Z.; You En Chan, J.; Trisno, J.; Ng, R. J. H.; Ruan, Q.; Qiu, C.-W.; Mortensen, N. A.; Yang, J. K. W., Nanophotonic Structural Colors. *ACS Photonics* **2020**.

8. Nishi, H.; Tatsuma, T., Full-Color Scattering Based on Plasmon and Mie Resonances of Gold Nanoparticles Modulated by Fabry–Pérot Interference for Coloring and Image Projection. *ACS Applied Nano Materials* **2019,** *2* (8), 5071-5078.

9. Xiong, K.; Tordera, D.; Jonsson, M. P.; Dahlin, A. B., Active control of plasmonic colors: emerging display technologies. *Reports on Progress in Physics* **2019,** *82* (2), 024501.

10. Kim, J.; Oh, H.; Seo, M.; Lee, M., Generation of Reflection Colors from Metal–Insulator–Metal Cavity Structure Enabled by Thickness-Dependent Refractive Indices of Metal Thin Film. *ACS Photonics* **2019,** *6* (9), 2342-2349.

11. Wang, Z.; Wang, X.; Cong, S.; Chen, J.; Sun, H.; Chen, Z.; Song, G.; Geng, F.; Chen, Q.; Zhao, Z., Towards full-colour tunability of inorganic electrochromic devices using ultracompact fabry-Pérot nanocavities. *Nature Communications* **2020,** *11* (1).

12. Hopmann, E.; Elezzabi, A. Y., Plasmochromic Nanocavity Dynamic Light Color Switching. *Nano Letters* **2020**.

13. Chen, D.; Wang, T.; Song, G.; Du, Y.; Lv, J.; Zhang, X.; Li, Y.; Zhang, L.; Hu, J.; Fu, Y.; Jordan, R., Dynamic Tunable Color Display Based on Metal–Insulator–Metal Resonator with Polymer Brush Insulator Layer as Signal Transducer. *ACS Applied Materials & Interfaces* **2019,** *11* (44), 41668-41675.

14. Xiong, K.; Tordera, D.; Emilsson, G.; Olsson, O.; Linderhed, U.; Jonsson, M. P.; Dahlin, A. B., Switchable plasmonic metasurfaces with high chromaticity containing only abundant metals. *Nano letters* **2017,** *17* (11), 7033-7039.

15. Kristensen, A.; Yang, J. K. W.; Bozhevolnyi, S. I.; Link, S.; Nordlander, P.; Halas, N. J.; Mortensen, N. A., Plasmonic colour generation. *Nature Reviews Materials* **2017,** *2* (1), 16088.

16. Xiong, K.; Emilsson, G.; Maziz, A.; Yang, X.; Shao, L.; Jager, E. W.; Dahlin, A. B., Plasmonic metasurfaces with conjugated polymers for flexible electronic paper in color. *Advanced Materials* **2016,** *28* (45), 9956-9960.

17. Kurokawa, Y.; Miyazaki, H. T., Metal-insulator-metal plasmon nanocavities: Analysis of optical properties. *Physical Review B* **2007,** *75* (3).

18. Dahlin, A. B.; Mapar, M.; Xiong, K.; Mazzotta, F.; Höök, F.; Sannomiya, T., Plasmonic Nanopores in Metal-Insulator-Metal Films. **2014,** *2* (6), 556-564.

19. Kerr, D. A., The CIE XYZ and xyY color spaces. *Colorimetry* **2010,** *1* (1), 1-16.

20. Faughnan, B. W.; Crandall, R. S.; Lampert, M. A., Model for the bleaching of WO3electrochromic films by an electric field. *Applied Physics Letters* **1975,** *27* (5), 275-277.

21. Hersh, H. N.; Kramer, W. E.; McGee, J. H., Mechanism of electrochromism in WO3. **1975,** *27* (12), 646.

22. Crandall, R. S.; Faughnan, B. W., Dynamics of coloration of amorphous electrochromic films of WO3 at low voltages. **1976,** *28* (2), 95.

23. Hashimoto, S.; Matsuoka, H., Mechanism of electrochromism for amorphous WO3thin films. *Journal of Applied Physics* **1991,** *69* (2), 933-937.

24. Lee, S.-H.; Cheong, H. M.; Tracy, C. E.; Mascarenhas, A.; Czanderna, A. W.; Deb, S. K., Electrochromic coloration efficiency of a-WO3−y thin films as a function of oxygen deficiency. *Applied Physics Letters* **1999,** *75* (11), 1541-1543.

25. Stolze, M.; Camin, B.; Galbert, F.; Reinholz, U.; Thomas, L. K., Nature of substoichiometry in reactively DC-sputtered tungsten oxide thin films and its effect on the maximum obtainable colouration by gases. **2002,** *409* (2), 254-264.

26. Bousquet, E.; Hamdi, H.; Aguado-Puente, P.; Salje, E. K. H.; Artacho, E.; Ghosez, P., First-principles characterization of single-electron polaron in WO3. *Physical Review Research* **2020,** *2* (1).

27. Triana, C. A.; Granqvist, C.-G.; Niklasson, G. A., Electrochromism and small-polaron hopping in oxygen deficient and lithium intercalated amorphous tungsten oxide films. *Journal of Applied Physics* **2015,** *118* (2), 024901.

28. Saenger, M. F.; Höing, T.; Robertson, B. W.; Billa, R. B.; Hofmann, T.; Schubert, E.; Schubert, M., Polaron and phonon properties in proton intercalated amorphous tungsten oxide thin films. **2008,** *78* (24).

29. Mahan, J. E. In *Physical Vapor Deposition of Thin Films*, 2000.

30. Thornton, J. A., Sputter Coating— Its Principles and Potential. *SAE Transactions* **1973,** *82*.

31. Lamont, L. T.; Turner, F. T., The role of dc self-bias potential in the control of rf sputtering. *Journal of Vacuum Science and Technology* **1974,** *11* (1), 47-51.

32. Rothen, A., The Ellipsometer, an Apparatus to Measure Thicknesses of Thin Surface Films. *Review of Scientific Instruments* **1945,** *16* (2), 26-30.

33. Ohring, M., The materials science of thin films. *Applied Optics* **1992,** *31* (34), 7162.

34. Green, S.; Backholm, J.; Georén, P.; Granqvist, C.-G.; Niklasson, G., Electrochromism in nickel oxide and tungsten oxide thin films: Ion intercalation from different electrolytes. *Solar Energy Materials and Solar Cells* **2009,** *93* (12), 2050-2055.

35. Rakić, A. D.; Djurišić, A. B.; Elazar, J. M.; Majewski, M. L., Optical properties of metallic films for vertical-cavity optoelectronic devices. *Applied Optics* **1998,** *37* (22), 5271.

36. Etchegoin, P. G.; Le Ru, E. C.; Meyer, M., An analytic model for the optical properties of gold. *The Journal of Chemical Physics* **2006,** *125* (16), 164705.

# Paper I

**High-contrast switching of plasmonic structural colors: inorganic versus organic electrochromism.**

Marika Gugole*, Oliver Olsson*, Kunli Xiong, Jolie C. Blake, José Montero Amenedo, Ilknur Bayrak Pehlivan, Gunnar A. Niklasson, and Andreas Dahlin

*ACS Photonics 2020 7 (7), 1762-1772*

*Contributed equally as first authors

ACS Photonics

pubs.acs.org/journal/apchd5

Article

# High-Contrast Switching of Plasmonic Structural Colors: Inorganic versus Organic Electrochromism

Marika Gugole,[‡] Oliver Olsson,[‡] Kunli Xiong, Jolie C. Blake, José Montero Amenedo, Ilknur Bayrak Pehlivan, Gunnar A. Niklasson, and Andreas Dahlin*

Cite This: *ACS Photonics* 2020, 7, 1762–1772

Read Online

ACCESS | Metrics & More | Article Recommendations | Supporting Information

**ABSTRACT:** Plasmonic structural colors have recently received a lot of attention. For many applications there is a need to actively tune the colors after preparing the nanostructures, preferably with as strong changes in the optical response as possible. However, to date, there is a lack of systematic investigations on how to enhance contrast in electrically induced color modulation. In this work we implement electrochromic films with plasmonic metasurfaces and compare systematically organic and inorganic materials, with the primary aim to maximize brightness and contrast in a reflective color display. We show nanostructures with good chromaticity and high polarization-insensitive reflectivity (~90%) that are electrochemically stable in a nonaqueous solvent. Methods are evaluated for reliable and uniform electropolymerization of the conductive polymer dimethylpropylenedioxythiophene ($PProDOTMe_2$) on gold. The resulting organic films are well-described by Lambert–Beer formalism, and the highest achievable contrast is easily determined in transmission mode. The optical properties of the inorganic option ($WO_3$) require full Fresnel models due to thin film interference, and the film thickness must be carefully selected in order to maintain the chromaticity of the metasurfaces. Still, the optimized fully inorganic device reaches the highest contrast of approximately 60% reflectivity change for all primary colors. The switching time is about an order of magnitude faster for the organic films (hundreds of ms). The bistability is very long (hours) for the inorganic devices and comparable for the polymers, which makes the power consumption essentially zero for maintaining the same state. Finally, we show that switching of the primary colors in optimized devices (both organic and inorganic) provides almost twice as high brightness and contrast compared to existing reflective display technologies with RGB subpixels created by color filters.

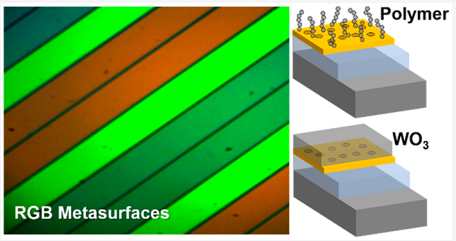


**KEYWORDS:** *metasurfaces, structural colors, electrochromism, reflective display, electronic paper*



Plasmonic nanostructures have found a broad range of applications, as they offer control of electromagnetic fields on the nanoscale. One application with strong recent interest is structural colors arising from resonances that occur in the visible.[1] Utilized since ancient times,[2] such colors have advantages such as high stability compared to organic dyes and the possibility to "print" with very high resolution compared to ink.[1] Also, due to the strong interaction with light, ultrathin (<1 $\mu$m) nanostructures or "metasurfaces" are sufficient to generate vibrant colors.[3] Recently, there has also been an increased interest in active plasmonic devices, where the optical properties can be changed on demand.[4−8] In particular, tuning of structural colors in this manner is highly interesting for new types of displays.[9,10] Modulation of transmitted or reflected light can be achieved in many ways.[9] For instance, liquid crystals can be implemented, even for addressing individual pixels.[11] Another approach is to create hybrid materials containing the plasmonic metal and conductive polymers, which makes it possible to perform redox switching in electrochemical cells.[5,12−15] Alternatively, inorganic electrochromic materials have been considered for display applications since the pioneering work of Deb.[16] Transition metal oxides, in particular, $WO_3$,[17] have been frequently studied due to their application in electrochromic windows.[18] Just during the last year, there has been a strong interest in implementing inorganic materials for new types of electrochromic devices.[4,6,7] Both organic and inorganic electrochromic materials are convenient to implement on plasmonic nanostructures, as they often have continuous metals that act as supporting electrodes. It may also be possible to electrochemically synthesize the electrochromic layer directly on the nanostructure.[5,13]

However, to date, there has been relatively little work on how to optimize the optical contrast in active plasmonic devices that transmit, reflect or scatter light. This is of obvious importance for tuning structural colors.[10] For plasmonic devices, early work was to a high extent focused on electrical

**Received:** March 11, 2020
**Published:** May 28, 2020

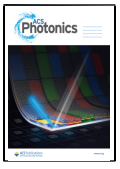







https://dx.doi.org/10.1021/acsphotonics.0c00394
*ACS Photonics* 2020, 7, 1762–1772

tuning of resonance shifts rather than intensity modulation.[14,15] In the field of electrochromic polymers (or their inorganic counterparts) high optical contrast, defined as difference in reflectivity or transmittance ($\Delta R$ or $\Delta T$), has long been the central benchmark because the spectra typically do not show any strong resonance features.[19−22] For plasmonic colors, high contrast is necessary if the nanostructures should be useful in reflective (or possibly "transflective") displays that rely on ambient light. Such "electronic paper" technologies are normally operating in black and white (electrophoretic displays or LCDs) due to the low reflectivity and contrast in color mode.[10] For instance, liquid crystals require polarizers that naturally only transmit 50% of the incident light. An additional intensity loss comes from the fact that, for color generation, subpixels are normally created by colored glass filters, which means that only a fraction of the area will display the set color.[23] An alternative subpixel design is found in the electrowetting display based on colored liquids,[24] but to date this technology has not made it to the market. In order to make electronic paper in color with good visual appearance, RGB subpixels must have both high absolute reflectivity and high switching contrast. Naturally, high intensity changes are also important for many other active plasmonic devices, such as tunable filters and so on.[12,13] Looking at existing literature, it remains unexplored in what ways inorganic materials can provide better performance than conjugated polymers. At the same time, there is currently a strong interest in combining inorganic electrochromism with plasmonics, but so far it has been used for tuning cavity resonances[4,7] or regulation of photothermal effects.[25]

In this work we present plasmonic metasurfaces that fulfill the main criteria for subpixels in a reflective color display: good chromaticity, high reflectivity, and, in particular, high-contrast switching. By selecting the right metals, we show that electrochromic switching is possible in nonaqueous electrolytes, which makes it possible to prepare highly stable and fully inorganic devices. Simple transmission measurements are shown to be sufficient for evaluating the maximum possible contrast of organic electrochromic films, while more advanced Fresnel models are used for the inorganic films. We show a systematic comparison of the highest achievable contrast in structural color switching using established organic and inorganic electrochromic materials. Under optimal conditions, our electrochromic metasurfaces provide sufficient brightness and contrast to clearly outperform existing reflective color display technologies that rely on glass filters to generate subpixels. In addition to contrast, we look at other parameters such as switching speed and power consumption. Although this study focuses on reflective color displays, our results should also be of general interest for other active plasmonic devices.

## THEORY

We first overview the theory for evaluating switching contrast before applying it in experiments. Consider a thin absorbing film of thickness $d$. If interference effects can be ignored, the transmitted light intensity $I$ (incident intensity $I_0$) through the film follows the Lambert−Beer law:[26]

$$E(\lambda) = \log\left(\frac{I_0(\lambda)}{I(\lambda)}\right) = \log\left(\frac{1}{T(\lambda)}\right) = \alpha(\lambda)d \tag{1}$$

Here, $E$ is the extinction, $T$ is the transmittance, and $\alpha$ is the absorbing capacity of the layer (inverse length, i.e., number density multiplied by cross-section). In reflection mode, the incident light passes through the film twice and the derivation is analogous. Upon switching, $\alpha$ changes between two values representing the colored and bleached states. The change in reflectivity is[19]

$$\Delta R = [\exp(-2\alpha_{ble}d) - \exp(-2\alpha_{col}d)]R_0 \tag{2}$$

Here $R_0(\lambda)$ is the reflectivity of the underlying surface.[27] The thickness that gives highest contrast can be calculated by deriving eq 2:[19]

$$d_{opt} = \frac{\log\left(\frac{\alpha_{col}}{\alpha_{ble}}\right)}{2[\alpha_{col} - \alpha_{ble}]} \tag{3}$$

Now we insert $d_{opt}$ into eq 2 to get the highest contrast:

$$\frac{\Delta R_{max}}{R_0} = \frac{\{\Delta R\}_{d=d_{opt}}}{R_0} = \exp\left(-\alpha_{ble} \times \frac{\log\left(\frac{\alpha_{col}}{\alpha_{ble}}\right)}{[\alpha_{col} - \alpha_{ble}]}\right) - \exp\left(-\alpha_{col} \times \frac{\log\left(\frac{\alpha_{col}}{\alpha_{ble}}\right)}{[\alpha_{col} - \alpha_{ble}]}\right) = \left[\frac{\alpha_{col}}{\alpha_{ble}}\right]^{1/(1-\alpha_{col}/\alpha_{ble})} - \left[\frac{\alpha_{col}}{\alpha_{ble}}\right]^{\alpha_{col}/\alpha_{ble}/(1-\alpha_{col}/\alpha_{ble})} \tag{4}$$

Remarkably, this shows that the highest achievable contrast $\Delta R_{max}$, in absolute numbers, depends only on the ratio $\alpha_{col}/\alpha_{ble}$ (and $R_0$). Previous studies have arrived at similar conclusions,[20,22] but, as far as we are aware, eq 4 has not been presented. We emphasize that it does not contain the film thickness. There is a certain thickness that gives the highest contrast (eq 3), but there is no need to know the thickness of the analyzed film in order to obtain the ratio $\alpha_{col}/\alpha_{ble}$ and, hence, the highest possible contrast. The critical ratio can be measured very easily because, by definition (eq 1), it is equal to the extinction ratio:

$$\frac{\alpha_{col}}{\alpha_{ble}} = \frac{E_{col}}{E_{ble}} \tag{5}$$

Hence, the highest contrast can be determined directly by the ratio of extinction values for the colored and bleached states using transmission mode measurements, as long as the background extinction is properly subtracted. Note that the thickness may change between colored and bleached states for organic films,[28] but this only introduces a dimensionless "swelling factor" into the $\alpha$ values, and the end result is the same. Note also that the highest contrast in transmission mode is identical ($\Delta T_{max} = \Delta R_{max}$) according to this model, but it occurs for a twice as thick film.

To get an accurate opaque/transparent type of contrast value across the visible, which accounts for the variation of eye receptor sensitivity with wavelength, the luminosity function can be used as weight:

$$\overline{\Delta R} = \frac{\int_{380nm}^{780nm} L(\lambda)\Delta R(\lambda)\mathrm{d}\lambda}{\int_{380nm}^{780nm} L(\lambda)\mathrm{d}\lambda} \tag{6}$$

Like in our initial work,[3] we use the $L(\lambda)$ function representing photoptic vision (good illumination conditions) since this is the likely scenario for display of structural colors.


https://dx.doi.org/10.1021/acsphotonics.0c00394
ACS Photonics 2020, 7, 1762−1772

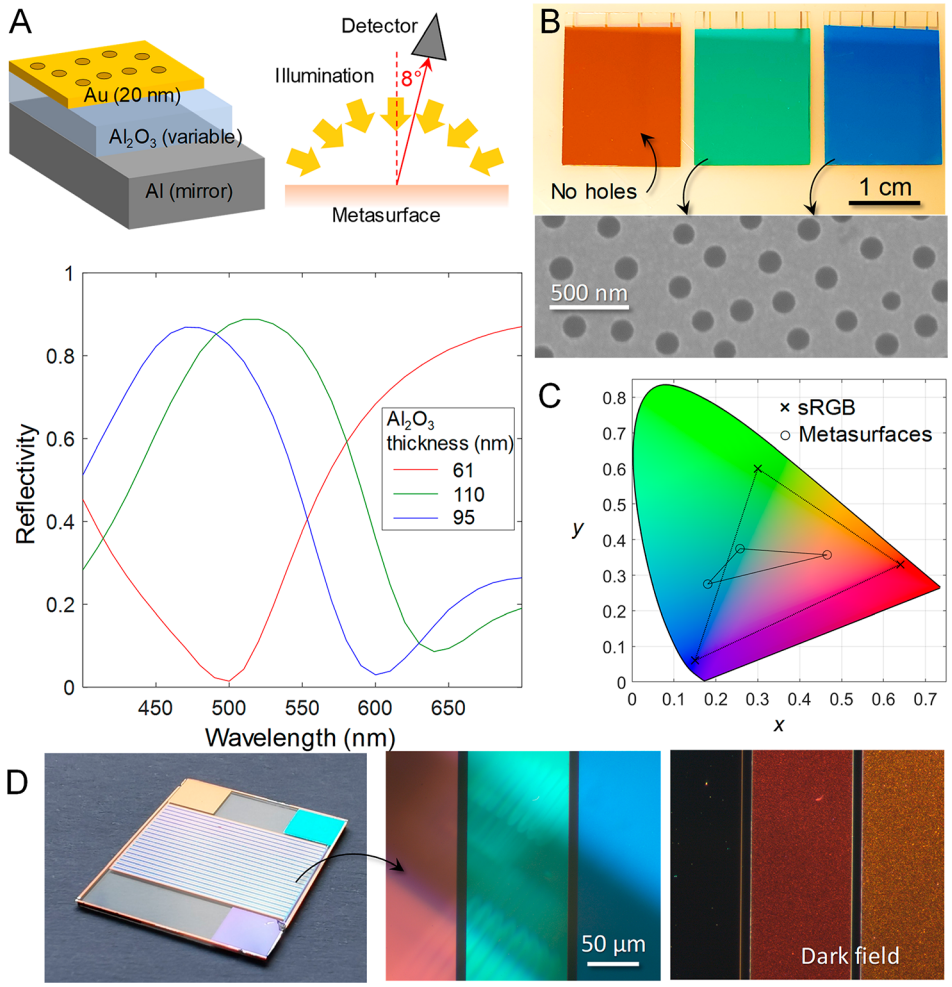


**Figure 1.** Metasurfaces based on an Al mirror, variable $Al_2O_3$ thickness, and a semitransparent Au with nanoholes. (A) Reflectivity in air under diffuse illumination (simulating ambient light) and collection angle of 8°. The values for alumina thickness represent the optimal primary colors. (B) Photo of metasurfaces. The electron microscopy image shows the nanoholes (not present on red samples). (C) CIE chromaticity coordinates compared to the standard RGB gamut. (D) A "white" surface made by RGB stripes. The microscopy images show the colors in bright or dark field illumination (same position).

To account for thin film interference, more advanced Fresnel models (transfer matrix method) can be used.[29] This requires accurate determination of the complex and wavelength-dependent permittivity of the electrochromic material in different oxidation states, which is fairly complicated.[30] The method based on the extinction ratio has the advantage that it only requires simple transmission mode spectra. These theoretical descriptions serve as guidelines when optimizing contrast (as shown below). In order to account for the plasmonic field enhancement, numerical simulations are preferable since the near-field distribution is multidimensional in nanostructures.[3]

## RESULTS AND DISCUSSION

Structural color generation was achieved by a combination of Fabry–Pérot modes (cavity resonances) and plasmonic effects using a triple layer consisting of a metal mirror, an insulator with varied thickness, and a thin top metal film with nanoholes.[3,27] The structures were prepared easily over large areas by colloidal lithography. Several different metals were tested, but not all were sufficiently stable in electrochemical cells, even with protective coatings.[27] In particular, the electrolyte imposes limitations as metals can dissolve in some solvents or react with certain ions.[31] We found that a combination of an aluminum base mirror and gold as the top thin film provided structures with good color quality and stability over a broad voltage range. For instance, it was possible to use nonvolatile and inert electrolytes such as propylene carbonate with $LiClO_4$.[17] Nonaqueous electrolytes are advantageous for device stability since unwanted Faradaic processes such as hydrolysis and gas formation can be avoided. It was also possible to directly dissolve the monomers for electropolymerization, which would require surfactants in aqueous environments.[3]

In order to evaluate the metasurface colors under ambient light, the reflectivity was measured with diffuse illumination using an integrating sphere (Figure 1A). This is a standard colorimetry test (ISO 17025, used, for instance, in the textile industry) that provides an accurate representation of ambient illumination in most scenarios. Thus, we consider the results in Figure 1 to be an accurate representation of the colors, even though fixed angle (specular) reflection could lead to better chromaticity. The optimal primary colors (R, G, B) were achieved with 61, 110, and 95 nm of $Al_2O_3$ spacer thickness. Photos and an electron microscopy image of RGB metasurfaces are shown in Figure 1B. Note that there was


https://dx.doi.org/10.1021/acsphotonics.0c00394
ACS Photonics 2020, 7, 1762–1772

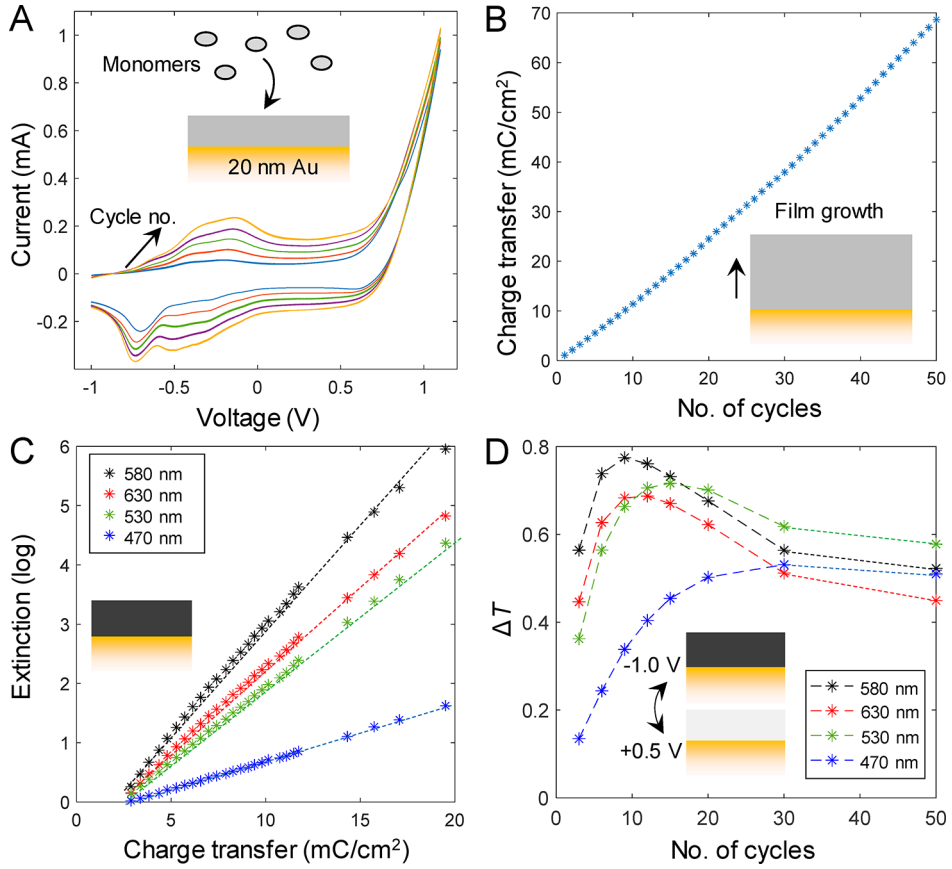


**Figure 2.** Electropolymerization and optical characterization of $PProDOTMe_2$ on Au. (A) Current during the first 5 CV scans for electropolymerization, represented by the current increase at +0.8 V. The scan rate was 200 mV/s and the electrode area was 1.0 $cm^2$. (B) Integrated current from all cycles vs cycle number. (C) Extinction in dark state vs integrated current with linear fits. (D) Contrast as $\Delta T$ for different thicknesses (cycle numbers) of the $PProDOTMe_2$ film, identifying the optimal thicknesses for different wavelengths representing RGB and also the wavelength of maximal contrast (580 nm). The contribution from the extinction of the thin Au film has been removed.

no nanoholes on the red samples (and thus no scattering) because they did not improve the color quality. This is because the plasmonic activity occurs in the red region, which was further confirmed by dispersion relation calculations (Figure S1). The chromaticity coordinates in the 1931 CIE 2D diagram are shown in Figure 1C, together with the standard RGB gamut. The metasurfaces have a reasonable gamut, similar to other plasmonic structures,[1] and it is well-oriented around the D65 white point (0.31, 0.33). Figure 1D shows an example of micropatterned metasurfaces (RGB stripes). The complementary colors seen under dark-field illumination represent the coloration contribution by resonant excitation of surface plasmons.[3,27] In summary, these metasurfaces have similar reflectivity and chromaticity as in previous work, but with the benefit of stability in nonaqueous electrolytes.

It is important to note that structural colors that rely on ambient light never provide both excellent chromaticity and reflectivity: If a surface would reflect a very narrow resonant wavelength band (~10 nm), the color quality would improve, but the visibility would be extremely poor because only a small fraction of the illumination light is reflected.[10] Therefore, a compromise between chromaticity and brightness is always necessary. In an emissive display (e.g., LED), the situation is different because the narrow emission bands can become clearly visible by increasing intensity (and power consumption). The metasurfaces offer a good balance between chromaticity and reflectivity with their line widths of ~100 nm, representing a third of the visible region for each primary color.

In order to switch the colors on and off in an optimal manner, we evaluated several conductive polymers prepared by electropolymerization, as well as tungsten oxide ($WO_3$) films prepared by reactive sputtering.[32] Starting with the polymers, we have previously tested polypyrrole[3] (PPy) and poly(3,4-ethylenedioxythiophene)[27] (PEDOT), but literature suggests that dimethylpropylene-dioxythiophene ($PProDOTMe_2$) gives better contrast, based on transmission mode measurements on transparent conductors.[21] However, there appears to be a lack of reports on electropolymerization of $PProDOTMe_2$ on thin gold films prepared by standard vacuum deposition. Such gold layers are frequently used in plasmonics for their long-term stability (especially in electrochemistry) and provide good structural colors (e.g., Figure 1). The work by the group of Reynolds has used porous gold structures in special cell configurations[33,34] or gold films formed by electroless precipitation.[35] For plasmonic structures, the polymer has only been implemented on aluminum.[12] Using previous results as a starting point, we evaluated different recipes for electropolymerization of $PProDOTMe_2$ on thin planar gold layers and found that the most homogeneous and reproducible films were achieved by voltage sweeps performed repeatedly. For comparison, maintaining a constant potential or current resulted in films that were not uniform and the process had poor reproducibility (Figure S2). Figure 2A shows cyclic


https://dx.doi.org/10.1021/acsphotonics.0c00394
ACS Photonics 2020, 7, 1762−1772

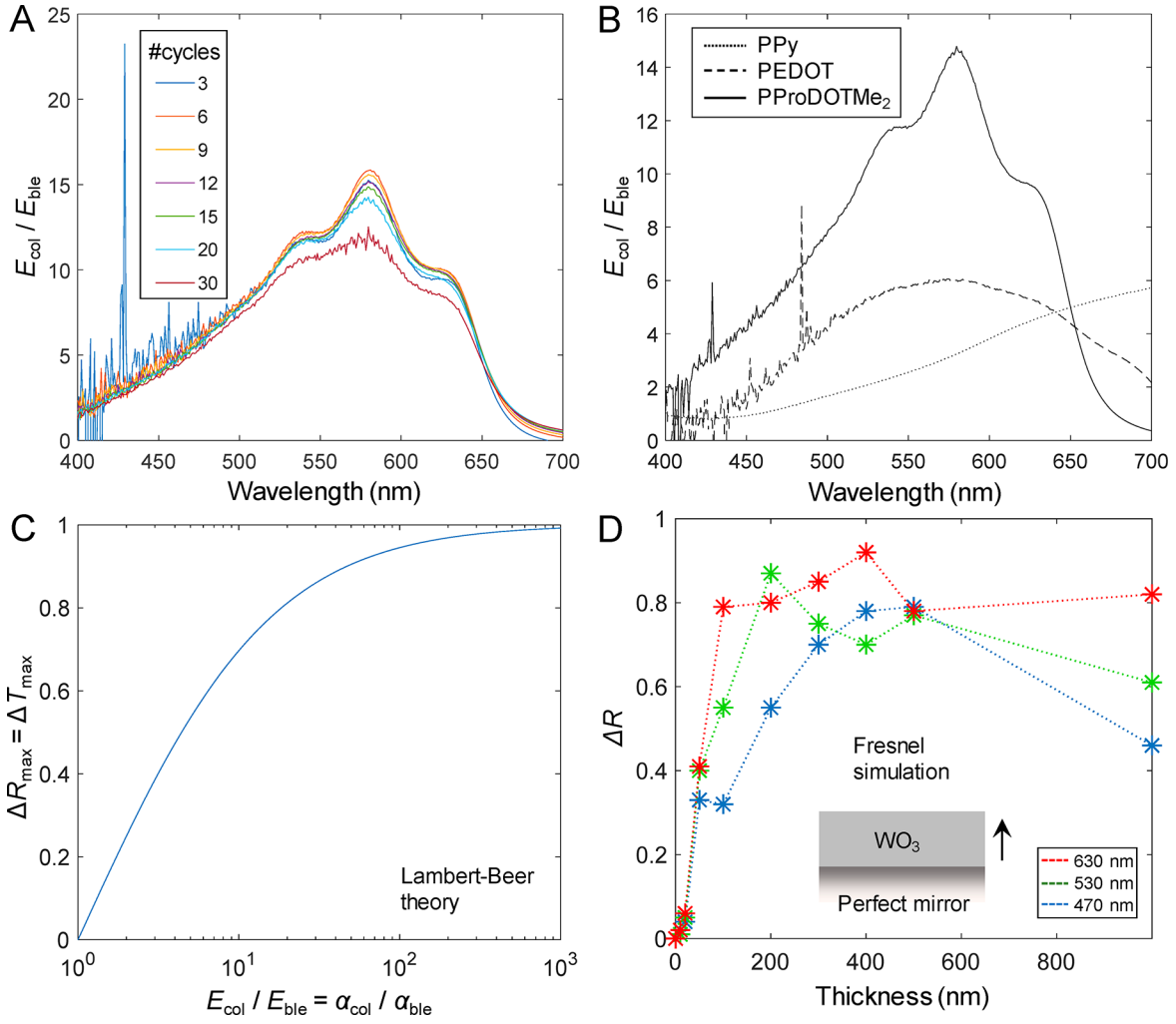


**Figure 3.** (A) Extinction ratio for different polymer thickness. The contribution from the Au support and the liquid cell was subtracted from the extinction values. (B) Extinction ratio for different electrochromic polymers. (C) Theoretical maximum contrast for a perfect mirror ($R_0$ = 1) as a function of extinction ratio (essentially a plot of eq 4). (D) Results of Fresnel models to determine contrast of $WO_3$ films of different thickness in reflection mode (normal incidence) for a perfect mirror support.

voltammetry results of the electropolymerization, which starts at about +0.8 V (vs $Ag/Ag^+$). The voltage range was from −1.0 to +1.1 V in order to ensure the formed polymer stayed to the surface. In subsequent cycles the oxidation and reduction peaks of the polymer film start to become visible. The scan rate was set as a compromise between precision and uniformity: faster sweeps give less polymer deposition per cycle and better precision in film growth, but less uniform coatings were observed. At 200 mV/s, the films were homogeneous over the whole area of 1 $cm^2$ by visual inspection. The integrated current (charge) from all voltage sweeps scaled almost linearly with cycle number (Figure 2B), showing that the same amount of polymer is added in each step. However, there was some variation in the charge transfer per cycle in different experiments, which means that it is important to record the current to know the end thickness. We also noted that intense light, such as the beam used to measure the spectrum, could influence the polymerization process. (Hence the light was off during polymerization.) The charge transfer was approximately linear with the dry thickness according to profilometer measurements, and 1 $mC/cm^2$ corresponded to a dry thickness of ∼10 nm (Figure S3). Assuming a density of ∼1 $g/cm^3$, the electron transfer per monomer grown is 1.9 (monomer weight 184 g/mol), which is close to the expected number of two electrons per bond formed.

We also measured the extinction of the $PProDOTMe_2$ films in the dark state (−1 V) as a function of charge transfer, showing a perfectly linear relation (Figure 2C), which verifies that the Lambert−Beer law (eq 1) is applicable. At voltages below −1 V or above approximately +0.5 V the change in transmission was negligible (<1%) for the polymer films. Upon switching the polymer (1 M $LiClO_4$ in PC) between transparent and absorbing (Figure 2D), the contrast was found to depend on film thickness, and an optimum for transmission mode could be identified, in agreement with eq 3. Note that the specific thickness that gives optimal contrast, is wavelength-dependent and does not necessarily give the highest optical contrast on a nanostructured surface that has plasmonic activity, because then the plasmons are also switched on and off.[3] However, it serves as a good first approximation to assume that the thickness which gives $\Delta R_{max}$ should be about half the value identified for transmission mode. The maximum contrast of 77% at 580 nm is in excellent agreement with previous reports for $PProDOTMe_2$ prepared on transparent conductors,[21] which shows that our electropolymerization procedure for gold works satisfactory.


https://dx.doi.org/10.1021/acsphotonics.0c00394
ACS Photonics 2020, 7, 1762−1772

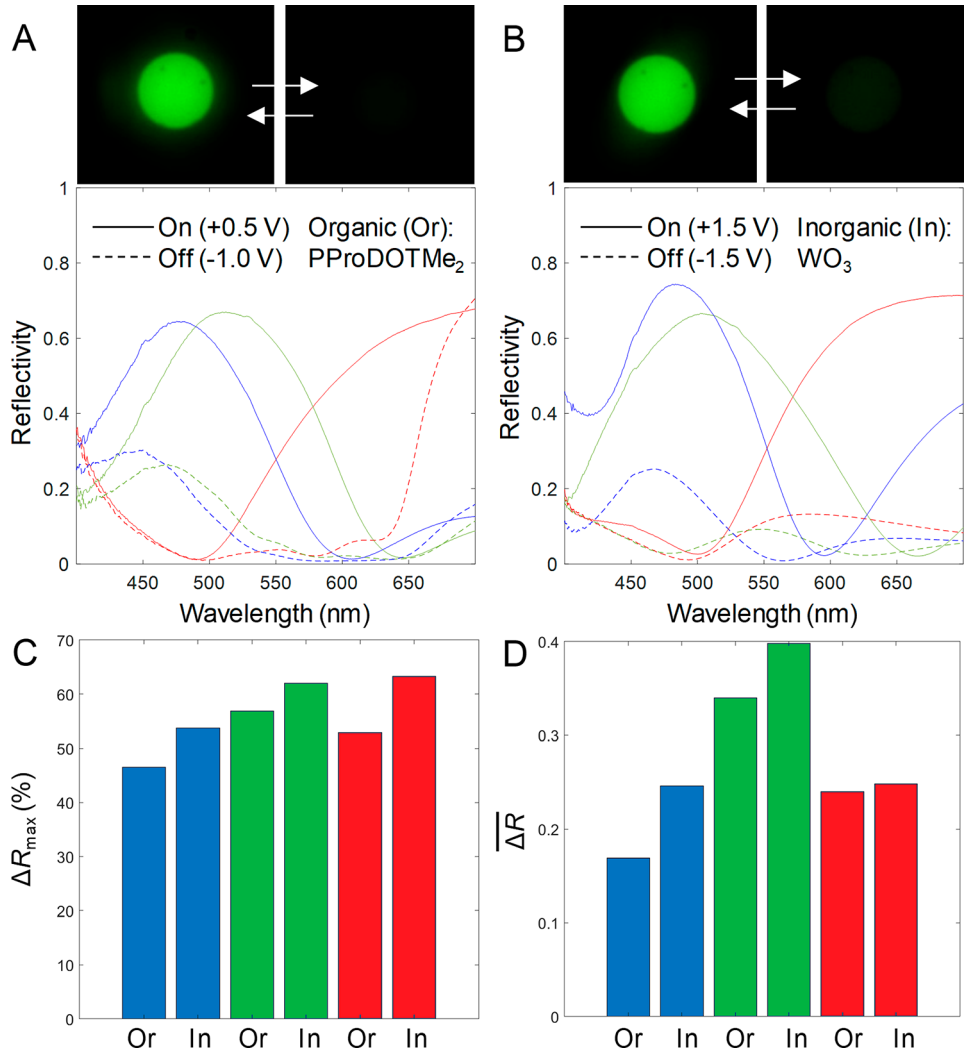


**Figure 4.** Optimized contrast for switching of metasurfaces with primary colors. (A) Reflectivity spectra in bright and dark states for metasurfaces with $PProDOTMe_2$ (organic, Or). The pictures show camera images of a ∼50 $\mu$m spot on a green sample illuminated by white light in "On" or "Off" states (same camera settings). (B) Same as (A) but for metasurfaces with $WO_3$ (inorganic, In). (C) Contrast comparison for each electrochromic metasurface in terms of highest change in absolute reflectivity (at whichever wavelength gives $\Delta R_{max}$). (D) Similar contrast comparison for each metasurface with the luminosity function as weight (eq 6).

To evaluate the contrast, we plotted the extinction ratio for the on and off states for different polymer thickness, which should remain constant according to eq 5. In order to acquire only the film properties, we subtracted the background extinction (mainly reflection) from the thin gold film and the flow cell. Indeed, the extinction ratio showed little variation (Figure 3A) and no trend of increasing or decreasing with thickness. To compare the different polymers, we plotted their averaged extinction ratios together (Figure 3B). From this comparison it is clear that, as suspected,[21] $PProDOTMe_2$ provides the highest extinction ratio over almost the whole visible. (However, the other polymers were much easier to synthesize as they were insensitive to how the voltage was applied during electropolymerization.) Figure 3C shows a semilog plot based on eq 4 to visualize how high extinction ratios that need to be achieved to generate a certain contrast in theory. One well-established conductive polymer not included in this comparison is polyaniline,[5,12,15] but it is generally not considered as a candidate for black/transparent switching.

Importantly, the switching properties of the inorganic $WO_3$ films (characterization in Figure S4) could not be evaluated in the same manner due to thin film interference as the real part of the refractive index was around 2.2 (Figure S5). This differs from the organic films, which have a refractive index ($n \approx 1.5$ for polymers) similar to that of the electrolyte ($n = 1.42$ for PC), which effectively removes one optical boundary. Full Fresnel models had to be used to evaluate the contrast, using literature values of the permittivity of $WO_3$ in bright and dark states[30] (keeping in mind that the exact values may depend on how the $WO_3$ is prepared). Figure 3D shows an example of calculated contrast in reflection mode by simulating a $WO_3$ film with variable thickness on a perfect mirror support for red, green, and blue (470, 530, and 630 nm, respectively). The simulated metal oxide film did not give the same smooth curves with a single maximum at a certain thickness, as observed for the experimental polymer characterization ($\Delta T$ in Figure 2D). Still, $\Delta R$ can clearly reach values considerably higher (>80%) than for all the polymers given that the thin film interference acts in favor of a large contrast at the wavelength of interest. Therefore, the $WO_3$ films may outperform $PProDOTMe_2$, although implementation on the metasurfaces requires more careful optimization.


https://dx.doi.org/10.1021/acsphotonics.0c00394
ACS Photonics 2020, 7, 1762−1772

Next, we present the highest reflectivity changes we could achieve for our metasurfaces with organic (Figure 4A) or inorganic (Figure 4B) electrochromism. When implementing $PProDOTMe_2$ on the metasurfaces, we electropolymerized a film close to the optimal value determined for each color (Figure 2D) and then continued to polymerize in steps (voltage sweeps) while monitoring the contrast when switching. Due to contribution from the resonant reflectivity of the metasurfaces, the ideal values of thickness (6 cycles for red, 9 for green and 15 for blue) were not identical but quite similar to those identified in transmission mode (Figure 2D) divided by two. The $WO_3$ thickness that gives optimal contrast on a given metasurface was instead selected based on Fresnel models excluding the nanoholes (Figures S6 and S7). Although such calculations do not include the plasmonic contribution to the coloration for blue and green samples, they enabled us to predict which thickness of $WO_3$ would make the thin film interference effects of all layers (four in total) favorable. This gave a $WO_3$ thickness of 130, 180, and 130 nm for R, G, and B, respectively. Thus, for both the organic and the inorganic samples, it is possible to avoid a pure trial and error approach when implementing electrochromism: The polymers should be precharacterized in the transmission mode and for the metal oxides the complex permittivity in both coloration states is needed. The end results show that the inorganic devices give the highest contrast for all colors. It did not matter if the contrast was evaluated as the highest $\Delta R$ at any wavelength (Figure 4C) or the $\Delta R$ weighted by the luminosity function (Figure 4D). Furthermore, the contrast of the inorganic film is indeed very high for all colors ($\Delta R \approx 50\%$), and so is the absolute reflectivity in the bright state (up to ~70%). Still, the organic films are not far off in performance ($\Delta R \approx 50\%$, reflectivity > 60%), and they are much easier to prepare, that is, electropolymerization as compared to reactive sputtering (with vacuum chamber and plasma). For comparison, in previous work with other materials and aqueous electrolytes,[3,27] the contrast was considerably lower, especially in the blue region (~25%).

Another important parameter for electrochromic devices is the switching speed. We performed a comparison between $PProDOTMe_2$ (Figure 5A) and $WO_3$ (Figure 5B) when switching by potential steps. The intensity of transmitted light at different wavelengths is monitored with high temporal resolution down to a few ms.[31] Here we simply picked a film thickness (200 nm) for polymer and metal oxide in the range where the highest contrasts were achieved. (A more detailed analysis of switching speed for different thickness and in different electrochemical cells is the subject of future work.) Figure 5A shows that the organic film is switching reasonably fast (<1 s) in both directions, and the speed is approximately the same for all wavelengths in the visible. The switch speed was not faster for PEDOT or PPy (not shown). The inorganic $WO_3$ is switching much slower (~10 s) from the bleached to the colored state, which can be attributed to the slow transport of $Li^+$ ions through the film.[36] Electron microscopy imaging indicated that the polymer films are much more permeable to an electrolyte (Figure S8). The reverse switch (removal of the intercalated $Li^+$) occurs at a speed comparable to that of the organic film, as expected.[25] As Supporting Information, we provide five different videos showing real-time switching of metasurfaces. (Detailed descriptions of the videos are also in the Supporting Information.) It should be kept in mind that the illumination is white and constant in all these videos.

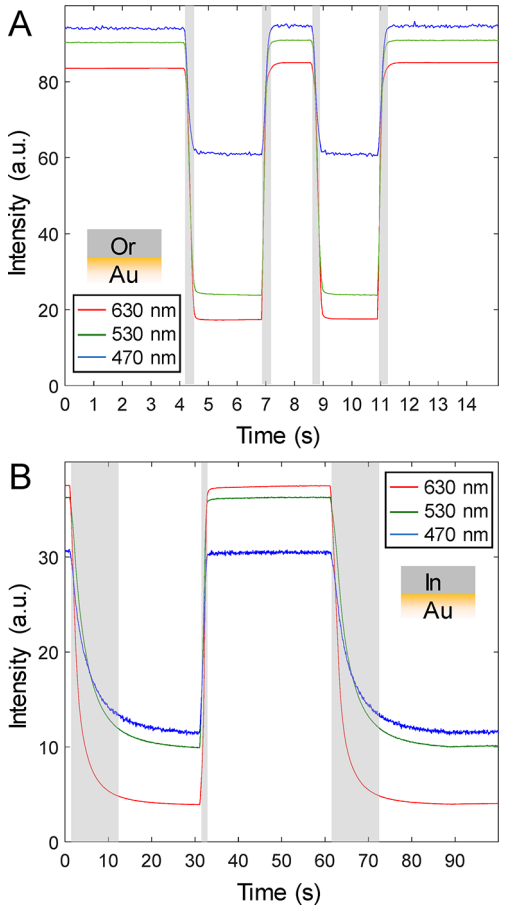


**Figure 5.** Comparing switching speed by intensity time traces at different wavelengths (square wave voltammetry). (A) Example of time trace when switching $PProDOTMe_2$ (Or) on gold in 1 M $LiClO_4$ in PC. The time it takes to reach 90% of the full intensity change is ~600 ms for dark to bright and ~800 ms for bright to dark. All wavelengths give approximately the same switching speed (±100 ms). (B) Example of $WO_3$ (In) switching in the same electrolyte. The time for reaching 90% of the total switch is marked in gray. The thickness of the $PProDOTMe_2$ and the $WO_3$ were both ~200 nm.

The main motivation for electronic paper technologies is power savings by many orders of magnitude as compared to emissive displays,[37] especially under bright conditions where emissive displays must increase their brightness to overcome ambient light. Unless the device is intended to switch very frequently, the most important parameter to evaluate the power consumption is bistability, that is, the time that a coloration state can be maintained at open circuit voltage. With full bistability, the power consumption is zero for a static state in a display device. We investigated how the intensity changed over time after disconnecting the voltage in the dark state for $PProDOTMe_2$ (Figure 6A) and $WO_3$ (Figure 6B). The intensity drifts back very slowly in both cases, although $WO_3$ shows slightly better performance. For the polymer, some wavelength dependence can be seen, while the inorganic film shows negligible changes for all colors over at least an hour. In the bright state, the bistability was essentially perfect for both devices since this is close to the equilibrium state (no intercalation in $WO_3$, anions in $PProDOTMe_2$). As an alternative measure of power consumption, the energy per area for one switch can be used.[3] This gave values of 1−2 mJ/cm$^2$ for $PProDOTMe_2$, and up to 40 mJ/cm$^2$ for $WO_3$, that is,


https://dx.doi.org/10.1021/acsphotonics.0c00394
ACS Photonics 2020, 7, 1762−1772

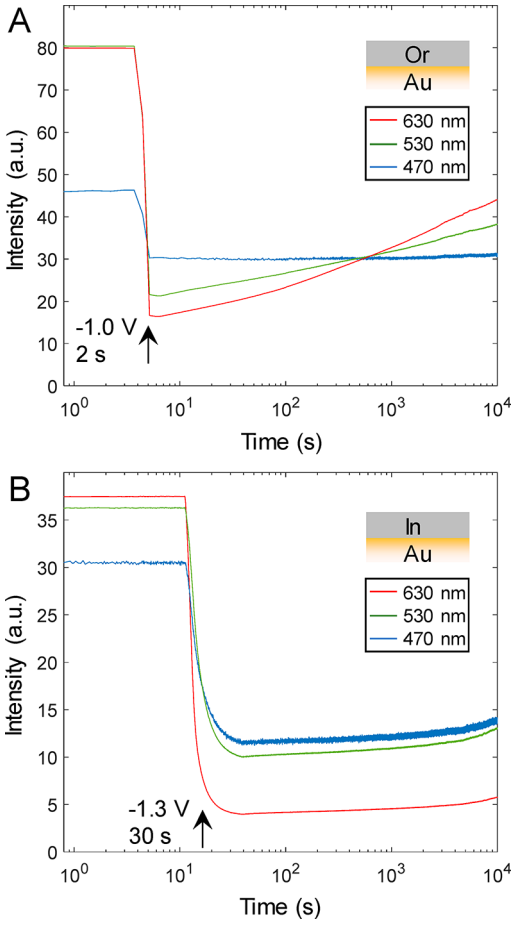


**Figure 6.** Bistability tests of organic (Or, A) and inorganic (In, B) electrochromic films on Au surfaces. The voltage is switched off after establishing the dark state by a negative pulse and the intensity is monitored over hours (note the logarithmic *x*-axes).

a noticeable difference that becomes important if the devices should be switched frequently.

Finally, we will show that with optimal electrochromic contrast, our metasurfaces can provide much better performance as RGB pixels in a reflective color display than existing technologies. In order to provide colors, electrophoretic displays and LCDs introduce color filters to generate RGB subpixels (Figure 7A). Such displays do exist, but they are generally not found on the market, which arguably is due to their poor image quality in terms of brightness and contrast.[10] For instance, E-ink markets the Triton, yet such e-reader devices are not found among suppliers (at the time of writing).[10] The metasurfaces are already red, green, or blue, as prepared, and their reflectivity is high as well as independent of polarization. In an LCD, 50% of the incident light is lost directly due to the polarizers, so we consider electrophoretic displays to be the most competitive option. (Yet, it should be noted that LCDs have other advantages, such as video speed.) We measured the reflectivity from a (black and white) Amazon Kindle device in the bright and dark states (Figure 7B), using the same instrument as for the metasurfaces. We then assumed that the color filters on RGB pixels would transmit 90% of each primary color (a typical value for band-pass filters). Hence, the reflectivity from a subpixel of any color in the electrophoretic display is given by the spectra in Figure 7B multiplied by 0.81. In Figure 7C, these values are compared with those of the metasurfaces. Notably, both brightness and contrast are almost twice as high for the metasurfaces, even when using the organic electrochromic films. Thus, it seems plausible that a reflective color display with RGB pixels containing the metasurfaces will have sufficient brightness and contrast to be of practical use in many scenarios. We emphasize, however, that the image quality (also including chromaticity) in such a display will never be as good as for emissive displays. The point is that the plasmonic electronic paper can operate with extremely low power consumption (Figure 6). At the same time, the image quality will be good enough for many applications, especially image display in bright environments.

## CONCLUSIONS

In conclusion, we have shown primary colored metasurfaces with high reflectivity that are electrochemically stable in a nonaqueous electrolyte. This opens new possibilities for implementation of both organic and inorganic electrochromic materials in order to switch the colors on and off. We present a comparison of $PProDOTMe_2$, which seems to be the best among established polymers for high-contrast broadband switching, and the well-studied transition metal oxide $WO_3$. We also compare both types of metasurfaces with electrophoretic displays (see Table 1). The inorganic device gives the highest contrast of over 60% for most wavelengths, but the polymer is not far behind in performance. Using the right methodology, the polymer films are easily synthesized by electropolymerization, while $WO_3$ films require reactive sputtering. The polymer also switches faster (<1 s), but $WO_3$ has essentially perfect bistability in the electrolyte used. If the optimized electrochromic metasurfaces are implemented in reflective color displays as RGB pixels they will provide superior image quality compared to subpixel generation by color filters. The power consumption of such a display will be extremely low or basically zero when showing a static image.

As a final point, it should be noted that there are a few reports of new types of organic[39] and inorganic[40] electrochromic films that claim extremely high contrast when switching between black and transparent states. Our study has focused on the well-established polymer $PProdDOTMe_2$ and transition metal oxide $WO_3$, both of which have been successfully implemented in electrochromic devices by many research groups worldwide. We believe it remains to be seen if the newer materials truly can outperform the established ones and the methodology presented in this work helps to perform the comparison.

## EXPERIMENTAL SECTION

**Chemicals.** Propylene carbonate (PC, purity 99%) was from Sigma-Aldrich. $LiClO_4$ (anhydrous) was from Fisher Scientific. $ProDOTMe_2$ was purchased from Sycon Polymers India Pvt. Ltd. and purified by making a dispersion in deionized water (~1 g monomer in 20 mL water) by sonication at 40 °C until a milky liquid was produced together with a brownish liquid. The milky liquid was transferred to another beaker, extracted, and recrystallized with hexane. Pyrrole and EDOT were purchased from Sigma and used without any further purification.

**Fabrication of Metasurfaces.** Al (with 5 nm Cr adhesion layer), $Al_2O_3$, and Au (with 1 nm Ti adhesion layer) were deposited by evaporation (Lesker PVD 225) onto glass substrates. Prior to Au deposition, colloidal lithography was


https://dx.doi.org/10.1021/acsphotonics.0c00394
ACS Photonics 2020, 7, 1762−1772

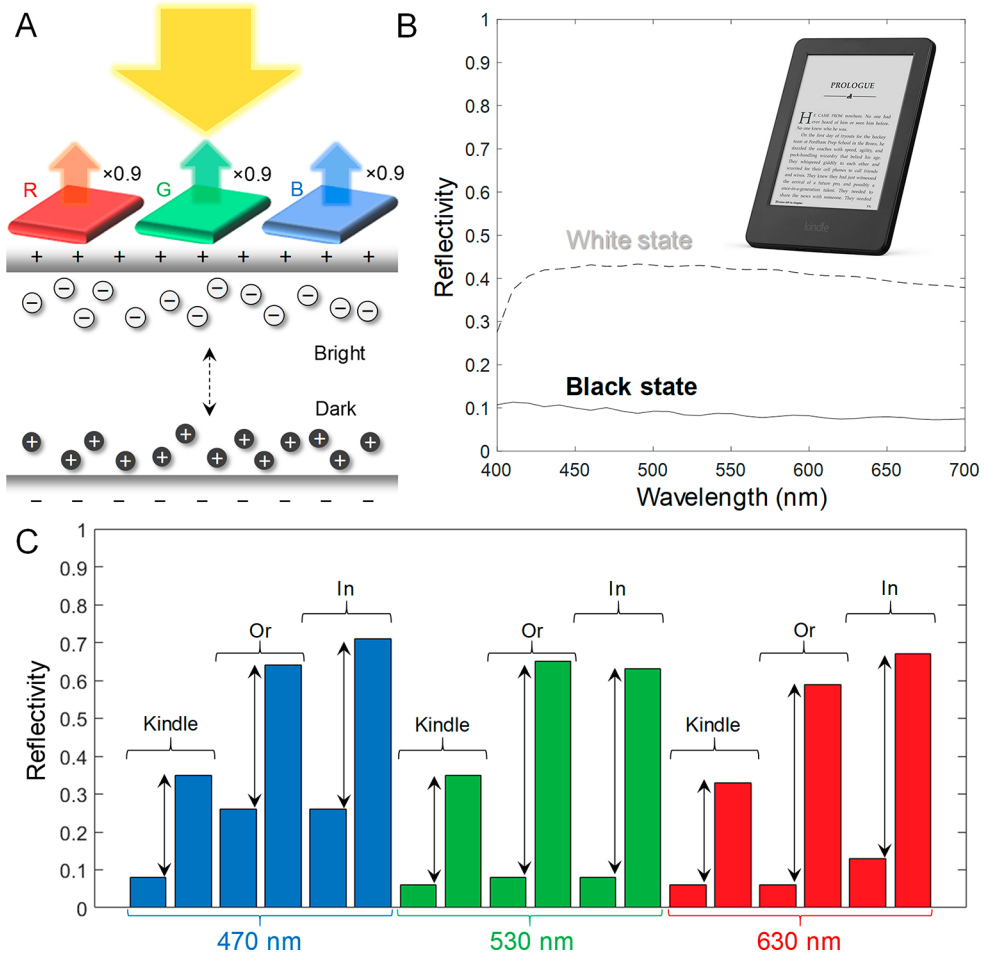


**Figure 7.** Comparison between metasurfaces and electrophoretic displays for electronic paper in color. (A) Principle of color generation by subpixels containing color filters, assuming 90% transmission of each primary color. (B) Diffuse reflectivity of black and white states of an Amazon Kindle device, measured with the same instrument as used for the metasurfaces. (C) Reflectivity in on and off states for three wavelengths, comparing the electrophoretic display with the metasurfaces having either organic (Or) or inorganic (In) films.

**Table 1**

| | metasurfaces with $PProDOTMe_2$ | metasurfaces with $WO_3$ | electrophoretic |
|---|---|---|---|
| preparation | electropolymerization directly on the surface | requires deposition by reactive sputtering | industrial production |
| brightness (reflectivity) | high (60−70%) | high (60−70%) | 40% in black/white, 35% for RGB subpixels |
| contrast | high (~50%) | higher (~60%) | 30% in black/white, 25% for RGB subpixels |
| optical modeling | Lambert−Beer formalism | full Fresnel models required | particle scattering/ absorption |
| switching speed | 0.1−1 s | 1−10 s, depends on switch direction | ~1 s |
| bistability | good overall, wavelength dependent | excellent (hours) | excellent |
| device stability (not systematically evaluated in this work) | excellent in terms of number of cycles[34] (~$10^5$); sensitive to intense light | may need to be regenerated after a certain number of cycles[38] (~$10^2$) in order to not lose performance; sensitive to water | commercially viable in black/white |

performed on $Al_2O_3$, as described previously,[3,27] using 147 nm polystyrene-sulfate particles (microParticles GmbH). For red samples the colloidal lithography step was omitted. Micropatterns were created by laser lithography, as described previously.[3,27]

**Electropolymerization.** For initial tests and for transmission mode measurements, substrates consisted of glass with 20 nm gold film (1 nm Cr) deposited in the same way as for the metasurfaces. The gold surface was first washed with acetone and isopropyl alcohol and dried with nitrogen. The substrate was placed in a custom-made spectro-electrochemical cell (Redox Me AB) with a Pt coil as counter electrode and an Ag electrode in contact with 0.01 M $AgNO_3$ and 0.1 M tetrabutyl ammonium perchlorate as reference ($Ag/Ag^+$). All


https://dx.doi.org/10.1021/acsphotonics.0c00394
ACS Photonics 2020, 7, 1762−1772

polymers were electrodeposited with a potentiostat (Gamry Interface 1010E) from a 10 mM monomer solution in 0.1 M $LiClO_4$/PC, degassed by a $N_2$ purge. Between every positive CV scan, a potential of −1 V was applied for 10 s to remove anions inserted in the polymer film. All voltages mentioned are versus the $Ag/Ag^+$ reference. No *iR* compensation was used. The dry thickness of the samples was measured with a profilometer (KLA Tencor Alpha-Step D-100).

**Sputtering.** $WO_3$ films were deposited by reactive RF sputtering inspired by previous recipes[32] (Nordiko 2000), with flow rates 32 and 8 sccm of Ar and $O_2$, respectively, at 20 mTorr and with 150 W power. The sample was kept as close as possible to the source at approximately 65 mm distance. The thicknesses and permittivity was analyzed using a spectroscopic ellipsometer (J.A.Wollam M2000). A dispersive model with three superimposed oscillators was assumed. XPS characterization was performed with a VersaProbe III (Physical Electronics).

**Opto-Electrical Measurements.** The diffuse reflectivity spectra of the metasurfaces (without electrochromic films) and of the Kindle device (Paperwhite 2 DP75SDI) were measured with a CM-700d spectrophotometer (Konika Minolta). This instrument also gives the CIE coordinates. Measurements of electrochromic surfaces during switching were performed in a home-built microscopy/reflection setup into which the electrochemical cell was placed and the potentiostat connected. $PProDOTMe_2$ was switched between −1.0 V and up to +0.8 V versus $Ag/Ag^+$ for the thickest films. PPy was switched between −1.0 V and +0.4 V versus $Ag/Ag^+$, while PEDOT was switched between −1.0 V and +0.4 V versus $Ag/Ag^+$. $WO_3$ was switched between −1.5 V and +1.7 V versus $Ag/Ag^+$ for thin Au films and −1.5 V and +1.5 V versus $Ag/Ag^+$ for metasurfaces. All switching was performed in PC with 1 M $LiClO_4$. A 4× air objective with NA 0.1 illuminated and collected light, representing an angular illumination range up to 4° to the surface normal for surfaces inside the electrolyte. A tungsten lamp (Azpect Photonics) was used and the spectrometer was a fiber-coupled photodiode array (B&WTek). A broadband dielectric mirror (BB05-E02, Thorlabs) was used to measure the reference reflection (no cell). It was verified that this mirror had essentially 100% reflectivity (>99%) using the Konika Minolta instrument. To account for light refraction, and so on, leading to an intensity loss in the liquid cell due to optics designed for measurements in air, the reflectivity spectrum of an Ag mirror was compared in air and inside the cell with electrolyte. All spectra were then corrected with a factor representing the ratio of these intensities (∼10% change). For transmission mode measurements, the reference intensity was simply measured without the liquid cell in place. The dark counts in the spectrometer (light source off) were always subtracted in all acquisitions. Note that extinction is defined using the natural logarithm and that it is additive. The contribution from the thin Au film and the flow cell could thus be removed by subtracting the corresponding extinction spectrum (before depositing an electrochromic film). The luminosity function was obtained from the Commission Internationale de l'Éclairage (CIE).

**Pictures and Videos.** RGB stripes were imaged using an Axiocam506 color camera in a microscope (Zeiss Axio Observer 7) with a 50× air objective designed for dark field illumination in reflection mode. Videos of switching of stripes and illuminated spots were recorded with a Thorlabs DCC1645C CMOS camera. Other photos and videos were obtained with mobile phones.

## ■ ASSOCIATED CONTENT

### Supporting Information

The Supporting Information is available free of charge at https://pubs.acs.org/doi/10.1021/acsphotonics.0c00394.

Video descriptions and Figures S1−S8 (PDF)

Five supporting videos (AVI)

## ■ AUTHOR INFORMATION


### Corresponding Author

**Andreas Dahlin** − *Department of Chemistry and Chemical Engineering, Chalmers University of Technology, 41296 Gothenburg, Sweden;* orcid.org/0000-0003-1545-5860; Email: adahlin@chalmers.se

### Authors

**Marika Gugole** − *Department of Chemistry and Chemical Engineering, Chalmers University of Technology, 41296 Gothenburg, Sweden*

**Oliver Olsson** − *Department of Chemistry and Chemical Engineering, Chalmers University of Technology, 41296 Gothenburg, Sweden*

**Kunli Xiong** − *Department of Chemistry and Chemical Engineering, Chalmers University of Technology, 41296 Gothenburg, Sweden*

**Jolie C. Blake** − *Department of Chemistry and Chemical Engineering, Chalmers University of Technology, 41296 Gothenburg, Sweden*

**José Montero Amenedo** − *Department of Materials Science and Engineering, Uppsala University, SE-75121 Uppsala, Sweden*

**Ilknur Bayrak Pehlivan** − *Department of Materials Science and Engineering, Uppsala University, SE-75121 Uppsala, Sweden;* orcid.org/0000-0002-4362-6148

**Gunnar A. Niklasson** − *Department of Materials Science and Engineering, Uppsala University, SE-75121 Uppsala, Sweden;* orcid.org/0000-0002-8279-5163

Complete contact information is available at: https://pubs.acs.org/10.1021/acsphotonics.0c00394


### Author Contributions

‡These authors contributed equally.

### Notes

The authors declare the following competing financial interest(s): Two authors (A.D. and K.X.) are co-founders of the company rdot displays AB, which works with reflective display technologies. O.O. has shares in this company. The authors have no active role in the company anymore. The company has not influenced the study in any way.

## ■ ACKNOWLEDGMENTS

We thank Anne Wendel at Chalmers for help with XPS analysis. Assoc. Prof. Magnus Jonsson at Linköping University and Dr. Peter Andersson Ersman at RISE are acknowledged for useful discussions. This work was financed by the Swedish Foundation for Strategic Research (EM16-0002).

## REFERENCES


(1) Kristensen, A.; Yang, J. K. W.; Bozhevolnyi, S. I.; Link, S.; Nordlander, P.; Halas, N. J.; Mortensen, N. A. Plasmonic colour generation. *Nat. Rev. Mater.* **2017**, *2*, 16088.

(2) Freestone, I.; Meeks, N.; Sax, M.; Higgitt, C. The Lycurgus Cup - A Roman nanotechnology. *Gold Bull.* **2007**, *40*, 270−277.

(3) Xiong, K.; Emilsson, G.; Maziz, A.; Yang, X.; Shao, L.; Jager, E. W. H.; Dahlin, A. B. Plasmonic metasurfaces with conjugated polymers for flexible electronic paper in color. *Adv. Mater.* **2016**, *28*, 9956−9960.

(4) Li, Y.; van de Groep, J.; Talin, A. A.; Brongersma, M. L. Dynamic tuning of gap plasmon resonances using a solid-state electrochromic device. *Nano Lett.* **2019**, *19*, 7988−7995.

(5) Shahabuddin, M.; McDowell, T.; Bonner, C. E.; Noginova, N. Enhancement of electrochromic polymer switching in plasmonic nanostructured environment. *ACS Appl. Nano Mater.* **2019**, *2*, 1713−1719.

(6) Wang, Z.; Wang, X.; Cong, S.; Chen, J.; Sun, H.; Chen, Z.; Song, G.; Geng, F.; Chen, Q.; Zhao, Z. Towards full-colour tunability of inorganic electrochromic devices using ultracompact fabry-perot nanocavities. *Nat. Commun.* **2020**, *11*, 302.

(7) Hopmann, E.; Elezzabi, A. Y. Plasmochromic nanocavity dynamic light color switching. *Nano Lett.* **2020**, *20*, 1876−1882.

(8) Atighilorestani, M.; Jiang, H.; Kaminska, B. Electrochromic-polymer-based switchable plasmonic color devices using surface-relief nanostructure pixels. *Adv. Opt. Mater.* **2018**, *6*, 1801179.

(9) Shao, L.; Zhuo, X.; Wang, J. Advanced plasmonic materials for dynamic color display. *Adv. Mater.* **2018**, *30*, 1704338.

(10) Xiong, K.; Tordera, D.; Jonsson, M. P.; Dahlin, A. B. Active control of plasmonic colors: emerging display technologies. *Rep. Prog. Phys.* **2019**, *82*, 024501.

(11) Franklin, D.; Frank, R.; Wu, S.-T.; Chanda, D. Actively addressed single pixel full-colour plasmonic display. *Nat. Commun.* **2017**, *8*, 15209.

(12) Xu, T.; Walter, E. C.; Agrawal, A.; Bohn, C.; Velmurugan, J.; Zhu, W.; Lezec, H. J.; Talin, A. A. High-contrast and fast electrochromic switching enabled by plasmonics. *Nat. Commun.* **2016**, *7*, 10479.

(13) Atighilorestani, M.; dos Santos, D. P.; Jaimes, R. F. V. V.; Rahman, M. M.; Temperini, M. L. A.; Brolo, A. G. Electrochemical control of light transmission through nanohole electrode arrays. *ACS Photonics* **2016**, *3*, 2375−2382.

(14) Jiang, N. N.; Shao, L.; Wang, J. F. (Gold nanorod core)/(polyaniline shell) plasmonic switches with large plasmon shifts and modulation depths. *Adv. Mater.* **2014**, *26*, 3282−3289.

(15) Leroux, Y. R.; Lacroix, J. C.; Chane-Ching, K. I.; Fave, C.; Felidj, N.; Levi, G.; Aubard, J.; Krenn, J. R.; Hohenau, A. Conducting polymer electrochemical switching as an easy means for designing active plasmonic devices. *J. Am. Chem. Soc.* **2005**, *127*, 16022−16023.

(16) Deb, S. K. In *Some aspects of electrochromic display systems*, Proc. 24th Electronic Components Conf., IEEE, 1974; pp 11−14.

(17) Green, S.; Backholm, J.; Georen, P.; Granqvist, C. G.; Niklasson, G. A. Electrochromism in nickel oxide and tungsten oxide thin films: Ion intercalation from different electrolytes. *Sol. Energy Mater. Sol. Cells* **2009**, *93*, 2050−2055.

(18) Granqvist, C. G. Electrochromics for smart windows: Oxide-based thin films and devices. *Thin Solid Films* **2014**, *564*, 1−38.

(19) Malti, A.; Brooke, R.; Liu, X.; Zhao, D.; Andersson Ersman, P.; Fahlman, M.; Jonsson, M. P.; Berggren, M.; Crispin, X. Freestanding electrochromic paper. *J. Mater. Chem. C* **2016**, *4*, 9680−9686.

(20) Padilla, J.; Osterholm, A. M.; Dyer, A. L.; Reynolds, J. R. Process controlled performance for soluble electrochromic polymers. *Sol. Energy Mater. Sol. Cells* **2015**, *140*, 54−60.

(21) Welsh, D. M.; Kumar, A.; Meijer, E. W.; Reynolds, J. R. Enhanced contrast ratios and rapid switching in electrochromics based on poly(3,4-propylenedioxythiophene) derivatives. *Adv. Mater.* **1999**, *11*, 1379−1382.

(22) Padilla, J.; Seshadri, V.; Sotzing, G. A.; Otero, T. F. Maximum contrast from an electrochromic material. *Electrochem. Commun.* **2007**, *9*, 1931−1935.

(23) Heikenfeld, J.; Drzaic, P.; Yeo, J. S.; Koch, T. A critical review of the present and future prospects for electronic paper. *J. Soc. Inf. Disp.* **2011**, *19*, 129−156.

(24) Hayes, R. A.; Feenstra, B. J. Video-speed electronic paper based on electrowetting. *Nature* **2003**, *425*, 383−385.

(25) Xu, J.; Zhang, Y.; Zhai, T.-T.; Kuang, Z.; Li, J.; Wang, Y.; Gao, Z.; Song, Y.-Y.; Xia, X.-H. Electrochromic-tuned plasmonics for photothermal sterile window. *ACS Nano* **2018**, *12*, 6895−6903.

(26) Kawahara, J.; Ersman, P. A.; Engquist, I.; Berggren, M. Improving the color switch contrast in PEDOT:PSS-based electrochromic displays. *Org. Electron.* **2012**, *13*, 469−474.

(27) Xiong, K.; Tordera, D.; Emilsson, G.; Olsson, O.; Linderhed, U.; Jonsson, M. P.; Dahlin, A. B. Switchable plasmonic metasurfaces with high chromaticity containing only abundant metals. *Nano Lett.* **2017**, *17*, 7033−7039.

(28) Wang, X.; Chen, K.; de Vasconcelos, L. S.; He, J.; Shin, Y. C.; Mei, J.; Zhao, K. Mechanical breathing in organic electrochromics. *Nat. Commun.* **2020**, *11*, 211.

(29) Junesch, J.; Sannomiya, T.; Dahlin, A. B. Optical properties of nanohole arrays in metal−dielectric double films prepared by mask-on-metal colloidal lithography. *ACS Nano* **2012**, *6*, 10405−10415.

(30) Triana, C. A.; Granqvist, C. G.; Niklasson, G. A. Electrochromism and small-polaron hopping in oxygen deficient and lithium intercalated amorphous tungsten oxide films. *J. Appl. Phys.* **2015**, *118*, 024901.

(31) Dahlin, A. B.; Zahn, R.; Voros, J. Nanoplasmonic sensing of metal-halide complex formation and the electric double layer capacitor. *Nanoscale* **2012**, *4*, 2339−2351.

(32) Yamada, Y.; Tabata, K.; Yashima, T. The character of WO3 film prepared with RF sputtering. *Sol. Energy Mater. Sol. Cells* **2007**, *91*, 29−37.

(33) Argun, A. A.; Berard, M.; Aubert, P. H.; Reynolds, J. R. Back-side electrical contacts for patterned electrochromic devices on porous substrates. *Adv. Mater.* **2005**, *17*, 422−426.

(34) Aubert, P.-H.; Argun, A. A.; Cirpan, A.; Tanner, D. B.; Reynolds, J. R. Microporous patterned electrodes for color-matched electrochromic polymer displays. *Chem. Mater.* **2004**, *16*, 2386−2393.

(35) Argun, A. A.; Reynolds, J. R. Line patterning for flexible and laterally configured electrochromic devices. *J. Mater. Chem.* **2005**, *15*, 1793−1800.

(36) Malmgren, S.; Green, S. V.; Niklasson, G. A. Anomalous diffusion of ions in electrochromic tungsten oxide films. *Electrochim. Acta* **2017**, *247*, 252−257.

(37) Fernandez, M. R.; Casanova, E. Z.; Alonso, I. G. Review of display technologies focusing on power consumption. *Sustainability* **2015**, *7*, 10854−10875.

(38) Wen, R.-T.; Granqvist, C. G.; Niklasson, G. A. Eliminating degradation and uncovering ion-trapping dynamics in electrochromic WO3 thin films. *Nat. Mater.* **2015**, *14*, 996.

(39) Zhang, Q.; Tsai, C.-Y.; Li, L.-J.; Liaw, D.-J. Colorless-to-colorful switching electrochromic polyimides with very high contrast ratio. *Nat. Commun.* **2019**, *10*, 1239.

(40) Cai, G.; Cui, M.; Kumar, V.; Darmawan, P.; Wang, J.; Wang, X.; Lee-Sie Eh, A.; Qian, K.; Lee, P. S. Ultra-large optical modulation of electrochromic porous WO3 film and the local monitoring of redox activity. *Chem. Sci.* **2016**, *7*, 1373−1382.




https://dx.doi.org/10.1021/acsphotonics.0c00394
*ACS Photonics* 2020, 7, 1762−1772

Supporting Information

# High-Contrast Switching of Plasmonic Structural Colors: Inorganic vs Organic Electrochromism

*Marika Gugole,[1‡] Oliver Olsson,[1‡] Kunli Xiong,[1] Jolie C. Blake,[1] José Montero Amenedo,[2] Ilknur Bayrak Pehlivan,[2] Gunnar A. Niklasson[2] and Andreas Dahlin.[1]**

1 Department of Chemistry and Chemical Engineering, Chalmers University of Technology, 41296 Gothenburg, Sweden.

2 Department of Materials Science and Engineering, Uppsala University, P.O. Box 534, SE-75121 Uppsala, Sweden.

‡ These authors contributed equally.

* Corresponding author adahlin@chalmers.se

Content:

Description of videos, figures S1-S8. Total 8 pages.

**Description of videos (merged into one .avi file) included as supporting online material:**

Green_PProDOTMe2_Spot: Switching a green sample with polymer in real-time. A reduced illumination spot is used (constant intensity).

Green_WO3_Spot: Switching a green sample with inorganic film in real-time. A reduced illumination spot is used (constant intensity).

Red_WO3: Switching a red sample with inorganic film in real-time. The illuminated region is ~1 mm wide. Note that the intensity is not homogenous here.

Blue_Stripes_PProDOTMe2: Selectively switching the blue stripes with polymer in real-time.

Green_Stripes_Cell: The green stripes on a region of the sample are being switched. A whole flow cell with electrodes is shown.

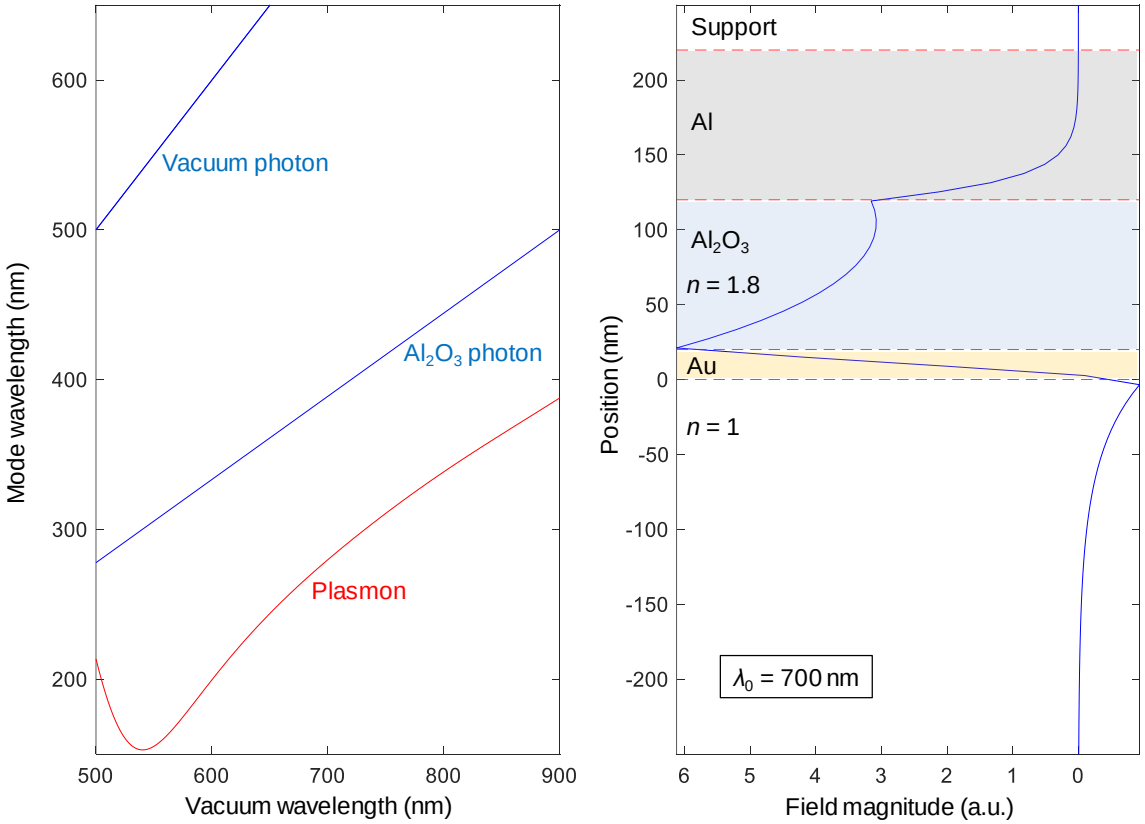


**Figure S1** Calculated surface plasmon dispersion relation in the thin film multilayers. The refractive index of $Al_2O_3$ was set to 1.8, which gave excellent agreement between Fresnel simulations and experimental reflectivity, and the thickness to 100 nm. The characteristic spacing between the colloids used gives a quasi-periodicity slightly below 300 nm, for which coupling is predicted at 700 nm. This is in agreement with the red-yellow scattering observed on green-blue samples. The field plot is generated at 700 nm. As expected, the plasmonic field is partly localized at the Al-$Al_2O_3$ interface.

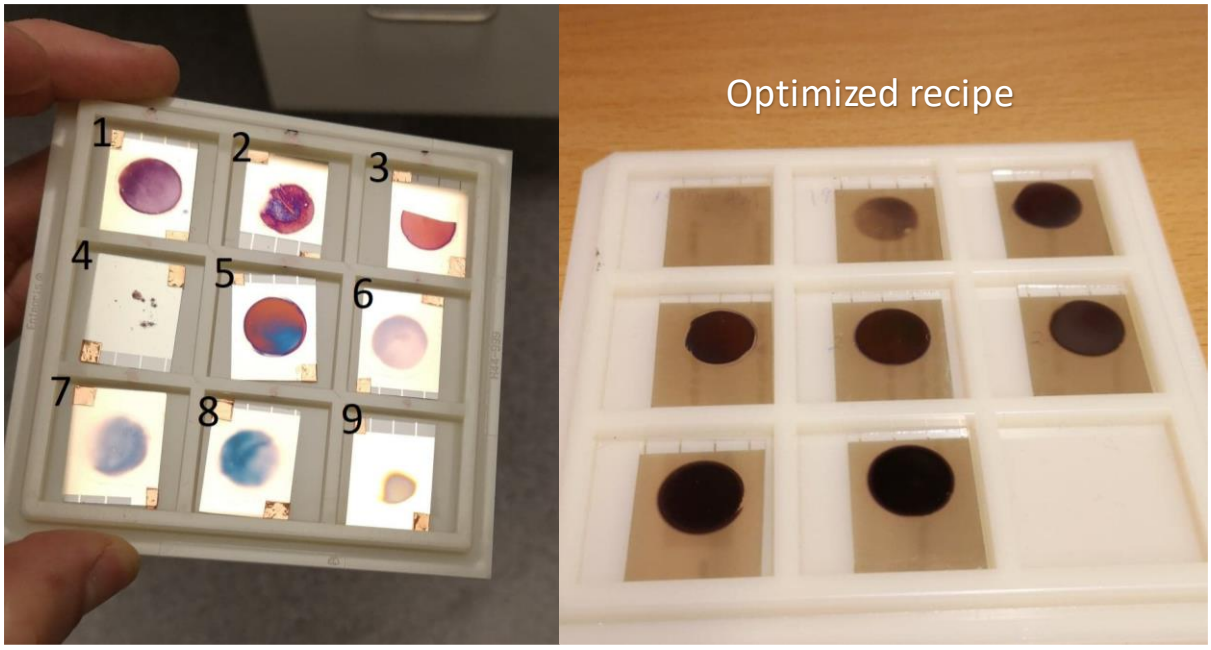


**Figure S2** The left picture shows samples prepared by other electrochemical methods, illustrating that it is not straightforward to create uniform films by electropolymerization. (1) Cyclic voltammetry 10× [1.5 V; −0.3 V] 100 mV/s, (2) Constant current [80 µA] 150 s, (3) Cyclic voltammetry 10× [1.5 V; −0.3 V] 100 mV/s, (4) Cyclic voltammetry on ITO (no polymer formed), (5) Cyclic voltammetry 28× [1.5 V; −0.3 V] 100 mV/s, (6) Cyclic voltammetry 3× [1.5 V; −0.3 V] 100 mV/s, (7) Constant potential [1.1 V then 1.2 V], (8) Constant current [40 µA then 80 µA], (9) Pulsed deposition [1.8 V 0.5 s; −0.3 V 0.5 s]. Note that these voltages were vs Ag/AgCl and another cell was used (which also influences quality and reproducibility). For comparison, the right image shows films of different thickness prepared by the optimized recipe.

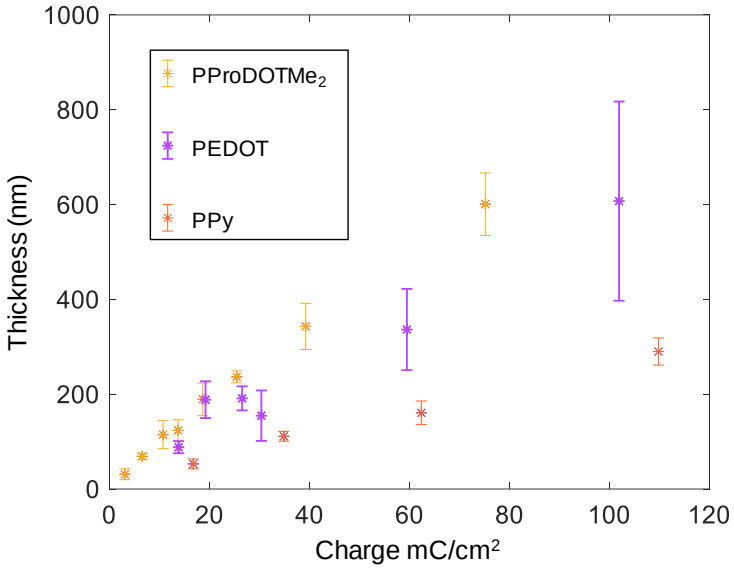


**Figure S3** Thickness measured by profilometer of different electropolymerized films.

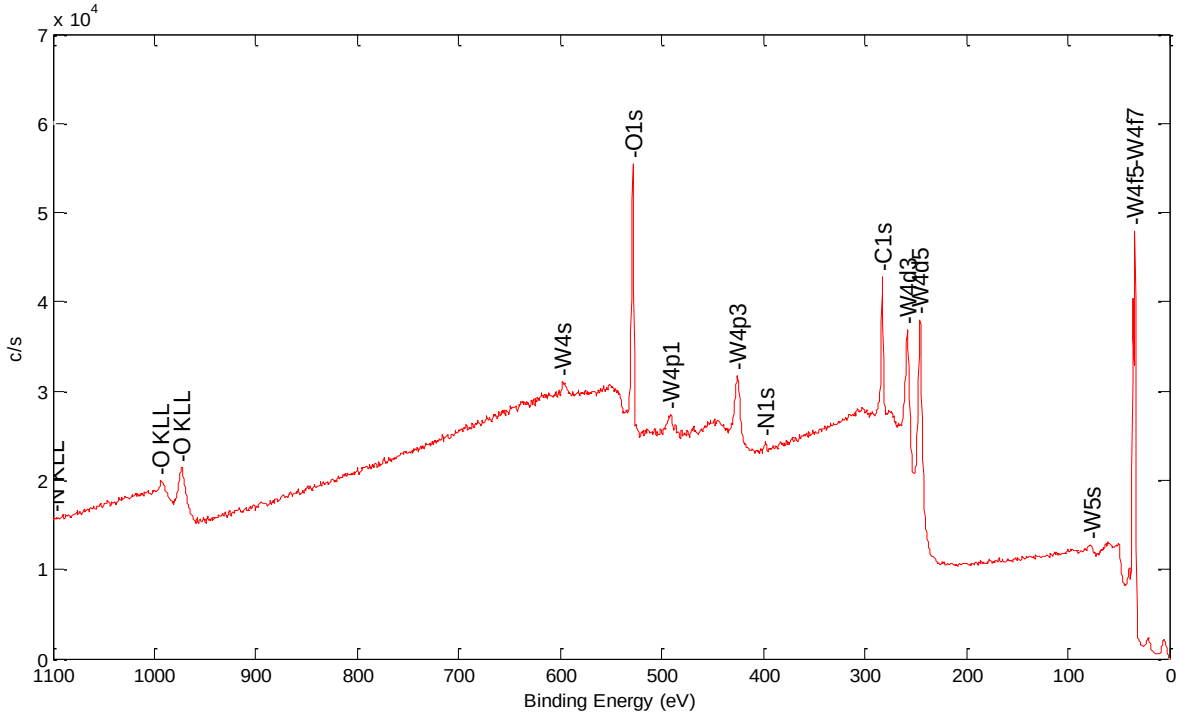


**Figure S4** X-ray photoelectron spectroscopy analysis of a $WO_3$ film prepared by reactive sputtering. Comparing the signal from the O1s and the W4f peaks gave a stoichiometry of O:W of 2.97 (which we refer to as $WO_3$).

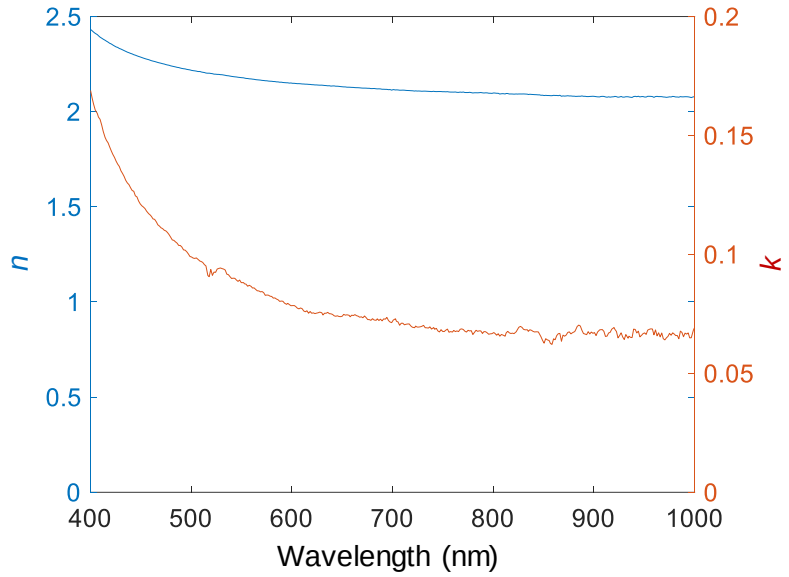


**Figure S5** Determination of as deposited $WO_3$ film permittivity by spectroscopic ellipsometry. The film was deposited on a glass slide where the other side was coloured black to avoid reflection. The thickness was allowed to vary and was fitted to 47.8 nm. Note that *n* is above 2, which gives rise to interference peaks in the visible already for relatively thin films. Note also that this film may be a little bit less absorbing than the "bright" state of $WO_3$ in experiments because it has never been exposed to $Li^+$. The *k* values in the literature data were ~50% higher, although *n* was identical (within measurement error). Hence, these data were not used to simulate $WO_3$ in its bright state but serve as a verification that our films have very similar optical properties to those presented in literature.

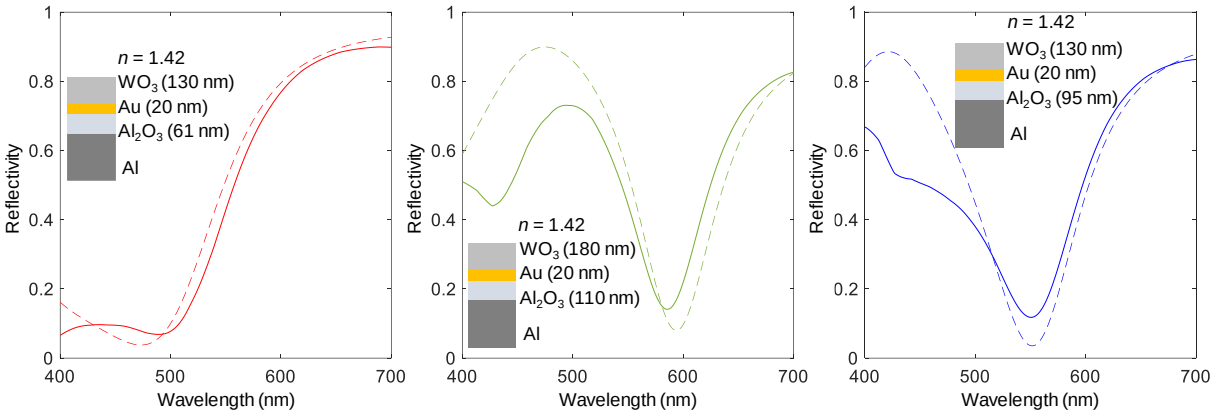


**Figure S6** Simulated reflectivity of metasurfaces when $WO_3$ and electrolyte is introduced on top. The $WO_3$ is in its bright state. The dashed lines are simulations of the same structure without the $WO_3$ and in air ($n$ = 1). These simulations do not take the nanoholes into account, which makes them inaccurate in the red region for blue and green samples as expected (compare with spectra in main text). However, the results work very well for describing the reflectivity maximum from the cavity resonance, which is sufficient for the purpose of finding a $WO_3$ film thickness that does not alter the color significantly. Simulations were performed as in previous work (see main text) and their accuracy is verified below.

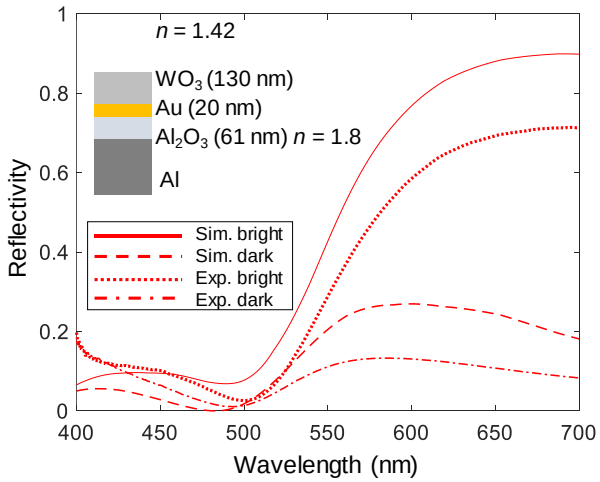


**Figure S7** Comparing simulations and experiments for a red sample with $WO_3$ in bright and dark states. The electrolyte is represented with refractive index 1.42. The simulated absolute reflectivity values are generally a bit shifted to higher values in the red region. Overall the agreement is considered to be satisfactory.

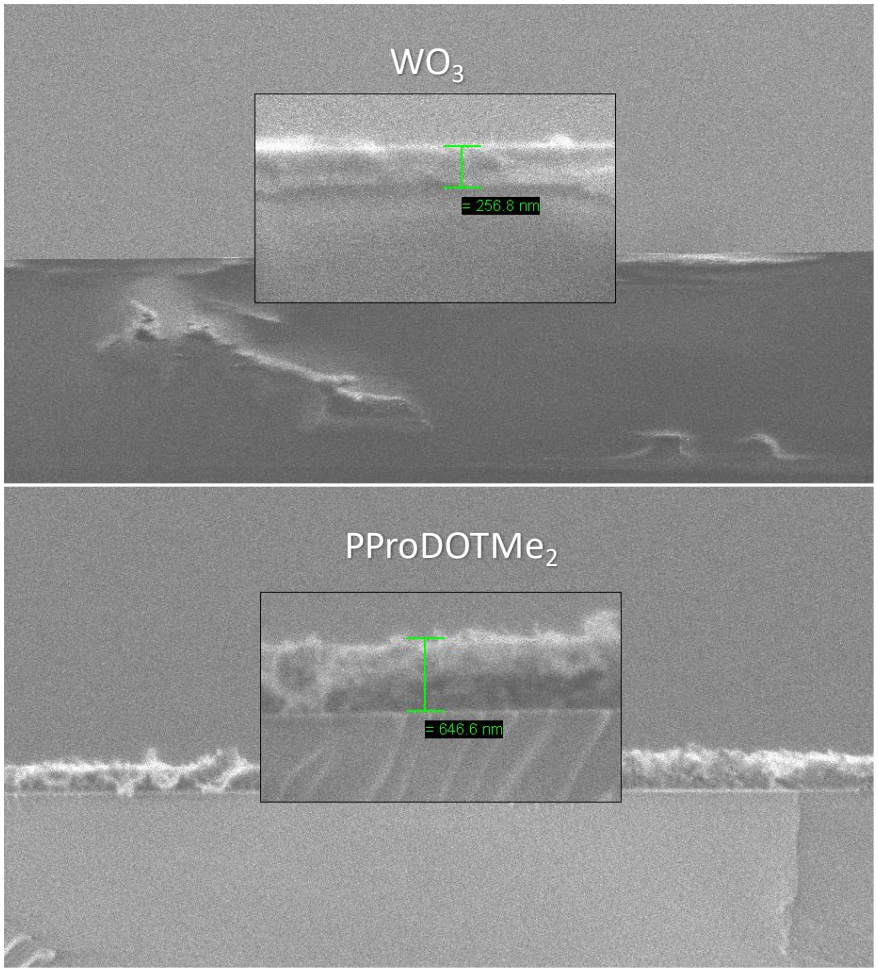


**Figure S8** Cross-section electron microscopy images of relatively thick electrochromic films. The porosity of $WO_3$ cannot be visualized since the pores are expected to be very small. For the polymer, the images indicate a highly porous soft network.

# Paper II

**Electrochromic Inorganic Nanostructures with High Chromaticity and Superior Brightness**

Marika Gugole, Oliver Olsson, Stefano Rossi, Magnus P. Jonsson, and Andreas Dahlin

*Manuscript*

# Electrochromic Inorganic Nanostructures with High Chromaticity and Superior Brightness

*Marika Gugole,[1] Oliver Olsson,[1] Stefano Rossi,[2] Magnus P. Jonsson[2] and Andreas Dahlin.[1]**

1 Department of Chemistry and Chemical Engineering, Chalmers University of Technology, 41296 Gothenburg, Sweden.

2 Laboratory of Organic Electronics, Department of Science and Technology, Linköping University, 60174 Norrköping, Sweden.

* Corresponding author: adahlin@chalmers.se

**Abstract**

The possibility of actively controlling structural colors has recently attracted a lot of attention, in particular for new types of reflective displays (electronic paper). However, it has proven challenging to achieve good image quality in such devices, mainly because many subpixels are necessary and the semi-transparent counter electrodes lower the total reflectance. Here we present an inorganic electrochromic nanostructure based on tungsten trioxide, gold and a thin platinum mirror. The platinum reflector provides a wide color range and makes it possible to "reverse" the device design so that electrolyte and counter electrode can be placed behind the nanostructures with respect to the viewer. Importantly, this makes it possible to maintain high reflectance regardless of how the electrochemical cell is constructed. We show that our nanostructures clearly outperform the latest commercial color e-reader in terms of both color range and brightness.

## Introduction

Supported by major advances in nanofabrication techniques, there has been a renewed interest in structural colors based on solid state materials with nanoscale features. In nature, such colors emerge from dielectric materials,[1] while humans have used metallic nanostructures supporting plasmon resonances since long ago.[2] In the last few years, the possibility to actively control structural colors has attracted a lot of attention.[3-7] Metallic nanostructures are particularly suitable for combining with electrochromic materials due to their conductive nature and have become highly interesting for various applications. In particular, reflective color displays or "electronic paper" technologies can offer great energy savings by replacing emissive displays (LCDs and LEDs) in various scenarios, especially under conditions of bright ambient light.[5] Very recently, several fully inorganic nanostructures based on metals and tungsten trioxide ($WO_3$) have been presented as strong candidates for durable electrochromic devices.[8-14] In contrast to organic electrochromism based on conducting polymers,[15] the use of $WO_3$ does not cause swelling of the material, i.e. the optical tunability is solely a result of the change in permittivity of the material upon ion intercalation.[16] Furthermore, $WO_3$ has proven stable enough for use in commercial devices such as smart windows.[4]

However, existing electrochromic devices based on $WO_3$ remain limited in terms of the main performance factors required for a reflective color display. The two most fundamental properties for good image quality are brightness (which translates to reflectance for electronic paper) and chromaticity (the color purity measured as the gamut in the CIE).[5] Although many innovative and promising nanoscale designs have been presented recently,[4] the colors may be limited to the green-red spectral region[11] and/or the reflectance is low.[10] In fact, the aspect of brightness is often neglected: if absolute reflectance values are presented at all, it is not explained properly how they

were measured. (For instance, the type of reference reflector becomes critical.) Without achieving both a strong reflection and a broad color range, the scope of applications for electrochromic nanostructures will be limited, even when it comes to simple decorative purposes. Maintaining high brightness is particularly critical for electronic paper technologies since only a fraction of the display surface will show a given color when using subpixels arranged side by side.[5] Because of this intensity loss, it is essential to find electrochromic surfaces that can provide many different colors as it reduces the number of subpixels needed. In some cases, this can be achieved with polarization-dependent reflection of colors and liquid crystals,[17] but such approaches still result in low absolute reflectance due to the requirement of polarizers.[18] In addition, regardless of the type of electrochromic surface used, the reflectance is always further reduced in practice because a counter electrode is needed in the device design.[19] This is typically achieved with minimally absorbing charge storing electrodes, which nevertheless eliminate a considerable fraction of the incident light.[20]

In this work we show a new design for inorganic electrochromic nanostructures which circumvents the problem of low reflectance while still providing an excellent color range. This is achieved by selecting the right metals and reversing the thin film layers, enabling all electrical components to be "hidden" behind the reflective surface. The devices show excellent performance in terms of both chromaticity and reflectance. Also, the power consumption is ultralow because of bistability (coloration memory). Finally, we propose a dual multichromatic pixel layout (instead of the conventional RGB) that enables high image quality in a reflective color display and show that this clearly can outperform a state-of-the-art electronic reader in color in terms of both brightness and color quality.

**Results and Discussion**

Inspired by recent work on tunable cavity resonances based on $Li^+$ intercalation in $WO_3$,[9-12, 21] we evaluated different nanostructures where $WO_3$ was sandwiched between a mirror and a semi-transparent metal film with nanoholes, generating a Fabry-Pérot cavity.[11, 13, 21-23] Colloidal lithography and standard thin film deposition techniques were used, which enable easy production of large-area samples. We tested different metals for extending the color range while maintaining stability in electrolyte environments. We found that platinum was ideal as the mirror, while 20 nm gold was used for the semi-transparent nanohole layer as previously.[13] A ~50 nm Pt mirror was sufficient to suppress transmission entirely due to the short penetration depth of incident light.[24] Also, due to the inert nature of both Pt and Au, the devices were highly stable with respect to oxidation, both in the presence of oxygen and upon applying anodic potentials.

For electrochromism based on conductive polymers, it has been shown that ions required for switching coloration state can be transported through opaque porous materials.[25, 26] Inspired by such work, we altered the "conventional" device outline by introducing the nanoholes in the Pt film instead, leading to the "reversed" design (Figure 1a). One reason why this is possible is the very thin Pt film, which prevents the colloids from becoming buried after metal deposition. The colloids could therefore be removed by carefully scraping the surface.[27] As a result, the observer can look through a fully transparent solid support directly onto the structural colors. In the reversed design, the electrolyte and counter electrode can be of practically any size and material suitable for efficient electrochemical performance and long-term stability. In comparison, the conventional design requires that the observer looks through both electrolyte and counter electrode in the display device,[19] which severely limits how the circuit can be configured and possible choices of materials.

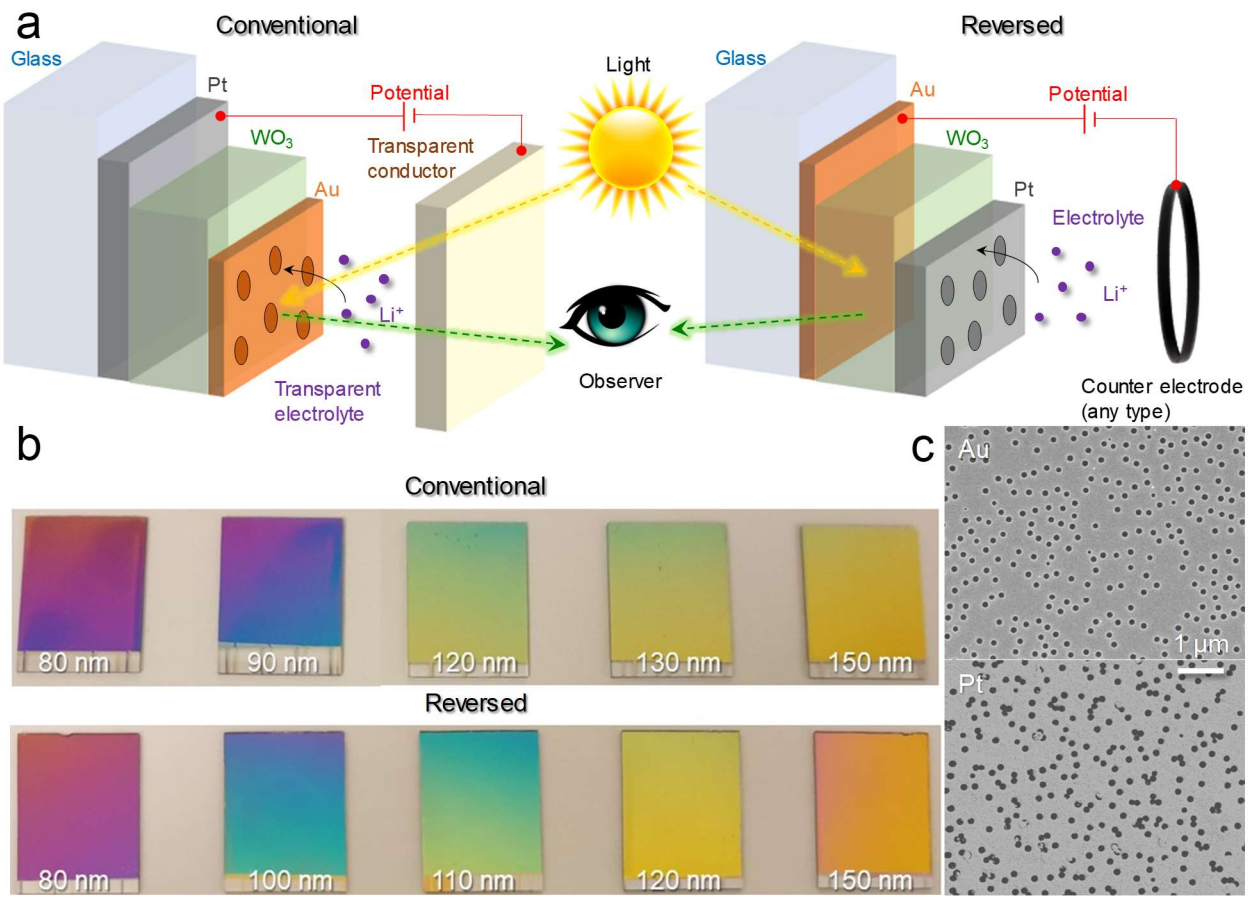


**Figure 1** Nanostructure and device design. (a) Schematics illustrating the conventional and reverse architectures. (b) Photos of samples with different thickness of $WO_3$. Note that the glass support is facing up for the reverse design. Color variations over the surface originate from the slightly non-uniform sputter coating over the sample dimensions (18×24 $mm^2$). (c) Electron microscopy images showing nanoholes in Au (conventional) or Pt (reversed).

Importantly, we observed no significant differences in optical response for the conventional and reversed designs. All colors could be achieved in both designs by changing the $WO_3$ thickness (Figure 1b). Furthermore, the nanohole arrays looked similar in electron microscopy images, although with some connected holes in Pt (Figure 1c). The reflectance (polarization insensitive) was high in absolute numbers and the spectra were very similar as long as the $WO_3$ thickness was

the same (Figure 2a). We concluded that any difference in the far field response from the two designs is smaller than the inherent sample-to-sample variation, which is mainly determined by the precision with which the $WO_3$ film thickness can be reproduced when sputtering (±10 nm). This implies that the nanoholes do not have a strong influence on the optical properties, i.e., the Fabry-Pérot cavity resonance is almost entirely responsible for the coloration. This differs from previous work with $Al_2O_3$ as the cavity, which gives rise to plasmonic activity that contributes to the structural colors.[13, 22, 23] Dark field imaging showed only weak red scattering from the nanoholes in Au and practically no scattering from holes in Pt (Fig. S1). Control samples without any nanoholes exhibited similar (within experimental variation) reflectance spectra in the visible (Fig. S2). As another control, changing hole diameter did not lead to any significant changes in the reflectance spectrum (Fig. S3). Thus, the purpose of the nanoholes is to allow transport of $Li^+$ ions to the $WO_3$ as shown by Hopmann et al.[11] However, finite difference time domain (FDTD) simulations on a square lattice[28] did suggest plasmonic activity in the near infrared for the conventional design (see Fig. S4 and related discussion).

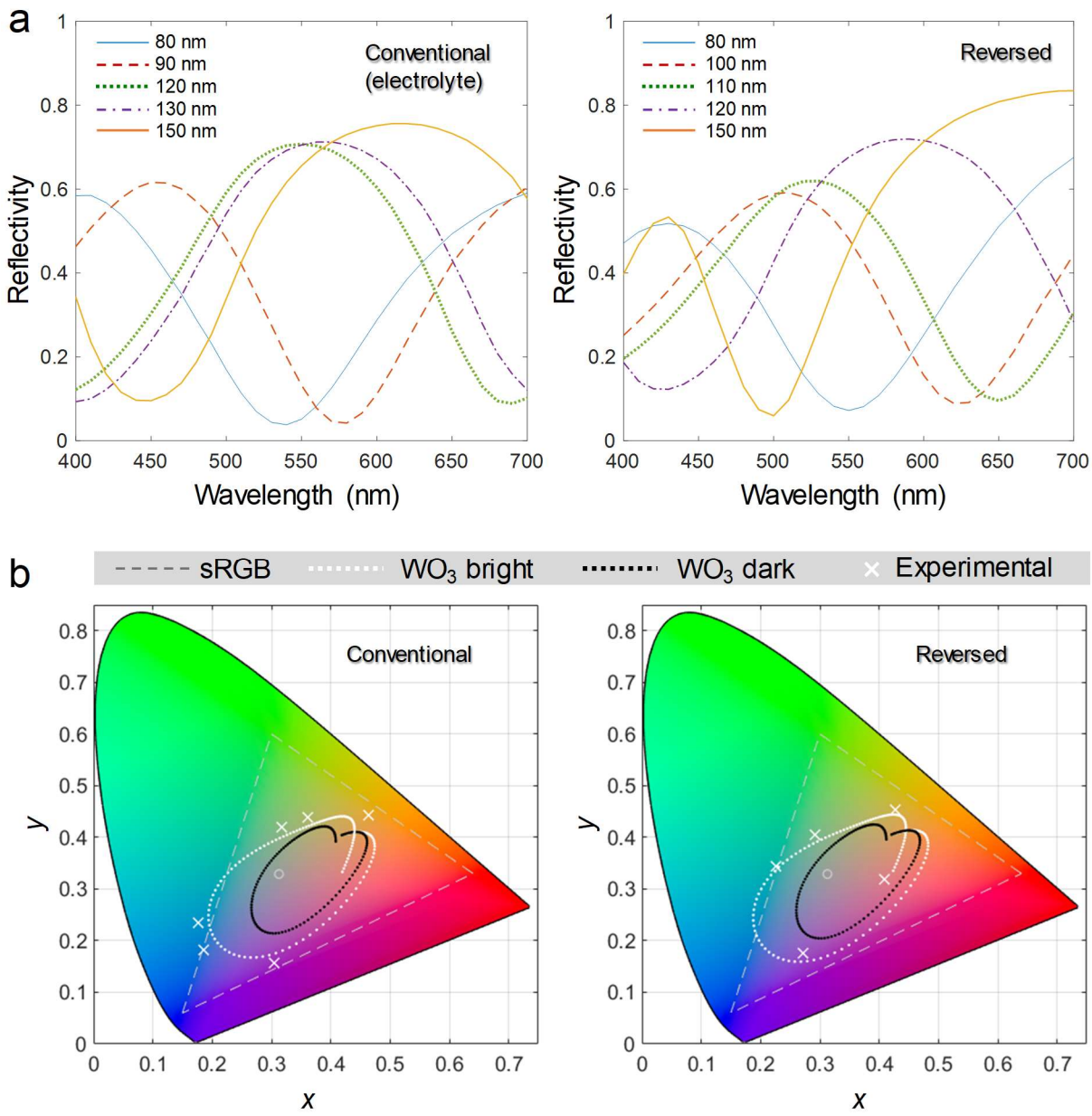


**Figure 2** Reflectance and color range. (a) Absolute reflectance spectra measured under diffuse illumination for different $WO_3$ thickness. (The conventional samples are immersed in a liquid which has the same refractive index as the electrolyte.) (b) Simulated color range in the CIE diagram for $WO_3$ thickness from 20 to 150 nm (white dots) and experimental data points (crosses). The black dots show the simulated color range when $WO_3$ is in its dark state. The circles indicate the D65 reference white point.

Due to the negligible contribution from plasmonic activity on the spectra, they were in good agreement with simple Fresnel simulations of the thin film system without nanoholes (Fig. S5). Literature data was used for the permittivity of Au,[29] Pt[24] and $WO_3$[16] (either the bright or the dark state). To estimate the total color range that can be obtained, we simulated the CIE coordinates generated by small stepwise changes in $WO_3$ thickness, resulting in lines in the *xy* chromaticity diagram representing a wide gamut around the white point (Figure 2b). Remarkably, most experimental data points appeared *outside* of the simulated gamut and some even outside the standard RGB range. The discrepancy between experiments and simulations is mainly due to minor differences in the permittivity of our $WO_3$ films[13] compared to literature data[16] (rather than the presence of the nanoholes). Simulating the cavities with $WO_3$ in its absorbing state leads to a smaller gamut (Figure 2b), which is due to the broadened spectral features when $WO_3$ is in its absorbing state. Nevertheless, a full color range is still generated. Increasing the thickness of $WO_3$ above ~150 nm did not extend the color range because multiple reflectance peaks start to appear within the visible, which is not beneficial for chromaticity for these nanostructures. Similarly, decreasing the thickness to tens of nm reduces color quality because the optical path length becomes too short. We note, however, that further improvements may be possible by double cavity structures.[21]

In order to dynamically tune the colors, a potential was applied to the nanostructures (ranging from +1.5 V to −1.5 V vs $Ag^+$) and the reflectance was monitored during $Li^+$ intercalation.[9-11, 13] For the reverse device design, the incident light illuminated the backside of the sample instead of going through the electrochemical cell. Figure 3 shows examples of color changes in terms of spectra and CIE coordinates. In brief, the reflectance maximum for the fundamental cavity mode moves across the visible due to changes in the permittivity of $WO_3$. There is once more almost

identical spectra for the conventional and reverse designs if the $WO_3$ thickness is similar (compare samples III and IV). Notably, even in the absorbing state when $Li^+$ is intercalated, the reflectance remains quite high (maximum >50%). For electrochromic applications, the brightness should also preferably be quantified in a manner that accounts for the wavelength dependent sensitivity of the eye (the luminosity function). Therefore, we also calculated the CIE *Y* value of the samples in their different coloration states. To establish some reference values for this parameter, a perfect broadband mirror has $Y = 100$, while we measured $Y = 63$ for white regions on a common newspaper and $Y = 84$ for an ordinary A4 paper (a very high value due to optical brightening agents). With black ink printed, the newspaper was reduced to $Y = 9$ and the printer paper was reduced to $Y = 5$ (spectra in Fig. S6). During $Li^+$ intercalation, *Y* generally decreased due to higher $WO_3$ absorption (see values in Figure 3b), but occasionally increased when the voltage was lowered if the color moved closer to green, i.e., the "bright" $WO_3$ state is not necessarily the brightest state of the whole nanostructure for the viewer. This is because the luminosity function peaks at 560 nm and illustrates how the *Y* parameter is an important complement to the reflectance values. The small hysteresis during switching is associated with the relatively fast voltage change and, most likely, a heterogenous distribution of $Li^+$ throughout the $WO_3$ film.

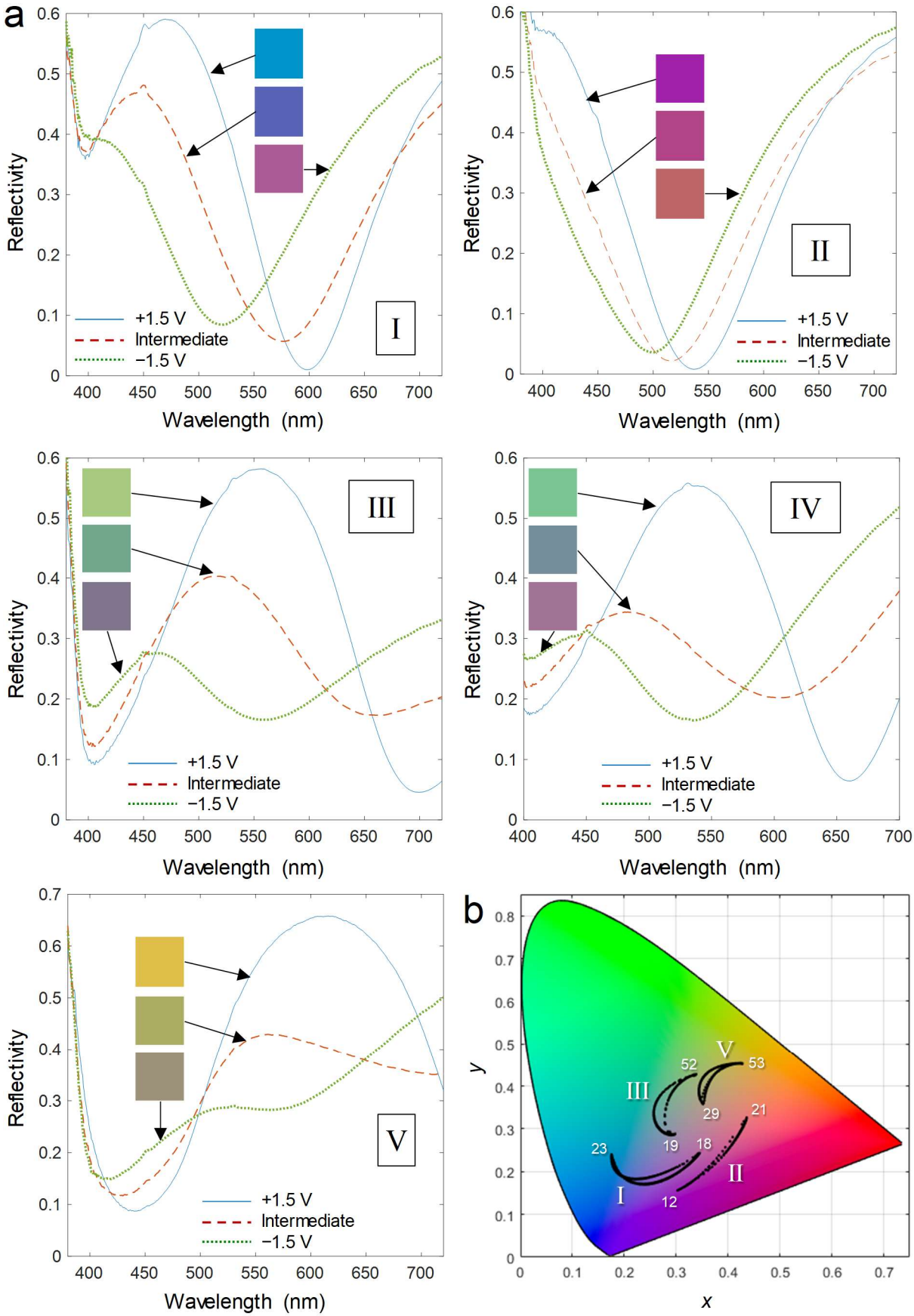
a
Reflectivity
Wavelength (nm)
+1.5 V
Intermediate
−1.5 V
I
II
III
IV
V
b
y
x
V
III
II
I
52
53
29
21
23
19
18
12

**Figure 3** Electrochemical color tuning. (a) Examples of reflectance changes when switching voltage between −1.5 V and +1.5 V vs ($Ag/Ag^+$). I: 100 nm $WO_3$ (conventional) II: 80 nm $WO_3$ (conventional) III: 120 nm $WO_3$ (conventional) IV: 110 nm $WO_3$ (reversed) V: 120 nm $WO_3$ (reversed) In all cases an example of an intermediate color state is shown. The squares show pseudo colors based on RGB values obtained from the CIE coordinates. (b) Corresponding movement in the CIE *xy* diagram. The numbers are the *Y* values at the end voltages. For all samples except III the higher Y corresponds to the bright state of the $WO_3$. (Sample IV is not included since it is similar to III.)

The switching dynamics showed that a complete switch took ~1 min (see supporting videos), which is slightly slower than for a $WO_3$ film in direct contact with the electrolyte.[13] This is expected because the nanohole array slightly hampers the transport of $Li^+$ ions. At the same time, the holes are necessary for tuning the cavity resonance (control samples without holes could not be switched). Furthermore, thicker $WO_3$ films took longer time to switch, which is expected since $Li^+$ needs to be transported through the whole layer. The speed can likely be improved by slightly increasing the amount of nanoholes or by altering the porosity of the $WO_3$,[30] but it is already sufficient for display applications where images do not necessarily need to be frequently updated (e.g. advertisement or decorative images). Importantly, all $Li^+$ intercalation levels (altered by voltage) exhibited bistability (Fig. S7). This means that the power consumption is essentially zero for maintaining any selected color throughout the switch and a only a low amount of energy is required for changing coloration state[13] (at the most 40 $mJ/cm^2$ for a full switch of the thickest $WO_3$).

We emphasize that the reflectance values we obtain can be maintained in real devices because of the reversed design, which is not influenced by how the electrochemical circuit is constructed

behind the nanostructures. In order to quantitatively show how important the reverse design is, we measured the reflectance loss for a sample in the conventional design using a vertical cell configuration with an indium tin oxide (ITO) coated glass cover. First, introducing the electrolyte leads to a small reflectance decrease (Figure 4a). Next, the loss in reflectance is an additional 20% when introducing a glass window and an ITO coating on this glass. (The corresponding loss in $Y$ is from 74 to 44.) Furthermore, the ITO film (130 nm thick and with the same area as the nanostructure) did not have sufficient charge storage capacity to completely switch the $WO_3$. This means that its effective capacitance needs to be increased, which is far from straightforward. One option is to introduce a minimally coloring charge storing polymer, but this leads to further intensity losses of tens of percent,[20] especially since light passes through twice. Commercial $WO_3$ devices often use nickel oxide as the counter electrode as it is anodically coloring, but the non-negligible absorption in its "bright" state leads to similar intensity losses.[31] Thus, in total, the reflectance is severe reduced (approximately cut in half) when a functioning flat-panel display device is constructed using the conventional approach. In contrast, our reverse design suffers no intensity losses at all since neither the electrolyte nor the counter electrode is in the light path (Figure 1a). There is also room for further improvements: the reflectance can become even higher on lower refractive index supports[32] (e.g. teflon) because faster propagation of the incident light wave leads to less absorption in the semi-transparent gold film. Also, anti-reflection coatings can be introduced on the other side of the solid support (facing the viewer) to further reduce the small reflection at this interface.

Because of the excellent brightness and chromaticity of our nanostructures, we hypothesized that they would outperform existing electronic readers in color. To quantitatively investigate this, we first performed measurements on the latest such device on the market at the time of writing:

the PocketBook Color, which is an electrophoretic display[33] that uses color filters to generate RGB subpixels using E-ink Kaleido™ technology. Reflectance spectra of the PocketBook showing the primary colors as well as white/black (all subpixels on/off) showed very low brightness (Figure 4b). This is not surprising considering that the reflectance of each electrophoretic cell is <50%, which is to be divided by more than a factor of three when subpixels are introduced.[13] Note that in order to ensure capturing all light from the e-reader, we measured with an integrated sphere that simulates ambient illumination and includes non-specular reflection.

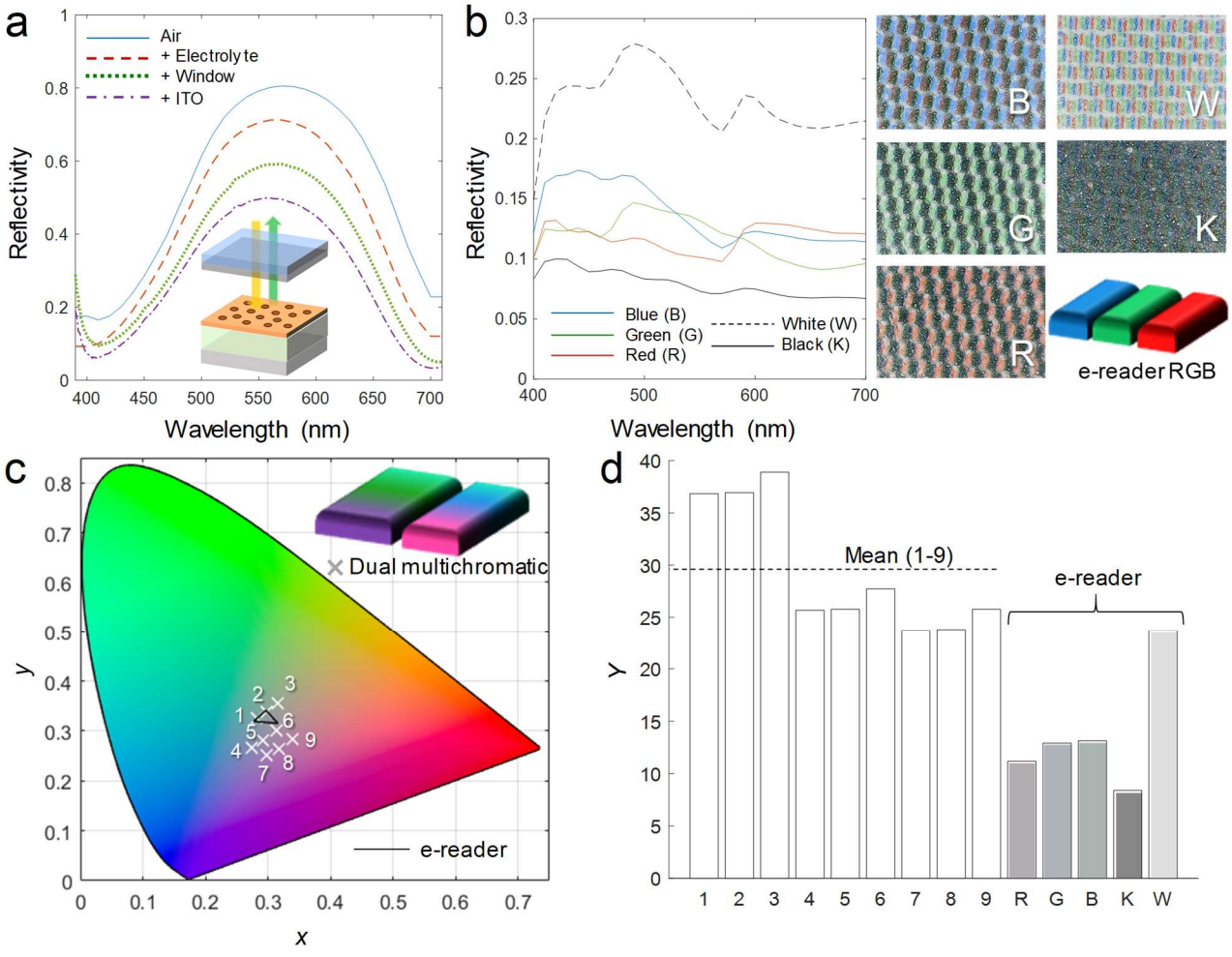


**Figure 4** Outperforming the latest commercial color e-reader. (a) Characteristic intensity losses in a conventional cell design as electrolyte and counter electrode are introduced. (b) Reflectance of

different colors from the latest commercial color e-reader. The corresponding images shows the pixels viewed under a microscope (images show 2.2×1.5 $mm^2$). (c) Example of colors that can be generated by a dual multichromatic subpixel outline (assuming 90% fill fraction for the display surface). For comparison, the RGB colors of the commercial e-reader are included. (d) Brightness comparison in terms of *Y* values for the dual multichromatic pixel layout compared to the e-reader RGB.

In contrast to RGB subpixels that are tuned in intensity, the electrochromic inorganic nanostructures truly alter their color, i.e. they move in the CIE diagram (Figure 3b). This opens up for new ways to introduce subpixels and perform color mixing by testing linear combinations of reflectance spectra at different voltages for some selected values of $WO_3$ thickness. This quickly becomes a complex multiparameter optimization process where it is important to find a balance between chromaticity and brightness. Here we will simply present an example to illustrate that our electrochromic nanostructures can easily outperform the commercial device in both respects, especially because of the reversed configuration. We show a dual pixel design assuming a display area covered to 35% by nanostructures with 90 nm $WO_3$ and to 55% by nanostructures with 110 nm $WO_3$ (both having the reverse design). The remaining 10% represents area needed for pixel separation and is assumed to have a flat reflectance spectrum of 50%. (The pixel fill fraction is thus assumed to be 90%, similar to that in commercial devices.) The reflectance spectra are generated by taking different coloration states for the two pixels with weight factors 0.35 and 0.55 (plus 0.1 with 50% reflection). Figure 4c shows 9 examples of colors in the CIE diagram that can be generated by selecting different voltages for the two pixels. For comparison, the much smaller color range of the commercial e-reader is also shown. Finally, we compare the *Y* values of our different colors with the e-reader, showing a strong enhancement also in terms of brightness

(Figure 4d). The mean value for the example colors generated by the dual pixel design is $Y = 29$, which is almost three times higher than for the primary colors of the e-reader. Furthermore, all 9 colors have a $Y$ value which is higher even than the fully "white" state of the e-reader.

## Conclusions

We have shown a new design for electrochromic inorganic nanostructures based on cavity resonances in $WO_3$ where a thin Pt film is used as the mirror. Besides providing a broad color range and high reflectance, the structures enable us to reverse the configuration in electrochromic devices so that the electrochemical cell ends up behind the reflective surface. This makes it possible to maintain high brightness regardless of electrolyte and counter electrode, which otherwise typically reduce the brightness by at least a factor of two. Furthermore, the nanostructures alter their color so much upon $Li^+$ intercalation that two different structures are sufficeint to generate all colors. Hence, we propose a dual multichromatic subpixel layout in order to improve brightness compared to RGB subpixels. This is the first clear demonstration of how electrochromic nanostructures outperform the latest commercial product of the market in terms of both chromaticity and brightness. Our nanostructure design enables new possibilities for electronic paper in color because of the improved image quality, which should be sufficient for the technology to replace energy costly emissive displays in many scenarios.

## Acknowledgements

This work was performed in part at Myfab Chalmers. The authors acknowledge funding from the Swedish Foundation for Strategic Research (EM16-0002).

## Supporting Information

Experimental section, 7 figures and related discussion, 2 videos. This material is freely available online.

## References


1. Sun, J.; Bhushan, B.; Tong, J. Structural coloration in nature. *RSC Adv.* 2013, 3, 14862-14889.
2. Kristensen, A.; Yang, J. K. W.; Bozhevolnyi, S. I.; Link, S.; Nordlander, P.; Halas, N. J.; Mortensen, N. A. Plasmonic colour generation. *Nat. Rev. Mater.* 2016, 2, 16088.
3. Kang, E. S. H.; Shiran Chaharsoughi, M.; Rossi, S.; Jonsson, M. P. Hybrid plasmonic metasurfaces. *J. Appl. Phys.* 2019, 126, 140901.
4. Zhang, W.; Li, H.; Hopmann, E.; Elezzabi, A. Y. Nanostructured inorganic electrochromic materials for light applications. *Nanophotonics* 2020, 10, 20200474.
5. Xiong, K.; Tordera, D.; Jonsson, M. P.; Dahlin, A. B. Active control of plasmonic colors: emerging display technologies. *Rep. Prog. Phys.* 2019, 82, 024501.
6. Daqiqeh Rezaei, S.; Dong, Z.; You En Chan, J.; Trisno, J.; Ng, R. J. H.; Ruan, Q.; Qiu, C.-W.; Mortensen, N. A.; Yang, J. K. W. Nanophotonic structural colors. *ACS Photonics* 2020, 8, 18-33.
7. Neubrech, F.; Duan, X.; Liu, N. Dynamic plasmonic color generation enabled by functional materials. *Sci. Adv.* 2020, 6, eabc2709.
8. Chen, J.; Wang, Z.; Liu, C.; Chen, Z.; Tang, X.; Wu, Q.; Zhang, S.; Song, G.; Cong, S.; Chen, Q.; Zhao, Z. Mimicking nature's butterflies: electrochromic devices with dual-sided differential colorations. *Adv. Mater.* 2021, 2007314.
9. Wang, Z.; Wang, X.; Cong, S.; Chen, J.; Sun, H.; Chen, Z.; Song, G.; Geng, F.; Chen, Q.; Zhao, Z. Towards full-colour tunability of inorganic electrochromic devices using ultracompact fabry-perot nanocavities. *Nat. Commun.* 2020, 11, 302.
10. Lee, Y.; Yun, J.; Seo, M.; Kim, S.-J.; Oh, J.; Kang, C. M.; Sun, H.-J.; Chung, T. D.; Lee, B. Full-color-tunable nanophotonic device using electrochromic tungsten trioxide thin tilm. *Nano Lett.* 2020, 20, 6084-6090.
11. Hopmann, E.; Elezzabi, A. Y. Plasmochromic nanocavity dynamic light color switching. *Nano Lett.* 2020, 20, 1876-1882.
12. Li, Y.; van de Groep, J.; Talin, A. A.; Brongersma, M. L. Dynamic tuning of gap plasmon resonances using a solid-state electrochromic device. *Nano Lett.* 2019, 19, 7988-7995.
13. Gugole, M.; Olsson, O.; Xiong, K.; Blake, J. C.; Montero Amenedo, J.; Bayrak Pehlivan, I.; Niklasson, G. A.; Dahlin, A. High-contrast switching of plasmonic structural colors: inorganic vs organic electrochromism. *ACS Photonics* 2020, 7, 1762-1772.
14. Xu, J.; Zhang, Y.; Zhai, T.-T.; Kuang, Z.; Li, J.; Wang, Y.; Gao, Z.; Song, Y.-Y.; Xia, X.-H. Electrochromic-tuned plasmonics for photothermal sterile window. *ACS Nano* 2018, 12, 6895-6903.
15. Wang, X.; Chen, K.; de Vasconcelos, L. S.; He, J.; Shin, Y. C.; Mei, J.; Zhao, K. Mechanical breathing in organic electrochromics. *Nat. Commun.* 2020, 11, 211.
16. Triana, C. A.; Granqvist, C. G.; Niklasson, G. A. Electrochromism and small-polaron hopping in oxygen deficient and lithium intercalated amorphous tungsten oxide films. *J. Appl. Phys.* 2015, 118.
17. Franklin, D.; Frank, R.; Wu, S.-T.; Chanda, D. Actively addressed single pixel full-colour plasmonic display. *Nat. Commun.* 2017, 8, 15209.
18. Franklin, D.; He, Z.; Mastranzo Ortega, P.; Safaei, A.; Cencillo-Abad, P.; Wu, S.-T.; Chanda, D. Self-assembled plasmonics for angle-independent structural color displays with actively addressed black states. *Proc. Nat. Acad. Sci.* 2020, 117, 13350.

19. Rai, V.; Singh, R. S.; Blackwood, D. J.; Zhili, D. A review on recent advances in electrochromic devices: a material approach. *Adv. Eng. Mater.* 2020, 2000082.
20. Knott, E. P.; Craig, M. R.; Liu, D. Y.; Babiarz, J. E.; Dyer, A. L.; Reynolds, J. R. A minimally coloured dioxypyrrole polymer as a counter electrode material in polymeric electrochromic window devices. *J. Mater. Chem.* 2012, 22, 4953-4962.
21. Rossi, S.; Jonsson, M. P. Highly reflective optical nanocavities for structural coloration by combining broadband absorber and Fabry–Pérot effects. *J. Opt.* 2020, 23, 015001.
22. Xiong, K.; Tordera, D.; Emilsson, G.; Olsson, O.; Linderhed, U.; Jonsson, M. P.; Dahlin, A. B. Switchable plasmonic metasurfaces with high chromaticity containing only abundant metals. *Nano Lett.* 2017, 17, 7033-7039.
23. Xiong, K.; Emilsson, G.; Maziz, A.; Yang, X.; Shao, L.; Jager, E. W. H.; Dahlin, A. B. Plasmonic metasurfaces with conjugated polymers for flexible electronic paper in color. *Adv. Mater.* 2016, 28, 9956-9960.
24. Rakic, A. D.; Djurisic, A. B.; Elazar, J. M.; Majewski, M. L. Optical properties of metallic films for vertical-cavity optoelectronic devices. *Appl. Opt.* 1998, 37, 5271-5283.
25. Argun, A. A.; Berard, M.; Aubert, P. H.; Reynolds, J. R. Back-side electrical contacts for patterned electrochromic devices on porous substrates. *Adv. Mater.* 2005, 17, 422-426.
26. Aubert, P.-H.; Argun, A. A.; Cirpan, A.; Tanner, D. B.; Reynolds, J. R. Microporous patterned electrodes for color-matched electrochromic polymer displays. *Chem. Mater.* 2004, 16, 2386-2393.
27. Xiong, K.; Emilsson, G.; Dahlin, A. B. Biosensing using plasmonic nanohole arrays with small, homogenous and tunable aperture diameters. *Analyst* 2016, 141, 3803-3810.
28. Malekian, B.; Xiong, K.; Kang, E. S. H.; Andersson, J.; Emilsson, G.; Rommel, M.; Sannomiya, T.; Jonsson, M. P.; Dahlin, A. Optical properties of plasmonic nanopore arrays prepared by electron beam and colloidal lithography. *Nanoscale Adv.* 2019, 1, 4282-4289.
29. Etchegoin, P. G.; Le Ru, E. C.; Meyer, M. An analytic model for the optical properties of gold. *J. Chem. Phys.* 2006, 125, 164705.
30. Kim, K.-W.; Yun, T. Y.; You, S.-H.; Tang, X.; Lee, J.; Seo, Y.; Kim, Y.-T.; Kim, S. H.; Moon, H. C.; Kim, J. K. Extremely fast electrochromic supercapacitors based on mesoporous WO3 prepared by an evaporation-induced self-assembly. *NPG Asia Materials* 2020, 12, 84.
31. Green, S.; Backholm, J.; Georen, P.; Granqvist, C. G.; Niklasson, G. A. Electrochromism in nickel oxide and tungsten oxide thin films: Ion intercalation from different electrolytes. *Sol. Energ. Mat. Sol. C.* 2009, 93, 2050-2055.
32. Brian, B.; Sepulveda, B.; Alaverdyan, Y.; Lechuga, L. M.; Kall, M. Sensitivity enhancement of nanoplasmonic sensors in low refractive index substrates. *Opt. Express* 2009, 17, 2015-2023.
33. Comiskey, B.; Albert, J. D.; Yoshizawa, H.; Jacobson, J. An electrophoretic ink for all-printed reflective electronic displays. *Nature* 1998, 394, 253-255.

For Table of Contents Only

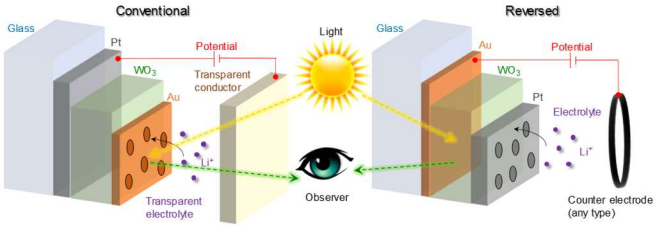

# Electrochromic Inorganic Nanostructures with High Chromaticity and Superior Brightness

*Marika Gugole,[1] Oliver Olsson,[1] Stefano Rossi,[2] Magnus P. Jonsson[2] and Andreas Dahlin.[1]**

1 Department of Chemistry and Chemical Engineering, Chalmers University of Technology, 41296 Gothenburg, Sweden.

2 Laboratory of Organic Electronics, Department of Science and Technology, Linköping University, 60174 Norrköping, Sweden.

* Corresponding author: adahlin@chalmers.se

**Brief description of videos**

Video 1: Switching in the conventional design. Colors covered are green, yellow and blue.

Video 2: Switching in the reverse design. Colors covered are blue, red and magenta.

**Experimental**

Materials: Propylene carbonate and poly(ethylene glycol) was purchased from Sigma. $LiClO_4$ (anhydrous) was purchased from Fischer Scientific. ITO glass was purchased from Naranjo substrates. For analyzing paper, a local newspaper (Expressen) was purchased and a black box was printed (Kyocera TASKalfa 356ci) on ordinary A4 paper (New Future Multi).

Nanofabrication: Supports were borosilicate microscopy cover glasses. Au and Pt films were deposited by physical vapor deposition (Lesker PVD 225). For the conventional design, a 5 nm Ti layer was included under Pt and a 1 nm Ti layer was included under Au to promote adhesion. For the reverse design, 1 nm Ti was used as adhesion between Au and glass. $WO_3$ was deposited by reactive sputtering (Nordiko 2000) with 32 sccm Ar and 8 sccm $O_2$ at 20 mTorr and 150 W. The $WO_3$ thicknesses was estimated by a spectroscopic ellipsometer (J.A.Wollam M2000). Colloidal lithography was performed on $WO_3$ using 147 nm polystyrene colloids (Microparticles). For the reversed samples, colloids were removed by carefully scraping the surface instead of using tape.[1]

Electrochemical measurements: A commercial liquid cell (RedoxMe) with an $Ag/Ag^+$ reference electrode and Pt counter electrode was used for three-electrode measurements with a potentiostat (Gamry Interface 1000/1010). When testing ITO it acted as both counter and reference electrode. All switching was performed in propylene carbonate with 1 M $LiClO_4$.

Optical measurements: The reflectance spectra were measured using diffuse illumination by a CM-700d spectrophotometer (Konika Minolta) and light collection at 8° against the surface normal. When measuring spectra of conventional samples (without doing any switching), poly(ethylene glycol) was mixed with milli-Q water in order to increase the refractive index to be the same as for propylene carbonate. To measure spectra during electrochemical switching, a home-built microspectroscopy setup was used.[2] The illumination and collection was with a 4× air objective (NA 0.10) and optical fibers were connected to the lamp (100 W tungsten) and the

[1] Xiong et al. *Analyst* **2016**, 141 (12), 3803-3810.

[2] Gugole et al. *ACS Photonics* **2020**, 7 (7), 1762-1772.

spectrometer (B&WTek photodiode array). When testing samples in the conventional design, light passed through a glass window and next to the Ag and Pt electrodes (see video). A broadband dielectric mirror (BB05-E02, Thorlabs) was used to measure the reference intensity. In order to ensure accurate absolute reflectance, the mirror used to obtain reference intensity was also measured in the CM-700d instrument.

Pictures: Photos of samples were taken with a Samsung S9 phone with standard settings. The commercial e-reader pixels were visualized with a digital handheld microscope. Red, green, blue, black and white regions of the test document which is on the device when purchased were visualized. Dark field images were recorded with an Axiocam506 color camera in a microscope (Zeiss Axio Observer 7) with a 50× air objective designed for dark field illumination in reflection mode.


**Figure S1** Dark field images showing weak deep red light scattering from nanoholes in Au. There is no significant scattering in the absence of holes. For holes in Pt the scattering is barely detectable and has no characteristic color.

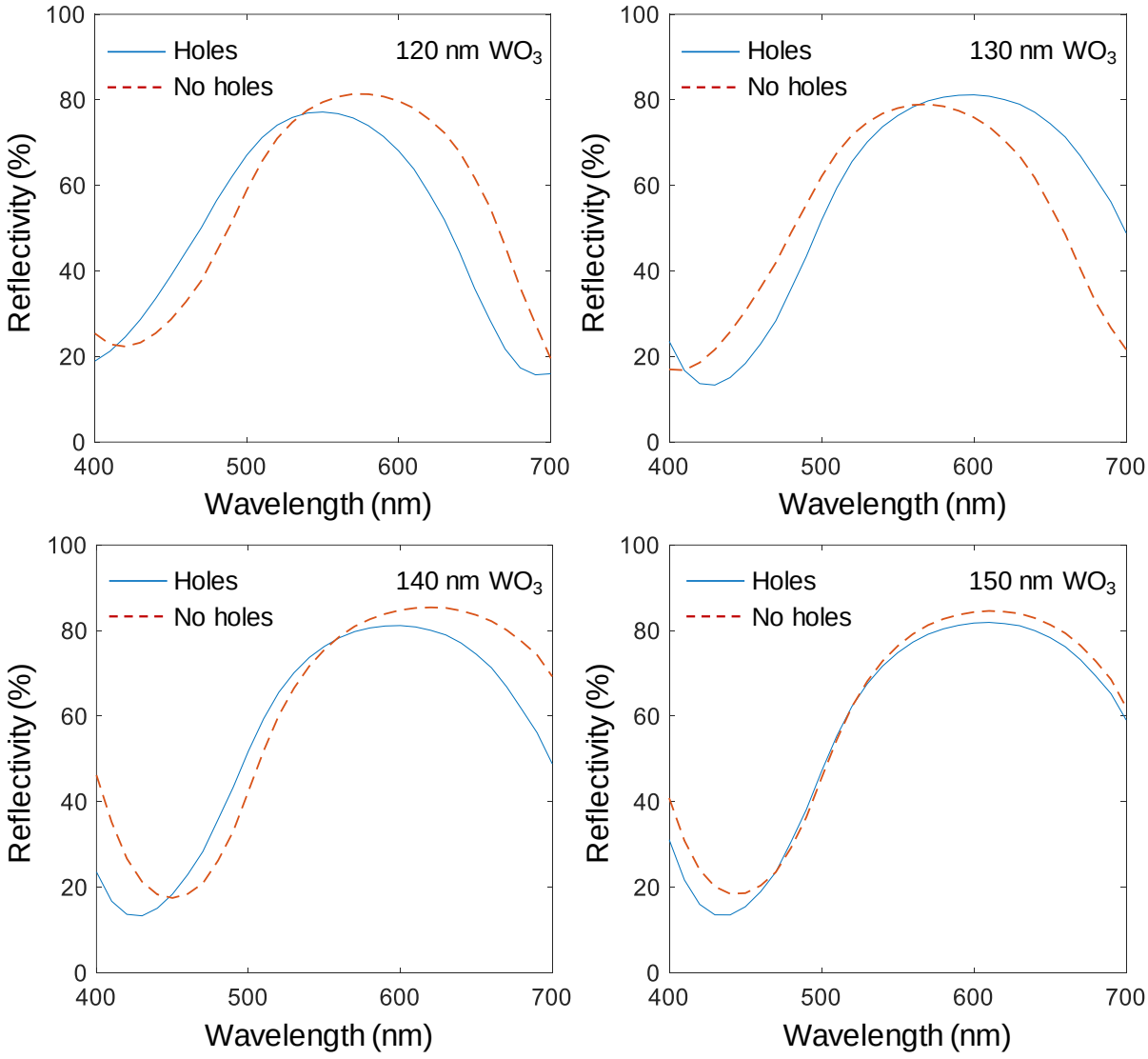


**Figure S2** Reflectance spectra of samples made by the conventional design but without nanoholes in the gold film. The spectral changes compared to having holes are not significantly larger than the inherent sample to sample variation.

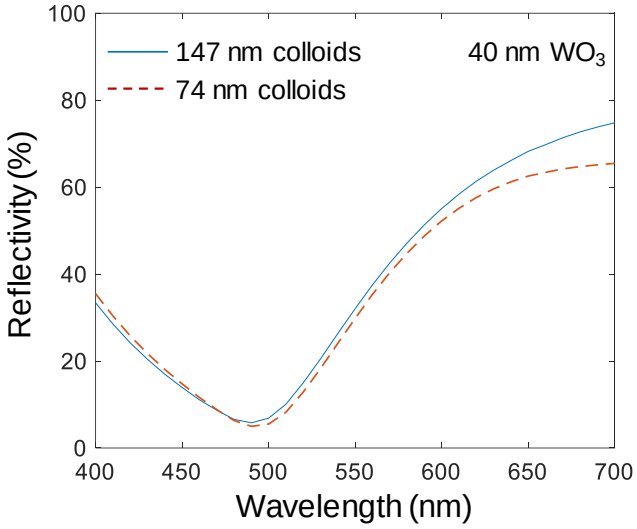


**Figure S3** Reflectance spectra of samples with different diameter of nanoholes (in Au). As in the previous figure, the spectral changes are not significant.

**Numerical simulations**

Simulations were preformed to find out if the lack of plasmonic activity in the visible is because the resonances are shifted to the NIR or if they are too damped. FDTD calculations in Lumerical were used similarly to previous work.[3] Periodic boundaries were used to model a square lattice in the surface plane. A perfectly matched layer was used in the direction perpendicular to the surface and the span of the FDTD simulation was 600 nm. The minimum mesh step was 2 nm, auto-non-uniform with a 2 nm mesh override over the nanoholes. The electric and magnetic field were recorded in continuous wave normalization, meaning that the fields are normalized by the Fourier transform of the source pulse.

The simulations confirm that the nanoholes do not significantly influence the spectra, at least not in the visible. For the conventional design, a clear minimum in reflectance appears just above 1000 nm when an array of nanoholes is present in Au. We attribute this reflectivity minimum to coupling to surface plasmons. For the reversed design, no such reflectance decrease appears, which is probably because coupling to plasmons occurs through the nanohole arrays. Since in the reverse cavity the Pt nanoholes are exposed to the WO3 layer, which has a much higher real and imaginary refractive index than the electrolyte, we expect the plasmonic resonance to be significantly red-shifted and dampened compared to the conventional design. Moreover, Pt is more absorptive than Au. This means that in the reversed design, damping is expected to become very high, thereby eliminating the resonance.

[3] Malekian et al. *Nanoscale Advances* **2019**, 1 (11), 4282-4289.

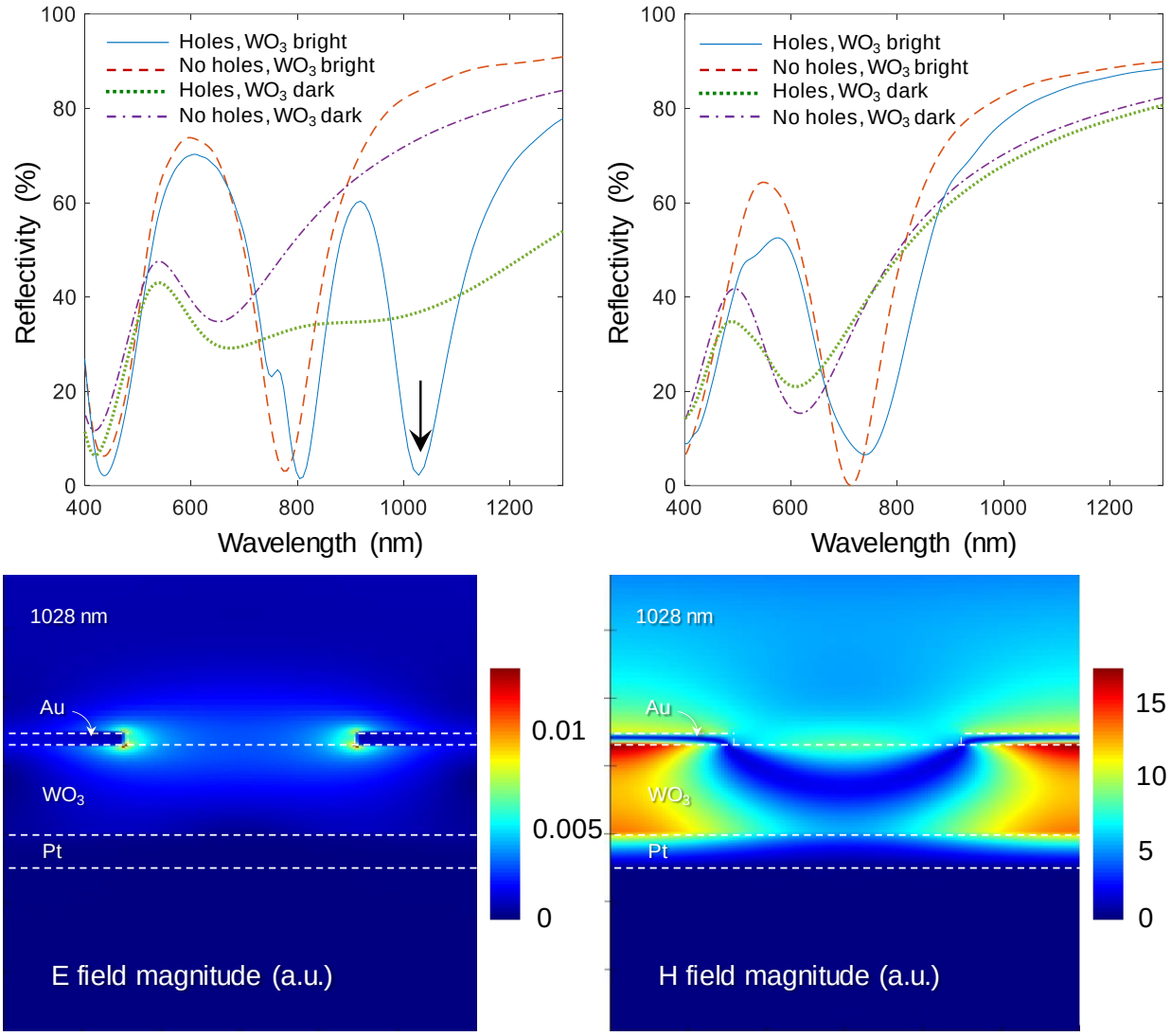


**Figure S4** FDTD simulations of the reflectance from the nanostructures with or without nanoholes. Left shows conventional, right shows reversed. The $WO_3$ thickness is 130 nm. The electrolyte refractive index was set to 1.4. The nanohole array has a periodicity of 300 nm. The near field is visualized at the reflection minimum (arrow), which only appears for the conventional design with $WO_3$ in its bright state. The left image shows the electric field and the right one shows the magnetic field. The polarization of the incident wave is along the image plane.

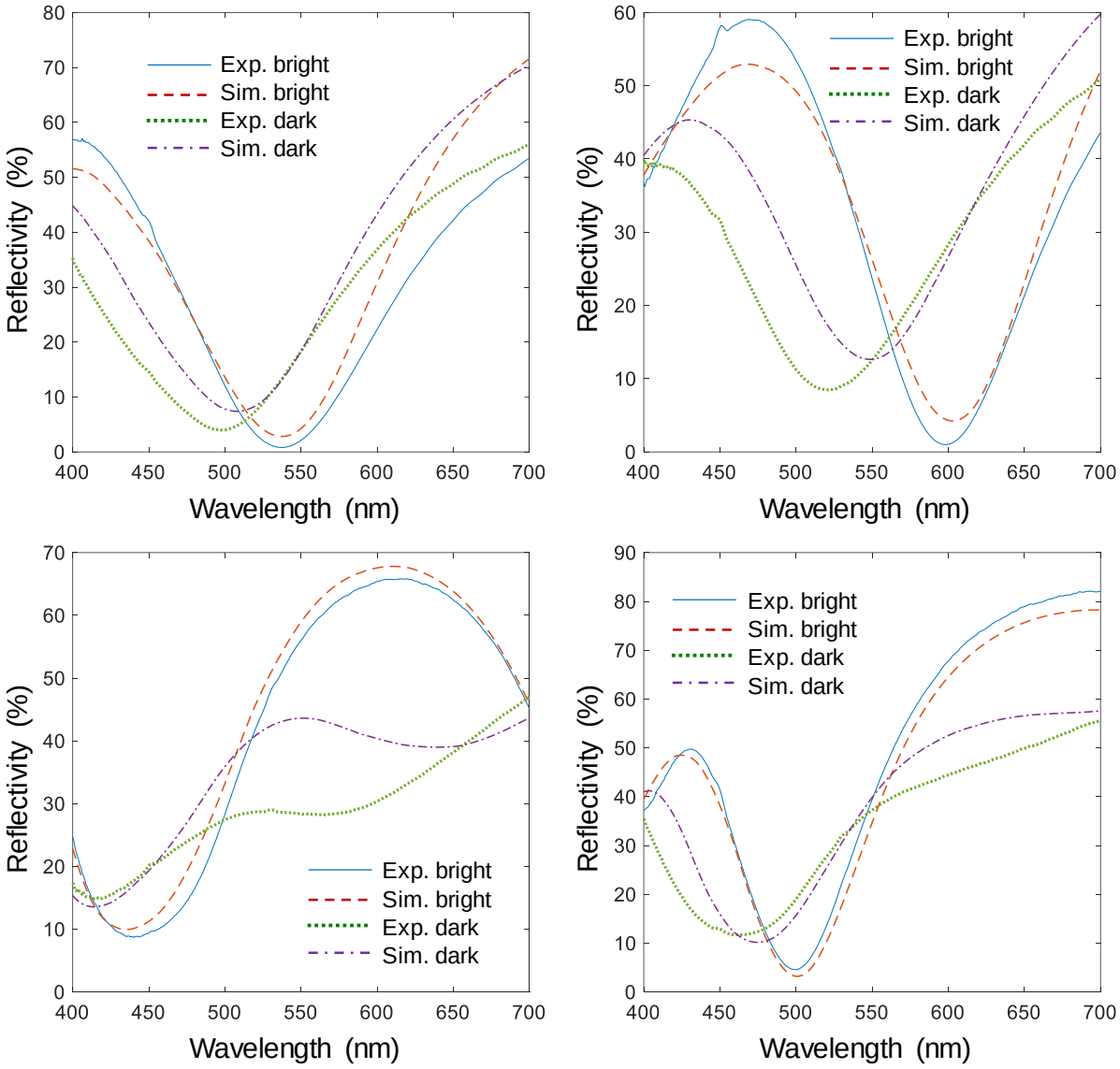


**Figure S5** Comparison of Fresnel models with experimental spectra. Top left: 80 nm $WO_3$ (conventional). Top right: 100 nm $WO_3$ (conventional). Bottom left: 130 nm $WO_3$ (reverse). Bottom right: 140 nm $WO_3$ (reverse). While the permittivity was fixed to literature values, the $WO_3$ thickness was allowed to vary by up to 20 nm to account for uncertainty in thickness. The discrepancy between experiments and calculations is mainly attributed to small differences in the actual permittivity of our $WO_3$ films compared to literature values. In particular, the film morphology, stoichiometry and degree of $Li^+$ intercalation in the bright and dark states may vary between studies.

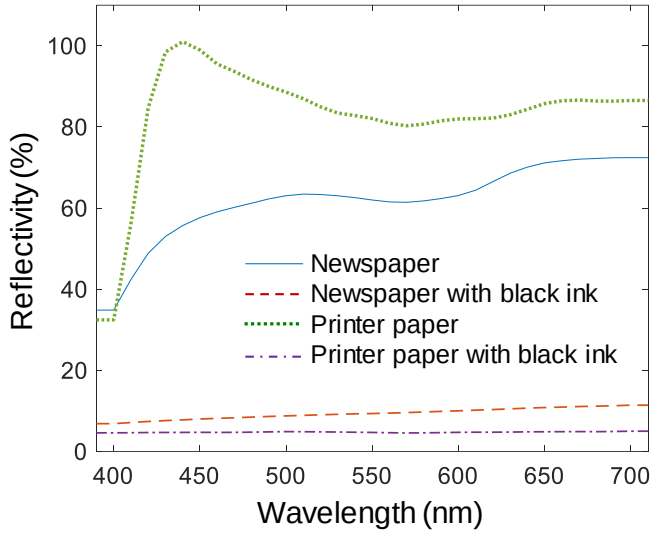


**Figure S6** Reflectance spectra measured for different common papers with and without black ink. The spectra were used to calculate characteristic *Y* values mentioned in the main text. Note that the printer paper contains fluorescent compounds which makes it possible to reach values even higher than 100% since higher energy incident light is absorbed and emitted at longer wavelengths.

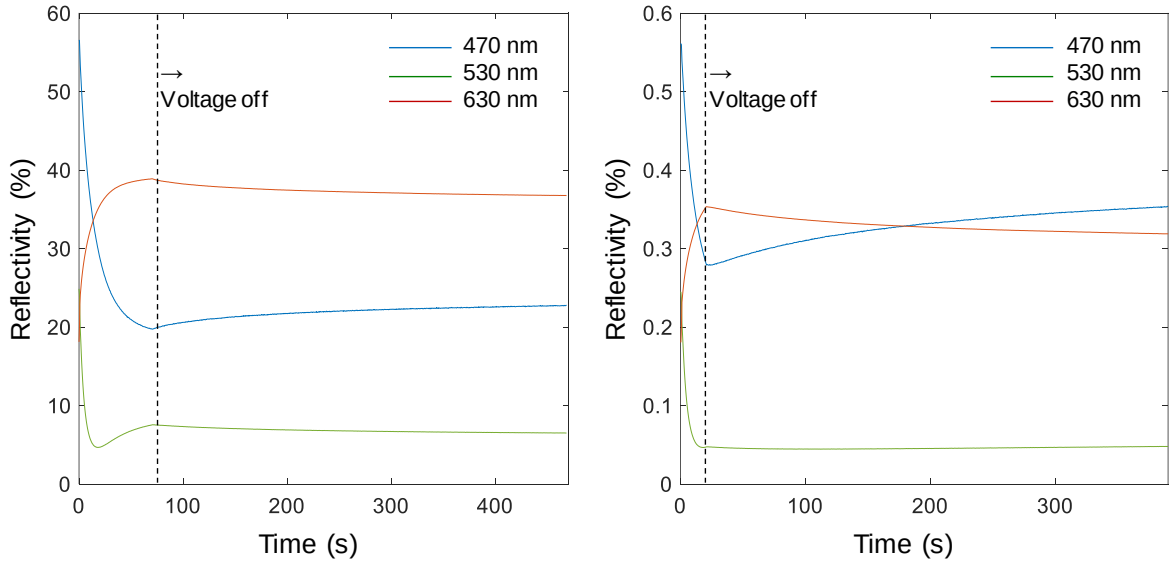


**Figure S7** Example data showing switching time and bistability. (Conventional sample, 90 nm $WO_3$.) Left: Reflectance levels are maintained at open circuit after a complete switch (−1.5 V applied from zero until 70 s). Right: Reflectance levels change little at open circuit after a partial switch (−1.5 V applied from zero until 20 s).